1-1-2015

Development and Characterization of Tool Compounds Targeting the Runt Domain's interaction With Cbfβ

Zaw Min Oo
University of Pennsylvania, aken.bates@gmail.com

Development and Characterization of Tool Compounds Targeting the Runt Domain's interaction With Cbfβ

Abstract

RUNX1 and CBFβ, which encode subunits of the core binding factor, are frequent targets of chromosomal aberrations in hematological malignancies. We previously determined that CBFβ (encoded by CBFB) is important for the transforming activity of the chimeric protein AML1-ETO protein (RUNX1-RUNX1T1) generated by the t(8;21), and other studies showed that normal Runx1 functions are essential for survival and maintenance of some leukemias lacking RUNX1 or CBFB mutations. Thus, we hypothesized that we could achieve therapeutic efficacy in multiple leukemias by targeting the Runx1:CBFβinteraction with small molecules. Using the structural information of the DNA binding Runt domain (RD) of Runx1 and its interface with CBFβ, we employed a computational screen for a library of 78,000 drug-like compounds, and further optimized our leads. The Runt domain inhibitors (RDIs) bind directly to the RD and disrupt its interaction with CBFβ. We showed that the RDIs reduced growth and induced apoptosis of t(8;21) acute myeloid leukemia (AML) cell lines, and reduced the progenitor activity of mouse and human leukemia cells harboring the t(8;21), but not normal bone marrow cells. The RDIs had similar effects on murine and human T cell acute lymphocytic leukemia (T-ALL) cell lines that did not harbor the t(8;21). Furthermore, our inclusion of a structurally related and weakly active compound as a control strongly support that the efficacies we observed were due to on target inhibition of RUNX functions. Our results confirmed that the RDIs might prove efficacious in various AMLs, and that a therapeutic window is available to specifically target malignant cells. We developed a pro-drug AI-9-59 with improved solubility and pharmacokinetic properties and assessed whether it has any in vivo efficacies in mouse leukemia models. Our results showed that the pro-drug was toxic to mice at dosage above 50 mg/kg and had no observable growth inhibitory effect on leukemia cells, suggesting that the concentration of the pro-drug necessary to inhibit endogenous core binding factor activity exceeds the maximum tolerated dose in mice. However, the expansion of granulocyte macrophage progenitors, and the gastrointestinal toxicity phenotype we observed suggested that the effects could be from on-target repression of RUNX proteins functions.

Degree Type
Dissertation

Degree Name
Doctor of Philosophy (PhD)

Graduate Group
Cell & Molecular Biology

First Advisor
Nancy A. Speck

Subject Categories
Cell Biology | Molecular Biology

DEVELOPMENT AND CHARACTERIZATION OF TOOL COMPOUNDS
TARGETING THE RUNT DOMAIN'S INTERACTION WITH CBFβ

Zaw Min Oo

A DISSERTATION

in

Cell and Molecular Biology

Presented to the Faculties of the University of Pennsylvania

in

Partial Fulfillment of the Requirements for the
Degree of Doctor of Philosophy

2015

Supervisor of Dissertation

Nancy A. Speck
Professor of Cell and Developmental Biology

Graduate Group Chairperson

Daniel S. Kessler
Associate Professor of Cell and Developmental Biology

Dissertation Committee:

Celeste M. Simon, Professor of Cell and Developmental Biology
Xianxin Hua, Professor of Cancer Biology
Warren Pear, Professor of Pathology and Laboratory Medicine
Wei Tong, Associate Professor of Pediatrics

ACKNOWLEDGEMENT

First and foremost, I would like to thank my advisor Dr. Nancy A. Speck for her mentorship and support over the years. I have learned so much from Nancy, and would like to take this opportunity to express my deepest gratitude.

I would also like to thank members of my thesis committee, Dr. Celeste M. Simon, Dr. Xianxin Hua, Dr. Warren Pear, and Dr. Wei Tong for their advice and help throughout my graduate career.

I am very grateful to my collaborators Dr. John Bushweller and Dr. Anuradha Illendula from University of Virginia. Much of my graduate work would not have been possible without their contribution.

I would like to thank past and present members of the Speck lab: Dr. Michael JF Chen, Dr. Liya Roudaia, Dr. Jing-mei Hsu, Dr. James Mangan, Dr. Xiongwei Cai, Dr. Joanna Tober, Dr. Yan Li, Chung-Tsai Lee, Amanda Yzaguirre, and Dana Bellissimo. I am fortunate to have you as colleagues, and I will always treasure our years in the Speck lab.

On a personal note, I would like to especially thank my wife Marybeth Tong, for her kind support, patience and her unwavering love. I would also like to thank my parents and my siblings for all their love and support.

ABSTRACT

DEVELOPMENT AND CHARACTERIZATION OF TOOL COMPOUNDS

TARGETING THE RUNT DOMAIN'S INTERACTION WITH CBFβ

Zaw Min Oo

Nancy A. Speck

RUNX1 and CBFβ, which encode subunits of the core binding factor, are frequent targets of chromosomal aberrations in hematological malignances. We previously determined that CBFβ (encoded by *CBFB*) is important for the transforming activity of the chimeric protein AML1-ETO protein (RUNX1-RUNX1T1) generated by the t(8;21), and other studies showed that normal Runx1 functions are essential for survival and maintenance of some leukemias lacking *RUNX1* or *CBFB* mutations. Thus, we hypothesized that we could achieve therapeutic efficacy in multiple leukemias by targeting the Runx1:CBFβ interaction with small molecules. Using the structural information of the DNA binding Runt domain (RD) of Runx1 and its interface with CBFβ, we employed a computational screen for a library of 78,000 drug-like compounds, and further optimized our leads. The Runt domain inhibitors (RDIs) bind directly to the RD and disrupt its interaction with CBFβ. We showed that the RDIs reduced growth and induced apoptosis of t(8;21) acute myeloid leukemia (AML) cell lines, and reduced the progenitor activity of mouse and human leukemia cells harboring the t(8;21), but not normal bone marrow cells. The RDIs had similar effects on murine and human T cell acute lymphocytic leukemia (T-ALL) cell lines that did not harbor the t(8;21). Furthermore, our inclusion of a structurally related and weakly active compound as a

control strongly support that the efficacies we observed were due to on target inhibition of RUNX functions. Our results confirmed that the RDIs might prove efficacious in various AMLs, and that a therapeutic window is available to specifically target malignant cells. We developed a pro-drug AI-9-59 with improved solubility and pharmacokinetic properties and assessed whether it has any *in vivo* efficacies in mouse leukemia models. Our results showed that the pro-drug was toxic to mice at dosage above 50 mg/kg and had no observable growth inhibitory effect on leukemia cells, suggesting that the concentration of the pro-drug necessary to inhibit endogenous core binding factor activity exceeds the maximum tolerated dose in mice. However, the expansion of granulocyte macrophage progenitors, and the gastrointestinal toxicity phenotype we observed suggested that the effects could be from on-target repression of RUNX proteins functions.

TABLE OF CONTENTS

LIST OF TABLES

LIST OF ILLUSTRATIONS

INTRODUCTION:

CHAPTER I:

CHAPTER II:

CHAPTER III:

xi

Introduction

Targeting Protein-protein interaction by small molecules

The past two decades have witnessed major advances in our understanding of the molecular mechanisms of diseases. As a consequence, drug discovery research has transitioned from searching for compounds with desired efficacy but against unknown targets to a target therapy approach. The aim of targeted therapy is to use our understanding of the cellular programs associated with the pathology of disease to design treatments with improved therapeutic efficacy. Although the majority of such studies have focused on targeting activated components of cytokine receptor signaling pathways, interest in targeting protein-protein interactions (PPIs) has grown in the past decade.

Protein-protein interactions play important roles in all aspects of cellular processes, particularly in the regulation of transcription where the assembly of protein-protein complexes is essential for appropriate gene regulation. PPIs, especially those involving transcription factors are highly attractive targets for developing inhibitors due to their biological importance, as many cancers either directly involve transcription factors, or indirectly modulate transcription factor activity. A variety of transcription factors have been identified as driving agents promoting tumorigenesis and cancer progression (1). Therefore, inhibiting PPIs involving transcription factors has a high therapeutic potential (2). However, until recently PPIs were considered undruggable due to several challenges. First, the contact surfaces involved in PPIs are large and lack the grooves and pockets for small molecule binding. Second, PPIs do not have natural small molecule substrate or ligand that can serve as starting scaffold for drug discovery.

1

Despite these challenges, research in identifying small molecule inhibitors of PPIs has made considerable progress in the past decade. Several recent technological advances facilitate this trend and provide hope for finding small molecules that target PPIs. We now have a better understanding of binding energetics at the macromolecular interface of PPIs. Although the protein-protein interfaces are large, mutational studies show that only a small subset of the residues involved contributes to most of the free energy of binding (3-5). The presence of such "hotspots" makes PPIs amenable to small molecule perturbations, and disrupting the interactions mediated by these hotspot residues proves to be effective in inhibiting PPIs. The identification of hotspot residues in turn allows for structure-based virtual screening to identify novel bioactive molecules. In virtual screening, large libraries of drug-like compounds that are commercially available are computationally screened against targets of known structure, and those that are predicted to bind well are experimentally tested. Structure-based virtual screening provides a more efficient and cost-effective approach over high-throughput screening (HTS) for identifying new lead compounds as it utilizes the knowledge of the three-dimensional (3D) structure of the biological target. I will provide several examples of small molecules targeting PPIs in distinct biological pathways.

MDM2-p53 inhibitors: a breakthrough in targeting PPI

One recent success story in targeting PPI is the development of small molecules that inhibit the interaction of MDM2 with p53 (6). p53 is a tumor suppressor gene that normally triggers growth arrest, senescence or apoptosis in response to cellular stress. p53 activation increases the expression of E3 ligase MDM2, which in turn binds p53, directly represses p53 DNA binding ability and tags p53 for proteasomal degradation (7). p53 mutations, detected in a variety of human cancers, disrupt p53's DNA binding and

transcriptional activity (8). Structurally, the N-terminal domain of MDM2 has a well-defined hydrophobic pocket that mediates p53 binding, suggesting that the pocket could be targeted with small molecule drugs to block the MDM2-p53 interaction (9). Nutlins, a family of cis-imidazoline analogs, were identified by screening for compounds that disrupt the MDM2-p53 interaction (10). Nutlins inhibit the interaction of MDM2 with p53, leading to stabilization of p53 levels, and restore p53 mediated apoptosis (10-13). The success of MDM2-p53 PPI inhibitors has significantly accelerated studies to target other PPIs with small chemical compounds as anticancer drugs.

STATs inhibitors

Signal transducers and activators of transcription (STATs) are a family of cytoplasmic transcription factors. One of the key structural features of STATs is the Src homology (SH) 2 domain, the phosphorylation of which activates STATs. Activated STATs form dimers that translocate to the nucleus and regulate transcription of target genes controlling cell growth, differentiation, and survival (14). In normal cells, STAT signaling is transient and tightly regulated. However, cancer cells frequently have persistent STATs activation from hyper-activation, overexpression of upstream tyrosine kinases, or loss of function of negative regulators. As activated STATs, particularly STAT3, drive the expression of genes involved in cell proliferation and survival, blocking STAT3 activity presents a useful strategy for drug discovery (14). The availability of the three-dimensional (3D) structure of phosphorylated STAT3 (15), and the existence of a clearly defined binding pocket for small molecules in the SH2 domain allowed virtual screening of chemical databases for the identification of small molecule inhibitors of the STAT3 SH2 domain (16, 17). The most recent compound discovered by this route, S3I-201, inhibits dimerization and DNA binding of pre-phosphorylated STAT3 and displayed

3

STAT3-dependent cellular effects in transcription, transformation, and apoptosis. Furthermore, S3I-201 is effective against a tumor cell line displaying constitutive STAT3 activity in a mouse model xenograft model (17).

BCL6 inhibitor

BCL6 (B cell lymphoma 6) is the most frequently involved oncogene in diffuse large B cell lymphomas (DLBCLs) (18). BCL6 is required for B cell maturation, during which BCL6 represses genes involved in sensing DNA damage or their downstream checkpoints (19-21). BCL6 is constitutively expressed in the majority of patients with aggressive B cell lymphomas (18), and mice engineered to constitutively express BCL6 in B cells develop DLBCL similar to the human disease (22, 23). BCL6 knockdown or peptide inhibitors kill DLBCL cells, demonstrating that BCL6 is required for survival of lymphoma cells and suggesting that BCL6 is a bone fide therapeutic target for DLBCL (19, 24, 25).

BCL6 is a member of the BTB/POZ family of transcription factors (26). BCL6 acts as a sequence specific transcription repressor by recruiting SMRT, N-CoR, and BCOR corepressors through its BTB domain (27, 28). Using structured-based virtual screening, a potent inhibitor of BCL6 BTB domain repressor activity was identified. The inhibitor binds to the BCL6 BTB domain, specifically inhibits BCL6, disrupts BCL6 transcriptional complexes and reactivates BCL6 target genes. The inhibitor selectively kills BCL6-dependent DLBCL cells, and suppresses human DLBCL xenografts in mice (29).

Menin-MLL inhibitors

Translocations involving the mixed lineage leukemia (*MLL*) gene are frequently found in acute myeloid leukemia (AML) and are associated with poor prognosis (30, 31).

The MLL protein is a histone H3 lysine 4 (H3K4) methyltransferase required for the expression of *HOX* family genes during hematopoietic differentiation (32, 33). Fusion of *MLL* with one of numerous partner genes results in chimeric proteins that upregulate MLL target gene expression, block hematopoietic differentiation, and promote proliferation (33-35). The function of the wildtype MLL as well as MLL fusion requires interaction between MLL and menin, a tumor suppressor encoded by *MEN1* (multiple endocrine neoplasia 1) (36). Loss of menin binding eliminates the oncogenic potential of MLL fusions (37, 38), and therefore targeting the menin-MLL interaction represents a potential therapeutic approach for the treatment of AML with the MLL translocation.

A single point mutation in the high-affinity menin-binding motif 1 (MBM1) in MLL is sufficient to abolish the menin-MLL interaction, suggesting the existence of a hotspot residue for this interaction (39, 40). Subsequently, Grembecka et al (41) reported the identification of a family of small molecules that inhibit the menin-MLL interaction. One of the compounds, MI-2 binds to menin, disrupts the menin-MLL interaction and downregulates the expression of the MLL target genes essential for leukemogenesis. MI-2 inhibits the proliferation of several leukemia cell lines harboring MLL translocation but has minimal anti-proliferation effect on leukemia cell lines without MLL fusions. Subsequent structure-based design resulted in MI-2-2 with improved binding affinity for menin and enhanced cellular potency (42). Therefore, the inhibitor represents a promising lead that may be developed into a new antileukemic drug for MLL leukemia.

CBFβ-SMMHC inhibitor

The chromosome inversion 16 inv(16)(p13;q22) is one of the most common chromosomal rearrangements in acute myeloid leukemia. The rearrangement fuses the core binding factor β (CBFB) gene to the myosin heavy chain (MYH11) gene and

generates the chimeric transcription factor fusion CBFβ-SMMHC. CBFβ-SMMHC cooperates with activating mutations in components of cytokine signaling pathways in leukemia transformation (43-46). Studies in mice and patient samples support the concept that inv(16) is a driver mutation that generates preleukemic progenitor cells that, upon acquisition of additional cooperating mutations, progress to leukemia (44, 45, 47, 48). CBFβ-SMMHC outcompetes wildtype CBFβ for binding to transcription factor RUNX1 (49), deregulates RUNX1-mediated transcription in hematopoiesis, and induces AML. Most recently, Illendula et al. reported the development of a PPI inhibitor that selectively binds to CBFβ-SMMHC and disrupts its binding to RUNX1 (50). Using a fluorescent resonance energy transfer (FRET) assay, the authors identified a lead compound that blocks the interaction of CBFβ-SMMHC with the Runt domain of RUNX1. As CBFβ-SMMHC is oligomeric in solution, the authors designed a bivalent analog of the lead compound with a seven-atom polyethylene glycol linker, resulting in the drug AI-10-49. AI-10-49 specifically binds to CBFβ-SMMHC, restores RUNX1 transcriptional activity and delays leukemia progression in mice. Treatment of primary inv(16) AML patient blasts with AI-10-49 triggers selective cell death (50). The work provides additional support for targeted therapy against transcription factor drivers of cancers.

These results demonstrate that targeting transcription factors with small molecules is feasible, and provide validation for our proposal to develop a novel class of small molecule inhibitors that target the RUNX proteins, a small family of DNA binding transcription factors, by interfering with their interaction with the non-DNA binding subunit core binding factor β (CBFβ).

Core-binding factor in development

RUNX proteins are members of the <u>c</u>ore-<u>b</u>inding <u>f</u>actor (CBF), a family of heterodimeric transcription factors that play major roles in hematopoiesis. The CBF family consists of three distinct DNA binding CBFα subunits (RUNX1, RUNX2, and RUNX3), and a common non-DNA binding CBFβ subunit (encoded by *CBFB*) (Figure 1).

Figure 1. The core binding factor subunits and genes.

Shown is the structure of the DNA binding Runt domain of Runx1 (gray) and the CBFβ subunit (blue) bound to DNA.
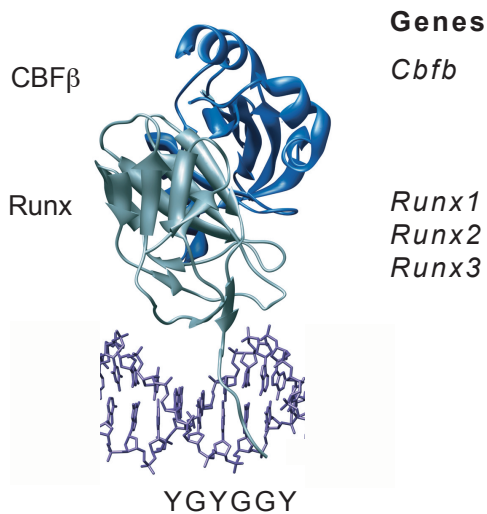
RUNX1, also known as acute myeloid leukemia 1 (AML1) or core-binding factor subunit alpha-2 (CBFA2), was initially identified from chromosome 21 in the t(8;21) (q22;q22) chromosomal translocation, frequently found in acute myeloid leukemia (AML) (51). RUNX proteins are evolutionally conserved (Figure 2). There are two well-studied RUNX homologs in *Drosophila*: runt and lozenge (52, 53). *runt* is a pair-rule gene involved in embryonic patterning and also plays a role in sex determination, segmentation and neural development (54, 55). *lozenge* is involved in hematopoiesis

7

and eye development (56). Subsequent work established that the RUNX proteins are sequence-specific DNA-binding proteins that bind to the polyomavirus enhancer and Moloney murine leukemia virus enhancer core sites, hence the name core-binding factors (57-61). All RUNX proteins have a highly conserved 128-amino-acid Runt domain in their N-terminal portion, which mediates both DNA binding and CBFβ heterodimerization (Figure 2). Through the Runt domain, RUNX proteins recognize the consensus sequence PyGPyGGT. The CBFβ subunit does not touch DNA but enhances the affinity of RUNX proteins for DNA (62), and protects them from ubiquitination and proteasomal degradation (63).

Figure 2. A diagrammatic representation of the structure of RUNX1, RUNX2 and RUNX3 together with *Drosophila runt* and *lozenge*.

The Runt domain, the activation domain (AD), and C terminal VWRPY motif, along with the size of each protein are indicated. m: mouse RUNX, h: human RUNX

8
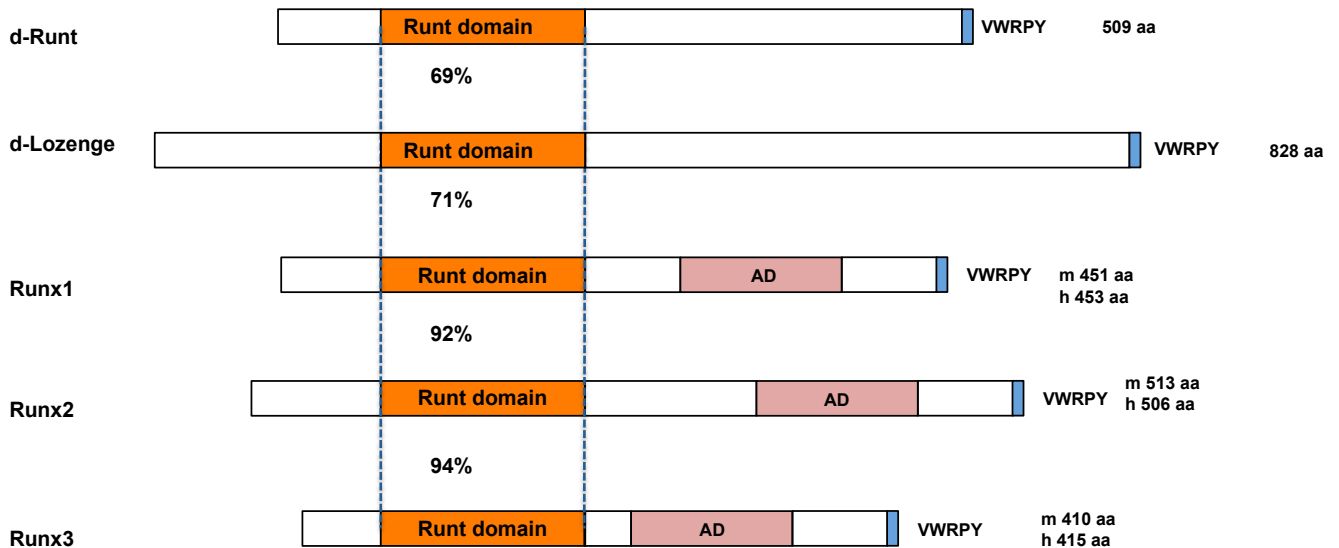
Numerous studies established that both Runx1 and CBFβ are critical for hematopoietic development. Runx1 is constitutively expressed in all hematopoietic lineages, except mature erythroid cells (64). In the conceptus, Runx1 is expressed in all sites of hematopoietic cell formation, including the vitelline and umbilical arteries, the yolk sac, the placenta, and the ventral portion of the dorsal aorta in the aorta-gonad-mesonephros (AGM) region (65-67) (Figure 3). In the embryo, hematopoietic stem and progenitor cells (HSPCs) emerge from Runx1-expressing vascular-endothelial-cadherin-positive endothelial cells called hemogenic endothelium, and Runx1 activity is essential for HSPC formation from these cells (65, 68-72). Thus RUNX1 is recognized as a mandatory transcription factor in embryonic hematopoiesis.

Figure 3. Schematic diagram of an E10.5 mouse embryo.

Sites of Runx1 expression in hemogenic endothelium are colored in red. These include the ventral aspect of the dorsal aorta in the aorta/gonad/mesonephros region, the umbilical artery, vitelline artery, and in areas of the yolk sac.
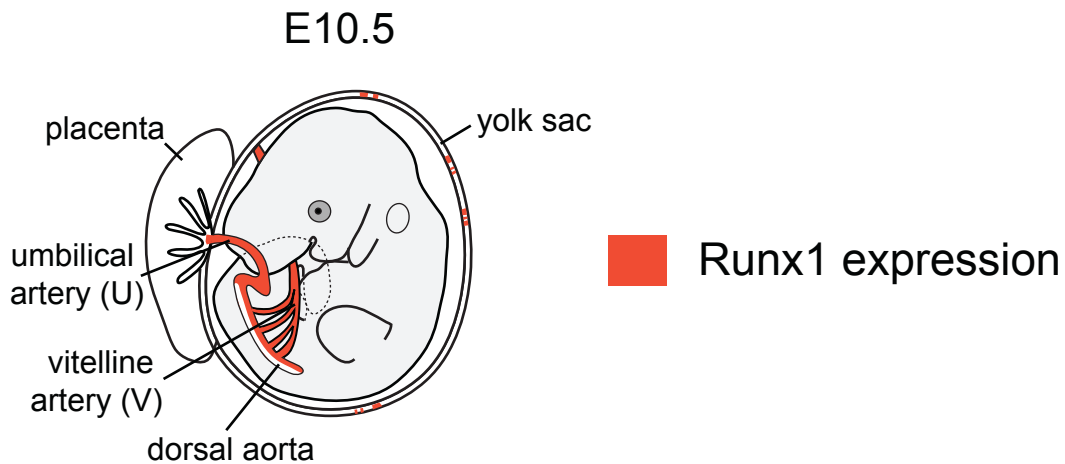
Homozygous deletion of Runx1 or CBFβ in mice results in nearly identical developmental defects including extensive hemorrhaging within the central nervous

system, and mid-gestation embryonic lethality between embryonic day 12.5-13.5 (73-76). *Runx1* or *Cbfb* deficient mouse embryos lack definitive hematopoietic progenitors, definitive enucleated erythrocytes, and mature myeloid-lineage cells (73-77), and the lack of definitive hematopoietic cells is observed in all sites of hematopoiesis (65, 67, 69, 70, 78) (Table 1). In addition, no transplantable hematopoietic stem cell (HSC) activity is found in the AGM region of *Runx1* deficient embryos (79). Chimeric animals made from *Runx1* or *Cbfb* deficient embryonic stem (ES) cells and wild type mouse blastocysts contain no ES-derived cells in adult hematopoietic tissues, which indicates that both genes are required in a cell-autonomous fashion (73, 75, 80). Therefore, both Runx1 and CBFβ are required to establish HSPCs during embryonic development.

Runx2, another member of the RUNX family, is primarily associated with osteoblast differentiation and bone formation (81, 82) (Table 1). Runx2 null mice died soon after birth, and the embryos and newborns showed a complete lack of bone formation and ossification, and the development of cartilage in Runx2 null mice was delayed (81, 82). Further studies established RUNX2 as a master transcription factor of osteoblast differentiation that controls both osteoblast differentiation and expression of osteoblast specific genes (83, 84).

The knockout of RUNX3 caused phenotypes in several different tissues (Table 1). Germline Runx3 knockout led to mice with defects in T-cell development, as well as gastrointestinal and neural disorders (85-88). During T-lymphocyte development, Runx3 is essential for silencing of CD4 expression and maturation of single positive CD8^{+} T cells. The absence of Runx3 results in defective cytolytic activity of T lymphocytes (86, 89). As Runx3 deficient mice spontaneously develop tumors in the intestine, lung and breast (90), RUNX3 may play a tumor suppressor role during the early stages of solid tumor formation.

Table 1. Knockout phenotypes of the core binding factor genes in mouse.

Gene	Phenotype	References
Runx1 -/-	Lethal at embryonic day (E) 11.2-12.5. Absence of definitive hematopoiesis.	(73, 74)
	Absence of intra-aortic hematopoietic clusters.	(65)
Runx2 -/-	Lethal at birth, failure of osteoblast differentiation and bone formation.	(81, 82)
	Perturbation of chondrocyte differentiation.	(91, 92)
Runx3 -/-	Hyperplastic gastric epithelia due to excessive proliferation.	(87)
	Loss of dorsal-root ganglion proprioceptive neuron function and ataxia.	(85, 88)
	Loss of homeostatic control of dendritic-cell function and lung inflammation.	(93)
Cbfb -/-	Lethal at E11.5-13.5. Failure of definitive hematopoiesis.	(75, 76)

Core-binding factor in adult hematopoiesis

As will be discussed later, we developed small molecule inhibitors of the RUNX proteins that disrupt the Runt domain's interaction with CBFβ. These function as pan-RUNX/CBFβ inhibitors. In order to anticipate and interpret the inhibitors' on-target activities, it is worth reviewing the murine phenotypes associated with Runx and CBFβ mutations, alone or in combinations. Conditional deletion of Runx1 in hematopoietic cells using the interferon inducible Mx1-Cre or pan-hematopoietic Vav1-Cre shows that once definitive hematopoiesis develops in the embryos, RUNX1 expression is not required to maintain HSCs (Table 2). Conditional knockout (cKO) of Runx1 does not cause hematopoietic failure in adult mice (94-96) but results in multi-lineage blocks in

lymphocyte and megakaryocyte development, and increase in the number of committed erythroid/myeloid progenitors. Runx1 deletion in the adult results in expansion of the lineage negative Sca1$^+$ Kit$^+$ (LSK) phenotypic HSPC population in the bone marrow (94, 97, 98) in a cell autonomous manner and reduces the frequency of functional long-term repopulating hematopoietic stem cells (LT-HSCs) in the bone marrow by 3-fold without affecting their self-renewal properties (97-99).

Runx1 loss in adult mice does not cause acute myeloid leukemia (AML) but establishes a pre-leukemic state that predisposes to AML following the acquisition of secondary mutations (99, 100). At the cellular level, Runx1-deficient HSPCs have slow growth, low biosynthesis and markedly reduced ribosome biogenesis (Ribi) (Figure 4). Runx1-deficient HSPCs have lower p53 levels, reduced apoptosis, an attenuated unfolded protein response, and are resistant to genotoxic and endoplasmic reticulum (ER) stress. The low biosynthetic activity and corresponding stress resistance provide a selective survival advantage to Runx1-deficient HSPCs, allowing them to expand in the bone marrow and outcompete normal HSPCs (101).

Young Runx3 cKO mice do not display gross hematopoietic abnormalities, and aged Runx3 cKO mice show a mild expansion of the LSK compartment, partially phenocopying Runx1 cKO mice (102) (Table 2). In contrast, Runx1;Runx3 double knockout (DKO) mice exhibited much more severe phenotypes. The DKO mice had decreased white blood cell and platelet counts, developed anemia, and died within 18 weeks post deletion. The DKO mice showed differentiation blocks in all hematopoietic lineages, and a 48-fold expansion in the LSK fraction that is followed by subsequent exhaustion in the HSPC compartment (103). Transplant experiments showed that the differentiation blocks and stem cell exhaustion in the DKO mice are cell autonomous (103). Therefore, Runx1;Runx3 double knockout mice show more pronounced

hematopoietic defects than Runx1 cKO mice, suggesting that RUNX family genes have compensatory mechanisms in hematopoiesis.

Conditional deletion of CBFβ, which should affect the activity of all three RUNX proteins, also shows more pronounced defects in hematopoiesis than *Runx1* cKO mice (Table 2). *Cbfb* cKO mice have marked differentiation blocks in all hematopoietic lineages and significant expansion of LSK and short-term HSCs (ST-HSCs) in the bone marrow (BM). *Cbfb* cKO mice showed progressive decreases in leukocyte, hemoglobin, and platelet counts, and died by 6 months of age due to bone marrow failure (104). Although fetal liver and BM cells from *Cbfb* cKO mice show significant increase in colony forming activity, recipient mice transplanted with *Cbfb* deficient cells have extremely low donor chimerism in the hematopoietic tissues, including HSPC fractions in the BM. These results showed that while the progenitors in the *Cbfb* cKO mice possess greater proliferative capacity, *Cbfb*-deficient HSCs were incapable of long-term engraftment (104, 105). In addition, *Cbfb* cKO mice are not born at Mendelian ratios. The fact that CBFβ deficient HSCs are much more severely compromised than Runx1 deficient HSCs suggests Runx2 and/or Runx3 contribute substantially to HSC functions and also suggests the existence of functional compensation by the remaining two *Runx* genes for Runx1 loss.

Table 2 . Conditional knockout phenotypes of the core binding factor genes in mouse.

Targeted Gene	Phenotype of conditional knockout		References
Runx1	Mx1-Cre	Normal HSC numbers. Normal myeloid cell compartment. Defective B and T cell differentiation.	(95)
	Mx1-Cre	Reduced competitive repopulating ability. Myeloid expansion in spleen and liver.	(94)
	Mx1-Cre Vav1-Cre	Expands phenotypic stem and progenitor population. Three-fold reduction in frequency of long term repopulating HSC but showed no exhaustion. Runx1 loss slowed HSC proliferation and reduced apoptosis.	(97)
	Vav1-Cre	Runx1 deficient HSPCs have slow growth, low biosynthesis, and markedly reduced ribosome biogenesis.	(101)
Runx3	Mx1-Cre	Old *Runx3* KO mice shows expanded LSK compartment.	(102)
Runx1 and Runx3	Mx1-Cre	The majority of double knock out mice developed bone marrow failure (BMF) and died within 18 weeks. BMF preceded by drastic expansion of the LSK compartment, followed by exhaustion. Differentiation blocks in all hematopoietic lineages.	(103)
Cbfb	Mx1-Cre Vav1-Cre	Differentiation blocks in all hematopoietic lineages. Significant expansion of LSK and ST-HSC populations. Stem cells incapable of long engraftment.	(104)
	Vav1-Cre	No significant perturbation in E14.5 fetal liver LSK and phenotypic long-term HSCs populations. Long term repopulating ability severely diminished.	(105)

Figure 4. Impact of loss of function *Runx1* mutations in hematopoietic stem cells (HSCs).
Runx1 directly occupies genes involved in ribosome biogenesis (Ribi). Loss of *Runx1* results in decreased ribosome biogenesis, and other phenotypes thought to be secondary to decreased ribosome biogenesis that are listed. From Cai et al. (101).

Decreased Ribosome Biogenesis
Decreased Cell Size
Decreased Translation Rate
Decreased Apoptosis
Attenuated UPR pathway
Lower p53
Decreased Metabolism
Increased Stress Resistance
Selective Advantage Over Normal HSCs
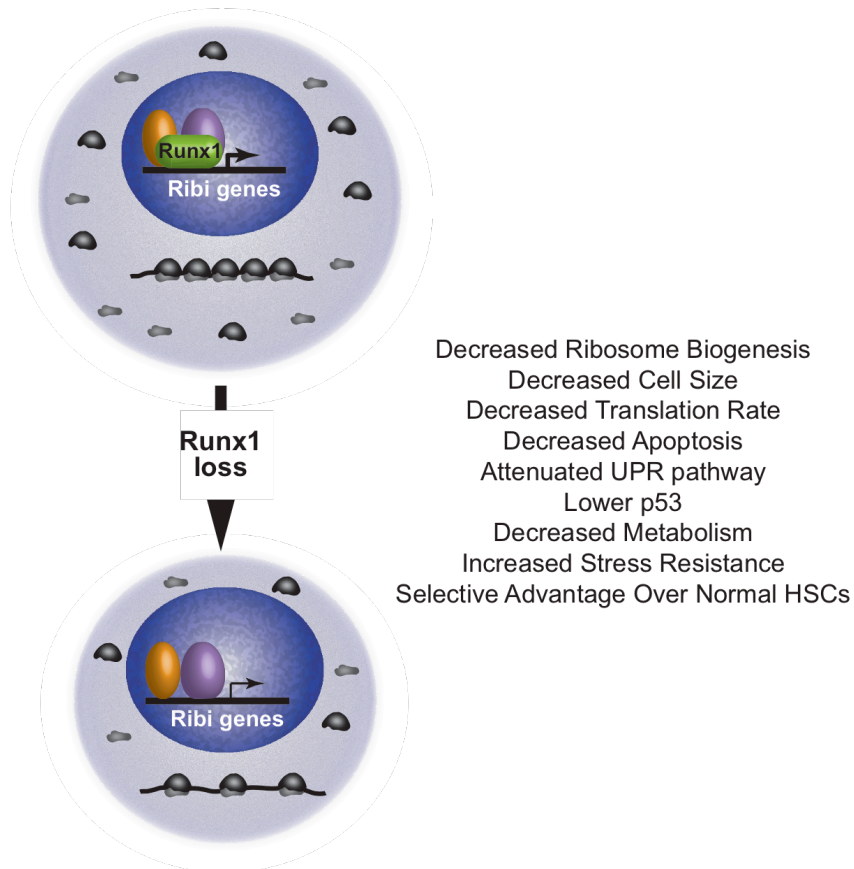
Core-binding factors in hematological diseases

The importance of the core binding factors in hematopoiesis is further underscored by the fact that both Runx1 and CBFβ are frequent targets of mutations and chromosomal aberrations in various hematological malignancies (Table 3). Characteristic genetic abnormalities include the t(8;21) and inv(16) in RUNX1 and CBFB

respectively. Each defines subgroups within the category of recurrent cytogenetic abnormalities, and confers a favorable prognosis.

Table 3. Chromosomal translocations and mutations affecting Runx1 and CBFβ in various hematological diseases.

Gene	Hematological disease	Mutations
RUNX1	AML-M2	AML1-ETO: t(8;21)(q22;q22) AML1-LRP16: t(11;21)(q13;q22) AML1-MTG16: t(16;21)(q24;q22)
	MDS	AML1-EVI: t(3;21)(q26.2;q22) AML1-MDS1: t(3;21)(q26.2;q22) AML1-EAP: t(3;21)(q26.2;q22) AML1-PRM6: t(1;21)(p36;q22)
	B-ALL	TEL-AML1: t(12;21)(p13;q22)
	AML-M0	Mono- or bi-allelic loss of function *RUNX1* mutation
	AML-M1	Loss of function *RUNX1* mutation
	CMML	Loss of function *RUNX1* mutation
	FPD/AML	Mono-allelic *RUNX1* mutation
CBFB	AML-M4 Eo	CBFB-MYH11: Inv(16)(p13;q22)

Abbreviations: AML, acute myeloid leukemia; AML-M0, minimally differentiated acute myeloid leukemia; AML-M1, acute myeloid leukemia without maturation; AML-M2, acute myeloid leukemia with maturation; AML-M4Eo, acute myeloid leukemia with bone marrow eosinophilia; CMML, chronic myelomonocytic leukemia; FPD/AML, familial platelet disorder with predisposition to acute myeloid leukemia; MDS, myelodysplastic syndrome.

t(8;21) AML and AML1-ETO

The 8;21 translocation t(8;21)(q22;q22) is one of the most common chromosomal aberrations in *de novo* AML, occurring in 10% of adult and 12% of pediatric AMLs (96, 106, 107). The t(8;21) breaks the *RUNX1* gene in intron 5, resulting in fusion of the N-terminal 177 amino acids of Runx1 (including the runt domain) to ETO (eight twenty-one, encoded by *RUNX1T1*) (108-112). This generates the chimeric protein AML1-ETO (Figure 5). ETO has no known role in hematopoiesis: homozygous loss of *Runx1t1* in mice resulted in gastrointestinal defects, but no hematopoietic deficiencies (113, 114). ETO contains four domains conserved with its Drosophila homologue nervy. Thus the chimeric protein AML1-ETO consists of the intact Runt domain and almost the entire coding region of ETO, including 4 functional domains named Nervy homology region (NHR) 1, NHR2, NHR3, and NHR4, the structures for all of which, along with their interacting proteins or peptides from those proteins, have been solved (115-120). Although AML1-ETO is an essential causative factor of t(8;21)-positive AML, the full length chimeric protein is not leukemogenic by itself, and can only induce AML in mice when combined with an additional oncogene such as an activated kinase, including Fms-like tyrosine kinase 3 internal tandem duplication (FLT3-ITD), TEL-PDGFBR, or activated KIT (121-123). AML1-ETO confers phenotypes different from loss of function Runx1 mutations. Genetic experiments in *Drosophila* showed that AML1-ETO acts as a constitutive repressor of Runx1 homologue lozenge (124). The phenotype of conditional knock-in mice in which AML1-ETO expression is activated in the adult bone marrow resembles a milder version of Runx1 loss, including increased numbers of granulocyte-monocyte (GM) progenitors and enhanced serial replating activity (125).

Figure 5. Schematic for AML1-ETO and its interacting proteins.

On top is a schematic diagram of RUNX1 in grey and ETO sequences in gold and orange. t(8;21) generates AML1-ETO which fuses the Runt domain to nearly all of ETO. Structures of conserved domains (grey or orange) and their interacting proteins or peptides from those proteins (blue), and DNA (purple) are shown below.
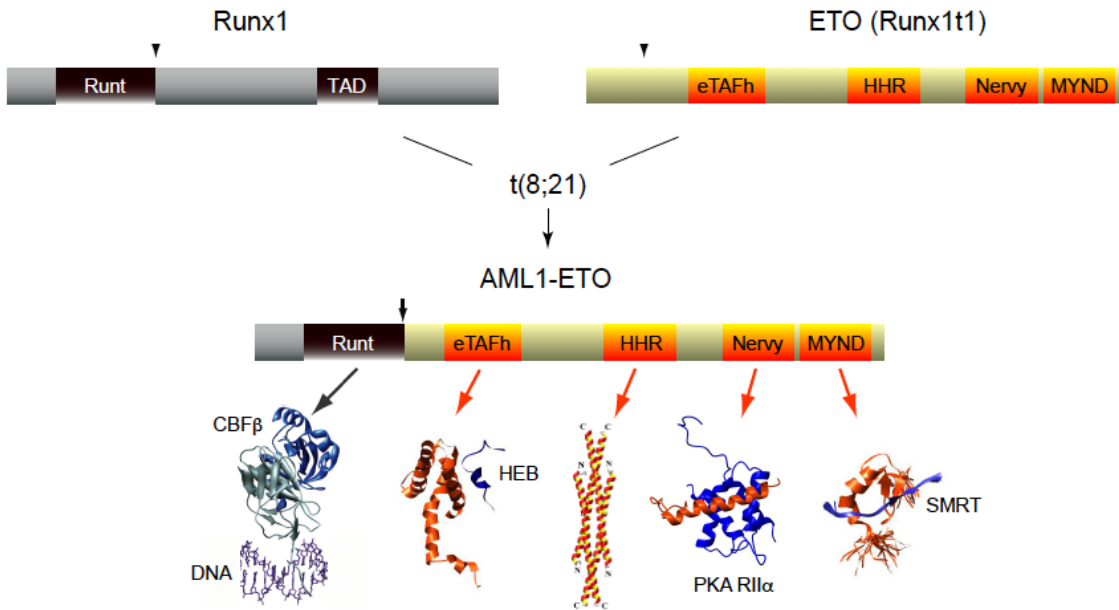
Clinically, t(8;21)-positive leukemia is associated with favorable prognosis, with 70% of patients achieving complete remission following standard therapy (126, 127) (Figure 6). However, many patients retain AML1-ETO expressing cells in their bone marrow due to incomplete eradication of the leukemic cells (128, 129). As a result 35-40% of these patients relapse within five years and have poor long-term survival (126, 127).

Figure 6. Survival curves of core binding factor leukemias compared to other leukemia types.

Favorable prognosis is associated with t(15;17), t(8;21), or inv(16) whether alone or in combination with other chromosomal abnormalities, with the possible exception of inv(16) or t(8;21) with complex karyotype. From Gulley et al. 2010 (128).
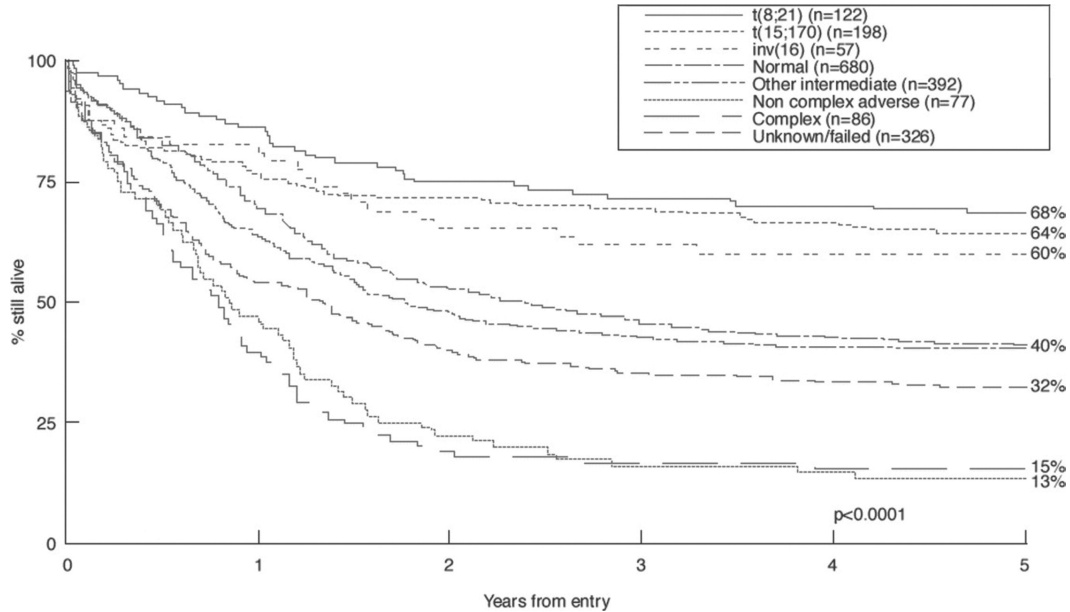
Mutations that specifically disrupt the interaction between individual domains in AML1-ETO and their associated proteins revealed that the Runt domain and the NHR2 domain (also known as hydrophobic heptad repeat or HHR) are essential for AML1-ETO's leukemogenic activity (130-133). The Runt domain of AML1-ETO mediates DNA binding and CBFβ binding, and both interactions are essential for AML1-ETO's leukemogenic activities (130, 132, 133). Amino acid substitutions in the Runt domain that either disrupt AML1-ETO's DNA binding or AML1-ETO's interaction with CBFβ severely impaired AML1-ETO's ability to transform hematopoietic cells, and abolished AML1-ETO's ability to initiate leukemia in cooperation with activated kinase TEL-PDGFBR in mice (130, 132) (Figure 7). Collectively these data demonstrated that

19

oligomerization and both DNA and CBFβ binding are required for AML1-ETO's leukemogenic activity.

Figure 7. Mutations that disrupt DNA or CBFβ binding impair AML1-ETO's leukemogenic activity. From Roudaia et al, 2009 (132).

A. Structures of the Runt domain and CBFβ are shown in gray and blue respectively, and the DNA is purple. The R174 residue in the Runt domain is shown in green, and the T161 and Y113 residues are in orange.

B. Schematic of transplantation. Bone marrow mononuclear cells harvested from 5-fluorouracil treated C57BL/6 mice were co-infected with MigR1 expressing AML1-ETO (or its mutated derivatives) and TEL-PDGFβR. IRES-mediated expression of EGFP marked AML1-ETO expressing cells while hCD4 marked TEL-PDGFβR expressing cells. One million transduced cells were transplanted along with 200,000 normal bone marrow cells into lethally irradiated mice.

C. Kaplan-Meier survival curve of mice after transplantation with retroviruses expression AML1-ETO (AE) or its mutated derivatives and TEL-PDGFβR (TP).

20
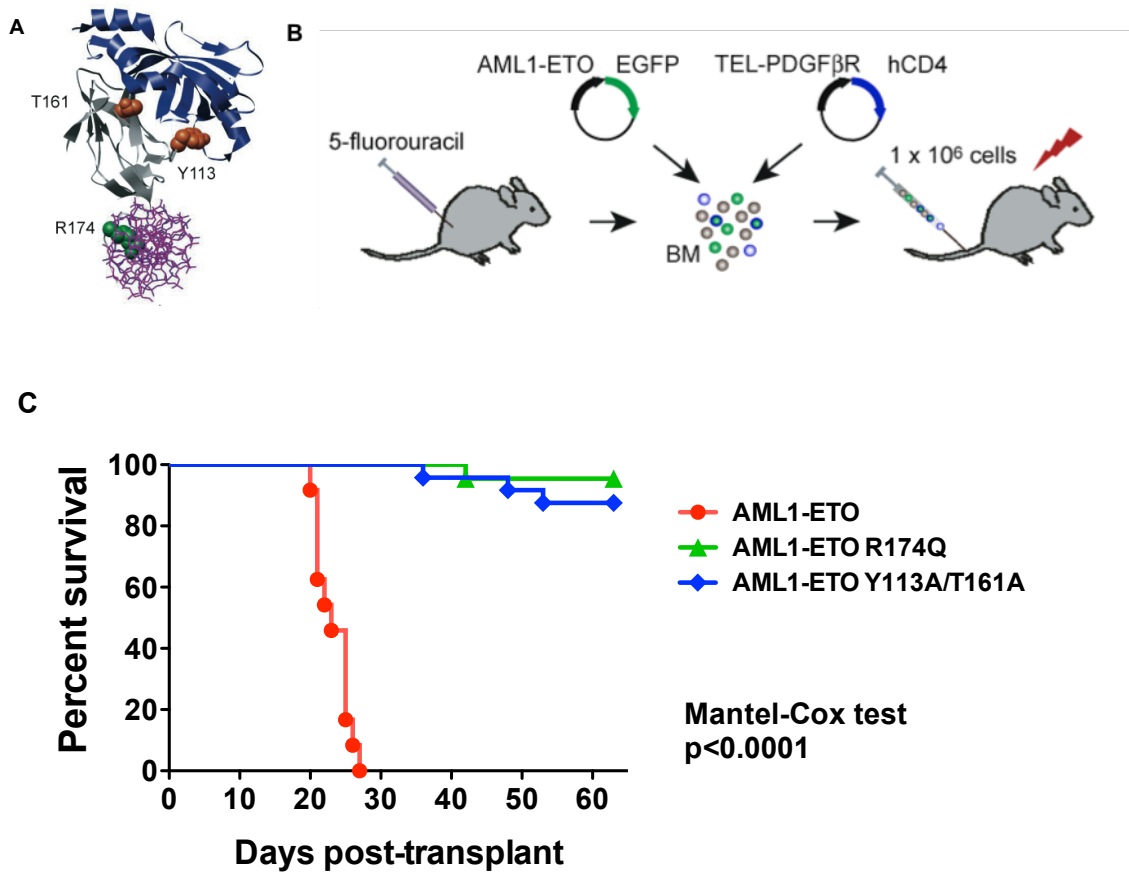
The NHR2 mediates tetramer (dimer of dimers) formation, and mutations that reduced the tetramer to a dimer abrogated AML1-ETO's leukemogenic activity (116, 131). Substitution of NHR2 by an oligomerization domain from the forkhead binding protein retained AML1-ETO's ability to confer serial replating activity to primary bone marrow cells, demonstrating that oligomerization per se is important for AML1-ETO's transforming ability (134).

On the other hand, NHR1, NHR3 and NHR4 are not essential for AML1-ETO's leukemogenic activity. The NHR1 (also known as the eTAFH domain) is homologous to several TATA binding protein-associated factors (TAFs) and interacts with E proteins (E2A and HEB). It has been proposed that AML1-ETO mediated silencing of E protein functions is important for t(8;21) leukemogenesis (119, 135). However, amino acid substitutions that disrupt NHR1's association with HEB did not impair AML1-ETO's ability to confer serial replating to primary mouse bone marrow cells (117), and deletion of the entire NHR1 domain had no effect on AML1-ETO's leukemogenic activity (130). The NHR3 (also known as the Nervy domain) shares homology with A-Kinase Anchoring Proteins (AKAPs) and interacts with the regulatory subunit of type II cAMP-dependent Protein Kinase (PKA RIIα) (136). Amino acid substitutions that disrupt the interaction of NHR3 with PKA RIIα did not affect AML1-ETO's ability to transform primary mouse bone marrow cells nor its leukemogenic activity (136).

The NHR4 (also known as the myeloid-Nervy-DEAF-1, MYND) appears to restrain AML1-ETO's leukemogenic activity, as mutations of NHR4 promote AML1-ETO's activity (137). NHR4 binds the silencing mediator of retinoid and thyroid hormone receptor (SMRT) and nuclear receptor co-repressor (N-CoR) complexes, as well as the DNA binding protein SON (138-140). Deletion of the C-terminal NCoR/SMRT interacting domain of AML1-ETO resulted in the formation of a more potent leukemogenic protein

21

(141). Interestingly, an alternative splice form of AML1-ETO that results in the formation of a C-terminal truncated protein called AML1-ETO9 (142). AML1-ETO9a is found in human leukemia cells, and introducing AML1-ETO9a alone into mouse hematopoietic cells results in the rapid development of leukemia in transplanted mice, suggesting that AML1-ETO9a does not require additional cooperating mutations (142).

Therefore, AML1-ETO has several interactions that may be targeted with small molecule inhibitors: the Runt domain:DNA interface, the Runt domain:CBFβ interface, and NHR2 mediated oligomerization. The interaction of CBFβ with the Runt domain is essential for the ability of TEL-AML1 (ETV6-RUNX1), frequently found in B-ALL, to promote the serial replating of B cell progenitors in vitro (132). This suggests that the interaction with CBFβ may be important for the activity of multiple chimeric Runx1 proteins.

Interestingly, no loss of function (LOF) *RUNX1* mutations in the remaining *RUNX1* allele were found in the favorable risk group with the characteristic genetic abnormality (8;21) (143, 144). Similarly, no LOF *RUNX1* mutations were found in AMLs containing the inv(16) (143, 144). These data suggest either that the t(8;21) and inv(16) were redundant with LOF *RUNX1* mutations, or that they were synthetically lethal. In support of the latter interpretation, recent studies have provided evidence that wildtype CBF functions are required for the maintenance and survival of leukemia cells. Specifically, knock down of wild type Runx1 reduced growth and induced apoptosis in t(8;21) cell lines, and also in AML1-ETO transformed human CD34 positive cells (145, 146). Knock down of Runx1 also induced apoptosis of MLL-AF9 transformed cells, and deletion of Runx1 and CBFβ extended the disease latency in a mouse MLL-AF9 model (146), suggesting that a subset of AMLs that do not harbor mutations in the CBF genes

22

may rely on continuous CBF function. T cell acute lymphocytic leukemia (T-ALL) also appears to rely on sustained Runx1 activity. A small molecule targeting cyclin-dependent kinase 7 displayed activity in a subset of cancer cell lines, including T-ALL, and its mechanism of action appeared to involve the down regulation of Runx1 expression (147). Taken together, these findings strongly suggest that, despite the proposed tumor suppressor function of Runx1 in normal hematopoiesis, a continued low level of normal Runx1 function is required to maintain cell growth or viability in a certain subset of leukemia. We hypothesize that these leukemias may be more sensitive to perturbations in the RUNX proteins' functions, and therefore small molecules interfering with Runx1:CBFβ interaction may achieve therapeutic efficacy in a wide range of leukemia.

In summary, we established the RD:CBFβ interface as viable drug target. In a previous study, we carried out structure-based mutagenesis study at the Runt domain of Runx1 to determine the energetic contribution of the amino acids in the Runt domain that contact CBFβ for heterodimerization. We identified two energetic hot spots at the heterodimerization interface of the Runt domain that contribute to the bulk of binding energy for heterodimerization with CBFβ (148). Herein we describe the identification small molecule inhibitors by screening for a library of compounds against the hot spot residues at the Runt domain:CBFβ interface, and the development of a tool compound that binds to the Runt domain of RUNX proteins and inhibits their interaction with CBFβ.

Chapter I: Development and characterization of thiazole compounds targeting to disrupt the Runt Domain:CBFβ interaction

Zaw Min Oo[1], Anuradha Illendula[2], Charles Schmidt[2], Yunpeng Zhou[2], Chung-Tsai Lee[1], Roger A. Rajewski[3], Nancy A. Speck[1], and John H. Bushweller[2]

[1]Abramson Family Cancer Research Institute and Department of Cell and Molecular Biology, University of Pennsylvania, Philadelphia, Pennsylvania, USA, 19104

[2]Department of Molecular Physiology and Biological Physics, University of Virginia, Charlottesville, Virginia, USA, 22908

[3]Department of Pharmaceutical Chemistry, University of Kansas, Lawrence, Kansas, USA, 66047

Abstract

RUNX1 and *CBFB*, which encode subunits of the core binding factor, are frequent targets of chromosomal aberrations in hematological malignancies. We previously determined that CBFβ (encoded by *CBFB*) is important for the transforming activity of the chimeric protein AML1-ETO protein (RUNX1-RUNX1T1) generated by the t(8;21), and other studies showed that normal Runx1 functions are essential for survival and maintenance of some leukemias lacking *RUNX1* or *CBFB* mutations. Thus, we hypothesized that we could achieve therapeutic efficacy in multiple leukemias by targeting the Runx1:CBFβ interaction with small molecule inhibitors. Using the structural information of the DNA binding Runt domain (RD) of Runx1 and its interface with CBFβ, we employed a computational screen for a library of 78,000 drug-like compounds, and further optimized our lead compounds. The Runt domain inhibitors (RDIs) bind directly to the RD and disrupt its interaction with CBFβ compounds reduced growth and induced apoptosis of t(8;21) acute myeloid leukemia (AML) cell lines, and reduced the progenitor activity of mouse and human leukemia cells harboring the t(8;21), but not normal bone marrow cells. The RDIs had similar effects on murine and human T cell acute lymphocytic leukemia (T-ALL) cell lines that did not harbor the t(8;21). Our results confirmed that the RDIs might prove efficacious in various AMLs, and that a therapeutic window is available to specifically target malignant cells.

Introduction

Acute myeloid leukemia (AML) often harbors non-random clonal chromosomal aberrations. Among them, the 8;21 translocation t(8;21)(q22;q22) is one of the most common in *de novo* AML, occurring in 10% of adult and 12% of pediatric AMLs (96, 106, 107). The translocation fuses the N-terminal 177 amino acids of Runx1 (also known as AML1, encoded by *RUNX1*) to ETO (eight twenty-one, encoded by *RUNX1T1*), generating the chimeric protein AML1-ETO, an essential causative factor of t(8;21)-positive AML (107). Runx1 is a sequence-specific DNA binding transcription factor and member of heterodimeric core binding factors (CBFs) that play important roles in hematopoiesis (106, 107). Loss of Runx1 during embryonic development results in a failure of hematopoietic stem cell (HSC) emergence, whereas loss in adult HSCs leads to a pre-leukemic state (79, 94, 96, 97, 99, 100). ETO, on the other hand, has no known role in normal hematopoiesis. Homozygous loss of *Runx1t1* in mice resulted in gastrointestinal defects, but no hematopoietic deficiencies (113, 114).

Clinically, t(8;21)-positive leukemia is associated with favorable prognosis, with 70% of patients achieving complete remission following standard therapy (126, 127). However, many patients retain AML1-ETO expressing cells in their bone marrow due to incomplete eradication of the leukemic cells (128, 129). As a result 35-40% of these patients relapse within five years and have poor long-term survival (126, 127). We hypothesize that direct therapeutic targeting of the chimeric protein AML1-ETO may reduce the rate of relapse and improve long-term survival.

AML1-ETO has five domains conserved with its *Drosophila* homologues: the Runt domain (RD) from Runx1, and four from ETO (eTAFH, HHR, Nervy, MYND) (107). We and others solved the structures of all five domains and their interacting partners,

and introduced amino acid substitutions to assess their contribution to AML1-ETO's transforming ability (62, 115-118, 120, 132, 134, 149-151). We determined that the interaction between the Runt domain of AML1-ETO and CBFβ, the non-DNA binding partner of all three RUNX proteins, is important for AML1-ETO mediated leukemogenesis (132). We introduced a single amino acid substitution into the Runt domain that disrupted DNA, but not CBFβ binding (R174Q), and a pair of mutations that impaired CBFβ but not DNA binding (Y113A/T161A). Both sets of mutations severely impaired AML1-ETO's ability to transform hematopoietic cells. Most importantly, both DNA and CBFβ binding were essential for AML1-ETO's ability to cooperate with the activated kinase TEL-PDGFβR to promote leukemia in mice. Collectively these data demonstrated that both DNA and CBFβ binding are critical for AML1-ETO's activity, and validated the AML1-ETO:CBFβ interaction as a viable drug target.

In addition, we determined that the interaction of CBFβ with the Runt domain is essential for the ability of TEL-AML1 (ETV6-RUNX1), frequently found in B-ALL, to promote the serial replating of B cell progenitors in vitro (132). This suggests that CBFβ may be important for the activity of multiple chimeric Runx1 proteins.

Recent studies have provided additional evidence that normal CBF functions are required for the maintenance and survival of certain leukemia cells. Specifically, knock down of wild type Runx1 reduced growth and induced apoptosis in t(8;21) cell lines, and also in AML1-ETO transformed human CD34 positive cells (145, 146). Knock down of Runx1 also induced apoptosis of MLL-AF9 transformed cells, and deletion of Runx1 and CBFβ extended the disease latency in a mouse MLL-AF9 model (146), suggesting that a subset of AMLs that do not harbor mutations in the CBF genes may rely on continuous CBF function. T cell acute lymphocytic leukemia (T-ALL) also appears to rely on

sustained Runx1 activity. A small molecule targeting cyclin-dependent kinase 7 displayed activity on a subset of cancer cell lines, including T-ALL, and its mechanism of action appeared to involve the down regulation of Runx1 expression (147).

Taken together, these findings strongly suggest that normal CBF function is required for the maintenance of leukemic stem cell functions in a certain subset of leukemia. We hypothesize that these leukemias may be more susceptible to perturbations in normal CBF functions. Therefore, small molecules interfering with Runx1:CBFβ interaction may achieve therapeutic efficacy in a wide range of leukemia. We have established the RD:CBFβ interface as viable drug target and have developed small molecules interfering with the RD:CBFβ interaction.

Herein we describe the development of a tool compound that binds to the Runt domain of RUNX proteins and inhibits their interaction with CBFβ. We also developed a pro-drug version of this tool compound to improve solubility and thereby potential utility in vivo. These Runt domain inhibitors (RDIs) inhibit growth in culture as well as clonogenic potential of AML1-ETO and T-ALL leukemia cell lines. The tool compounds show clear effects on the expression of well-characterized RUNX1 target genes. Analysis of genome-wide changes in gene expression identified lipid and sterol biosynthesis and ribosome biogenesis pathways, which are RUNX regulated (152, 153), as significantly affected by inhibitor treatment.

Materials and Methods

Virtual screening

Details of the virtual screen are described in the Supplemental Methods. In brief, the computer program LUDI/InsightII (154) was applied for virtual screening of CAP (Chemicals Available for Purchase, 78,000 compounds) library to the CBFβ binding interface on the Runt domain structure. Compounds from CAP library were docked and ranked by the scoring function (Energy Estimate 1) implemented in the LUDI program (155). The 500 best-scored hits (compounds with the predicted binding affinity < 300 μM as evaluated by LUDI's empirical scoring function) were subjected to visual inspection of their potential interactions with the Runt domain. Compounds with diverse scaffolds and involved in at least two hydrogen bonds with the Runt domain were selected for experimental evaluation.

Fluorescence resonance energy transfer (FRET) assays

Cerulean-Runt domain and Venus-CBFβ were expressed, purified and used in FRET assays as described previously (50, 156). Cerulean-Runt domain and Venus-CBFβ proteins were used at a concentration of 100 nM for all assays.

Saturation transfer difference NMR

Saturation transfer difference (STD) NMR experiments (157, 158) were performed with 30 μM Cerulean-Runt domain or Venus-CBFβ, 800 μM AI-7-54 or AI-8-45, 10% D_2O, and 5% DMSO in 50 mM KP_i, 100 mM KCl, 10 mM K_2SO_4, 2 mM $MgSO_4$, pH 7.5 in a final volume of 200 μL. All STD experiments were performed using a 600 MHz Bruker

NMR spectrometer at 25°C with saturation times of 500, 750, 1000, 1500, and 2000 ms. Samples were irradiated at 0.4 ppm (protein) and 30 ppm (off-resonance control) and the difference spectra calculated using MestReNova*Chemical*

Chemical synthesis

Details of the chemical synthesis including relevant NMR and mass spec data are provided in Supplementary Information.

Pharmacokinetics

Detailed methods are provided in the Supplemental Methods.

Mice

All mouse procedures were approved by the University of Pennsylvania University Animals Resource Center (ULAR) and Institutional Animal Care and Use Committees (IACUC) of the University of Pennsylvania and the University of Kansas. C57BL/6 mice were used in all studies.

Human samples

Patient AML specimen pheresis and bone marrow mononuclear cells were obtained from the University of Pennsylvania Stem Cell and Xenograft Core, under the approval from the University of Pennsylvania Institutional Review Board (IRB).

Mouse and human cell lines

Kasumi-1 (ATCC), Jurkat E6-1 (ATCC), 8946 T-ALL, and 720 T-ALL cell lines were cultured in RPMI 1640 (Corning Cellgro) supplemented with 10% fetal bovine serum

(FBS) and 1% penicillin/streptomycin at 37°C under 5% CO_2. K562 (ATCC) cell line is cultured in Iscove's Modified Dulbecco's Medium (IMDM) supplemented with 10% FBS. 720 T-ALL cells were derived from a $Tcf12^{+/-}$ mouse expressing a $Tal1$ transgene under the control of the Lck promoter (159). 8946 T-ALL cells are derived from a murine T-ALL induced with a doxycycline-repressible human c-MYC transgene (160).

MTT Cell Proliferation Assay

Mouse and human leukemia cell lines (10^4 cells/200 µl) were plated in a 96-well flat-bottom plate and cultured with DMSO (vehicle), 1 µM Staurosporine, or RDIs (12.5, 25, 50, or 100 µM) for 24, 48, and 72 hours. After treatment, 10 µl of 5 mg/ml MTT solution (3-(4, 5-dimethylthiazolyl-2)-2, 5-diphenyltetrazolium bromide) (Sigma-Aldrich) was added to each well cultured at 37°C for 4 hours. The plate was centrifuged at 300 g for 5 minutes, the media removed, and 100 µl of DMSO (Sigma-Aldrich) was added to solubilize the resulting reagent formazan and incubated at room temperature for 10 minutes. The plate was then analyzed by measuring absorbance at 540 nm wavelength in a SpectraMax plate reader (Molecular Devices). Data are plotted as percentage of viable cells relative to DMSO.

CFU-C Assay

Frozen human AML samples, and mouse leukemic bone marrow cells were thawed and cultured in RPMI 1640 with 10% FBS for two hours. Live cells were washed and recovered, and subsequently plated in Human Methylcellulose Complete Media HSC003 (R&D Systems) in 5% CO_2 at 37°C for 14 days, or in Methocult GF M3434 (Stem Cell Technologies) and incubated in 5% CO_2 at 37°C for 7 days, for human and mouse cells, respectively. All classes of myeloid and/or erythroid colonies consisting of at least 40

31

cells were counted according to manufacturer's recommendations.

Western blotting

Murine leukemic cells treated with RDIs or DMSO were harvested and lysed with RIPA buffer (25mM Tris•HCl pH 7.6, 150mM NaCl, 1% NP-40, 1% sodium deoxycholate, 0.1% SDS). Total protein lysates were resolved on 4-12% SDS-PAGE gels, transferred to a nitrocellulose membrane (GE Life Sciences), and probed with primary antibodies. Proteins of interest were visualized by chemi-luminescence (Pierce). The following antibodies were used for immunoblotting: caspase-3 (Cell Signaling, #9662), p53 (Santa Cruz, DO-1; Leica, CM5), and actin (Santa Cruz, N21).

Flow cytometry

Cells were stained with fluorochrome-conjugated antibodies for 30 minutes at 4°C and washed with 2% FBS in PBS prior to analysis. Apoptosis analysis (Annexin V-APC; BD Biosciences) was performed according to the manufacturer's recommendations on a LSR II flow cytometer (BD Biosciences). The data were analyzed using FlowJo v.9.8 (TreeStar).

Gene expression analysis (quantitative real-time PCR and microarrays).

RNA for quantitative real-time PCR (qRT-PCR) was isolated with the RNeasy Kit (QIAGEN), and total RNA was reverse-transcribed using cDNA Reverse Transcription Kit (Applied Biosystems). The cDNA produced was used for quantitative real-time PCR using SYBR Green technology (Applied Biosystems). Primers are listed below:

	Sybr green primer set	
Gene	Forward	Reverse
Dhcr24	CAT CGT CCC ACA AGT ATG	CTC TAC GTC GTC CGT CA
Cdkn1a	TTC CGC ACA GGA GCA AAG T	CGG CGC AAC TGC TCA CT
Deptor	TTG TCG TCT CTG TCA ATG GCC TCA	TTG TCC TTG GGC TGT CA GAA TCA
Csf1r	ACC AAA TGG CCC AGC CTG TAT TTG	TGC TTG GCA GGT TAG CAT AGT CCT
Cebpa	TGA GAA AAA TGA AGG GTG CAG	CGG GAT CTC AGC TTC CTG T
Hprt	CTC CTC AGA CCG CTT TTT GC	TAA CCT GGT TCA TCA TCG CTA ATC

Gene expression analysis (microarrays)

RNA for microarray was isolated with the RNeasy Kit (QIAGEN). Total RNA quantity and integrity were verified using Bioanalyzer (Agilent Technologies), and amplified using Ambion WT Expression Kit (Applied Biosystems). Microarray experiments were performed on GeneChip Mouse Gene 2.0 ST Array (Affymetrix) at the University of Pennsylvania Molecular Profiling Facility, according to the manufacturer's instructions.

Affymetrix probe intensity (cel) files were analyzed using Partek Genomics Suite (v6.6, Partek, Inc., St. Louis, MO). The data was normalized using Robust Multichip Average Algorithm (RMA), and technical controls were excluded to leave 34,365 transcript IDs available for statistical analysis. A one-way ANOVA followed by 3 pairwise comparisons (t-tests) were performed across the samples, each yielding a p-value for each transcript ID. The p-values were further corrected using the Benjamini-Hochberg procedure for false discovery rate (FDR). Fold-change in expression level for each transcript ID was calculated for the 3 pairwise comparisons.

To identify genes that are differentially expressed following treatment, the data was filtered to retain transcript IDs that demonstrated a false discovery rate of 5% and have a mean fold change of at least 1.5, up or down in AI-7-54 vs AI-8-45 treated cells. 87 IDs (78 unique genes) met these cutoffs. Hierarchical clustering was performed using Pearson correlation and average linkage. The colors red and blue are used to indicate the log-2 intensity of each gene relative to the mean of AI-7-54 treatment.

Microarray experiments were performed according to the manufacturer's instructions using GeneChip Mouse Gene 2.0 ST Array (Affymetrix) at the University of Pennsylvania Molecular Profiling Facility. Detailed methods, including data analysis for the microarray are provided in the Supplemental Methods. Significantly perturbed KEGG pathways (161) were identified using the functional annotation tool available at DAVID (http://david.abcc.ncifcrf.gov/summary.jsp) (162).

Statistical analyses

Statistical analyses were performed using the Graph Pad Prism 6.0 software package.

Results

Virtual screening to identify lead compounds targeting the Runt domain

We conducted a virtual screen utilizing the computer program LUDI (154) to identify initial lead compounds that bind to the Runt domain at the CBFβ interface (62, 150) and inhibit CBFβ binding. We employed the LUDI/CAP (Chemicals Available for Purchase) library containing 78,000 commercially available drug-like compounds, i.e. compounds that meet Lipinski's Rule of Five (163), which states that drug-like compounds should have molecular weight lower than 500, lipophilicity (logP) lower than 5, less than five hydrogen bond donors, and less than ten hydrogen bond acceptors. These compounds were docked to the CBFβ binding surface on the Runt domain using LUDI and ranked by the scoring function implemented in the program (164) for theoretical binding efficacy estimation. Based on the LUDI results and a visual inspection of the predicted interactions with the protein for the 500 top scoring compounds, we selected 100 compounds with diverse molecular scaffolds for experimental screening.

Evaluation of compound efficacy using a fluorescence resonance energy transfer (FRET) assay

We used Cerulean-Runt domain and Venus-CBFβ fusion proteins at a 100 nM concentration for compound screening by fluorescence resonance energy transfer (FRET) (50, 156) (Figure 1). Compounds were screened at 200 μM in a competition experiment using the fluorescence emission ratio (emission intensity at 525 nm / emission intensity at 474 nm, FRET ratio) as a read-out. The dynamic range for the FRET assay was determined by adding a 20-fold excess of untagged CBFβ and the

associated change in the FRET ratio was defined as 100% inhibition. Five compounds showed 20% - 60% inhibition of the Runt domain - CBFβ interaction at 200 μM. Four of these compounds were discontinued due to toxicity, covalent binding to the protein, or promiscuous inhibition. The fifth compound, the aminotriazole AI-9-76 (Figure 2, Scheme 1) was identified as an initial hit. As the hydrazine moiety in AI-9-76 is a potential source of toxicity, we made O (oxadiazole2-thione) and S (thiadiazole2-thione) substitutions (Figure 2, Scheme 1). While the O substitution (AI-9-75) resulted in a loss of activity, the compound with an S substitution (AI-7-54) retained activity in the FRET assay.

Figure 1. Schematic diagram of FRET assay. From Matheny et al, 2007 (165).

A. Cerulean is excited at 433 nm and emission from Cerulean and Venus detected at 474 nm and 525 nm, respectively.

B. Fluorescence spectra of Cerulean-Runt domain and Venus-CBFß showing the FRET effect. The black curve is the spectrum of Cerulean-Runt domain + Venus-CBFß at a concentration ~4-fold below K_d. The red curve is the spectrum of Cerulean-Runt domain + Venus-CBFß at a concentration ~4-fold above the K_d.
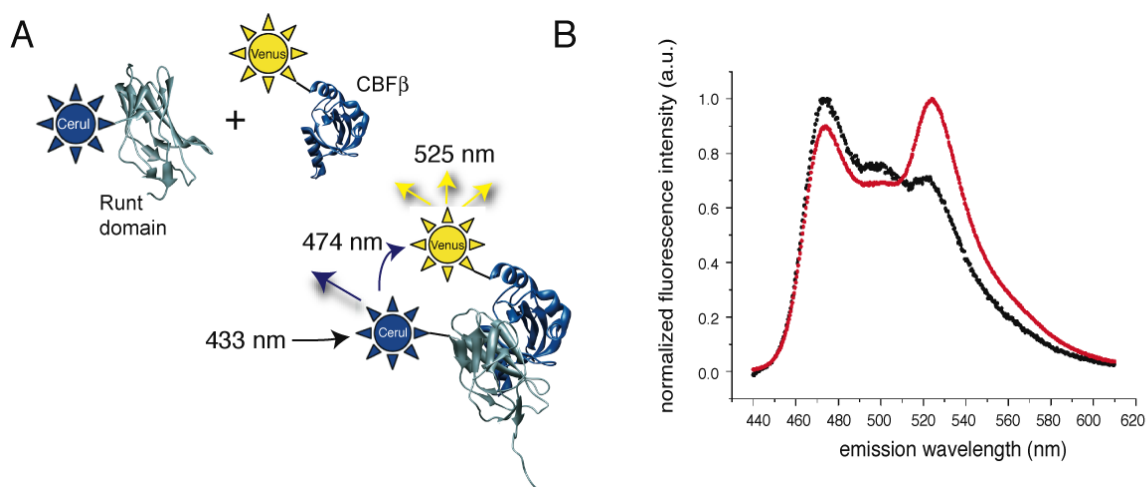
Figure 2. Library of analogs synthesized.

Schemes 1-5 illustrate the synthetic routes used for library generation and refer to sets of compounds described in the main text.

Scheme 1

AI-9-76 (1)   AI-9-75 (2)   AI-7-54 (3)

Scheme 2

4a. R = Thiophen-2-yl
4b. R = Phenyl
4c. R = 6-Methyl-2-pyridyl
4d. R = Pyrazin-2-yl

Scheme 3

5a. R = 2F
5b. R = 3F
5c. R = 3F
5d. R = 2-CH$_3$
5e. R = 2-OCH$_3$
5f. R = 2-CH$_3$; 4-F

Scheme 4

6a.   6b.   6c.

6d.   6e.   6f.

Scheme 5

7a. R = 2-CH$_3$
7b. R = 3-CH$_3$
7c. R = 3F
7d. R = 3-OCH$_3$
7e. R = 4-OCH$_3$
7f. R = 3-Cl **(AI-8-45)**
7g. R = 4-Cl
7h R = 2,3-di-Cl
7i. R = 3-Cl,-4-OCH$_3$
7j. R = 3-COOH
7k. R = 3-CF$_3$
7l. R = OCF$_3$
7m. R = 3-Cl, 4-(2-methoxyethoxy)**(AI-9-54)**
7n. R = 3-N,N-di-CH$_3$

37
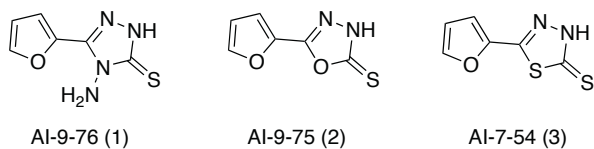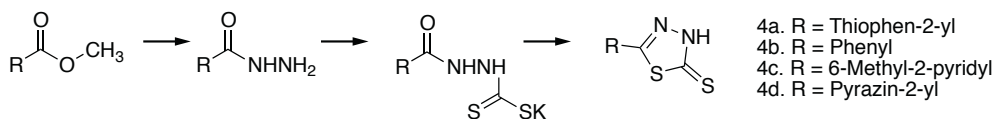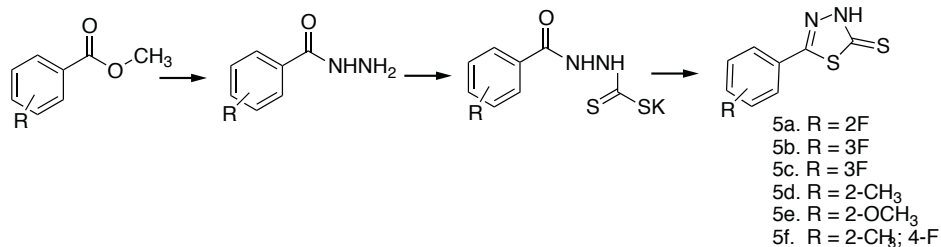
Verification of ligand binding to the Runt domain by Nuclear Magnetic Resonance (NMR) spectroscopy

The FRET assay detects inhibition of CBFβ – Runt domain binding by small molecules, but cannot determine to which protein the compound binds. In order to establish that the lead compound does indeed bind to the Runt domain, we employed Nuclear Magnetic Resonance (NMR) spectroscopy. Two-dimensional ^{15}N-^{1}H heteronuclear single quantum coherence (2D ^{15}N-^{1}H HSQC) spectra have been used very effectively to detect binding to proteins as well as to localize the site of binding. However, ^{15}N-^{1}H HSQC spectra of the Runt domain are very poor and missing almost half of the peaks due to exchange broadening (166), thus we were not able to detect any chemical shift changes upon addition of AI-7-54 (not shown). Spectra of the Runt domain bound to DNA are of good quality but the addition of our inhibitors resulted in precipitation. To overcome these obstacles, we utilized saturation transfer difference (STD) experiments (157, 158) that rely on the transfer of saturation from the protein to bound ligand to detect binding. To enhance the sensitivity of the experiment, we increased the size of the proteins by using Cer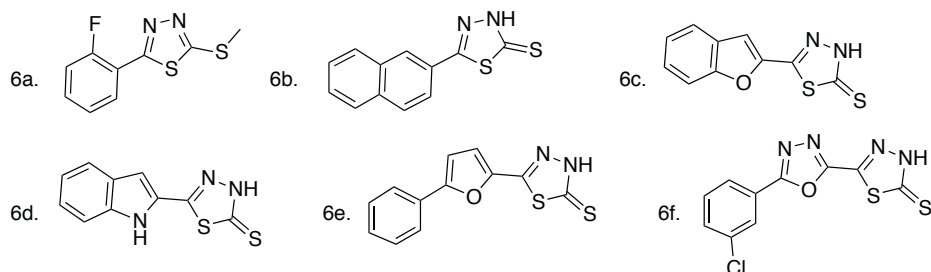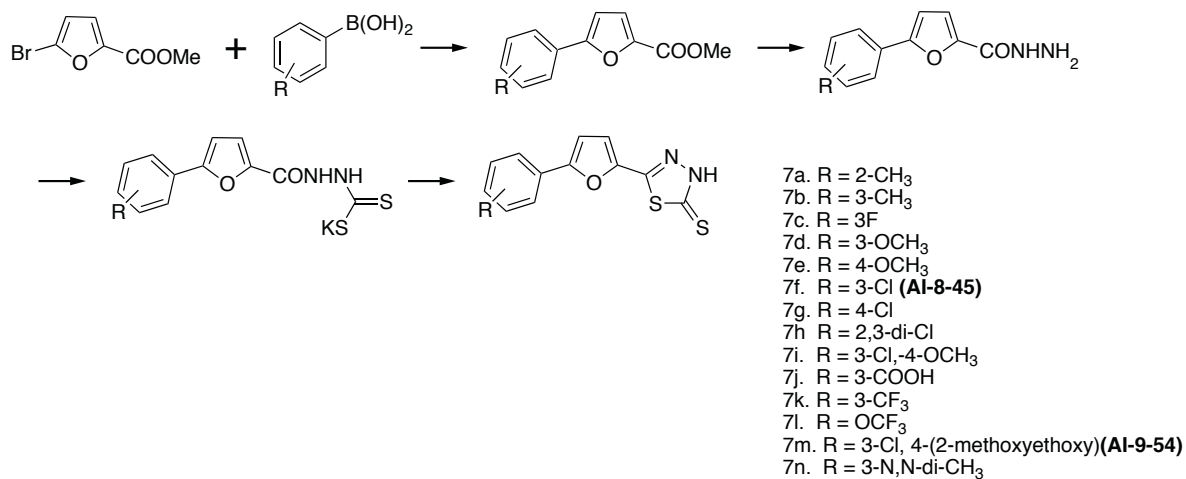ulean-RD and Venus-CBFβ, the same protein constructs that were used in the FRET assay. A saturation transfer effect was observed only for the AI-7-54 plus Cerulean-Runt domain mixture (Figure 3A), indicating that AI-7-54 binds to the Runt domain. Importantly, the absence of signals on the Venus-CBFβ STD spectrum confirms that AI-7-54 does not interact with either CBFβ or Venus (nor by analogy to Cerulean which has a very similar primary sequence). To confirm this, we collected high quality ^{15}N-^{1}H HSQC spectra for CBFβ in the presence of AI-7-54 and observed no chemical shift changes (not shown). Taken together, these results confirm that the Runt domain is the protein to which AI-7-54 binds.

Development of inhibitors with increased potency

The STD NMR and FRET data confirmed that the AI-7-54 scaffold is a valid initial lead. Indeed, the 1,3,4-thiadiazole heterocyclic ring system has been reported to have a wide range of pharmacological activities in the literature (167). To further develop this class of compounds, we performed a structure activity relationship (SAR) analysis, first by replacing the furan ring in AI-7-54 with thiophene, phenyl, 6-methyl-2-pyridyl, and pyrazine (Figure 2, Scheme 2). The phenyl substitution (**4b**, yielding 5-phenyl-1,3,4-thiadiazole-2(3*H*)-thione) improved the activity (IC_{50} = 11 ± 1.3 µM), whereas other substitutions yielded compounds that were inactive or weaker than AI-7-54. The addition of several substitutions into the phenyl ring based on the 4b scaffold did not improve activity (Figure 1, Scheme 3). Based on this initial round of synthesis, we further elaborated the molecule as shown in Figure 2, Scheme 4. Methylation of the thioamide in compound **5a** yielding 2-(2-fluorophenyl)-5-(methylthio)-1,3,4-thiadiazole (Figure 2, Scheme 4, **6a**) resulted in a complete loss of activity, clearly defining the importance of the thioamide moiety. We then introduced a series of substitutions for the phenyl ring (Figure 2, Scheme 4). Substitution with benzofuran (**6b**), and replacement of the furan ring with an oxadiazole (**6d**) resulted in a complete loss of activity. On the other hand, compound **6c** in which a benzene ring was added to the furan of AI-7-54 was active (IC_{50} = 13 ± 1.9 µM). We explored the SAR around compound **6c** by introducing a series of substitutions into the phenyl ring (Figure 2, Scheme 5). Introduction of a 3-Cl yielding the compound 5-(5-(3-chlorophenyl)furan-2-yl)-1,3,4-thiadiazole-2(3*H*)-thione (**AI-8-45**) (**7f**) improved the activity, however AI-8-45 has somewhat limited solubility. STD NMR analysis of AI-8-45 showed that protons in the furan ring as well as protons on the phenyl ring are in close contact with the protein (Figure 3B), consistent with the SAR. To improve the solubility we introduced 3-Cl pus 4-methoxyethyl ether yielding **AI-9-54** (**7k**)

that had similar activity as AI-8-45 in the FRET assay (Figure 3D). The SAR for this library of analogs was somewhat flat with no dramatic improvements in activity, so we selected two of the most active compounds (Table 1), AI-8-45 (IC_{50} = 2.0 ± 1.1 µM) and AI-9-54 (IC_{50} = 1.8 ± 0.6 µM) for use as tool compounds for biological studies. We used the starting scaffold AI-7-54 that has a 12-fold higher IC_{50} (24 ± 7µM, Figure 3C) as a negative control.

Figure 3. NMR STD and FRET data for Runt domain inhibitors.

A.　　　Results of NMR saturation transfer (STD) analysis for AI-7-54. The structure of AI-7-54 is shown with a 1D ^{1}H NMR spectrum of the compound below. Arrows indicate resonance assignments. The middle spectrum shows 1D difference spectrum for Cerulean-Runt domain + AI-7-54. Bottom spectrum shows 1D difference spectrum for Venus-CBFβ, demonstrating a lack of binding.

B.　　　Results of STD analysis for AI-8-45, as in panel A.

C,D.　　Results of FRET analysis for the initial lead AI-7-54 (C) and optimized compounds AI-8-45 and AI-9-54 (D). Calculated IC_{50} values are shown.
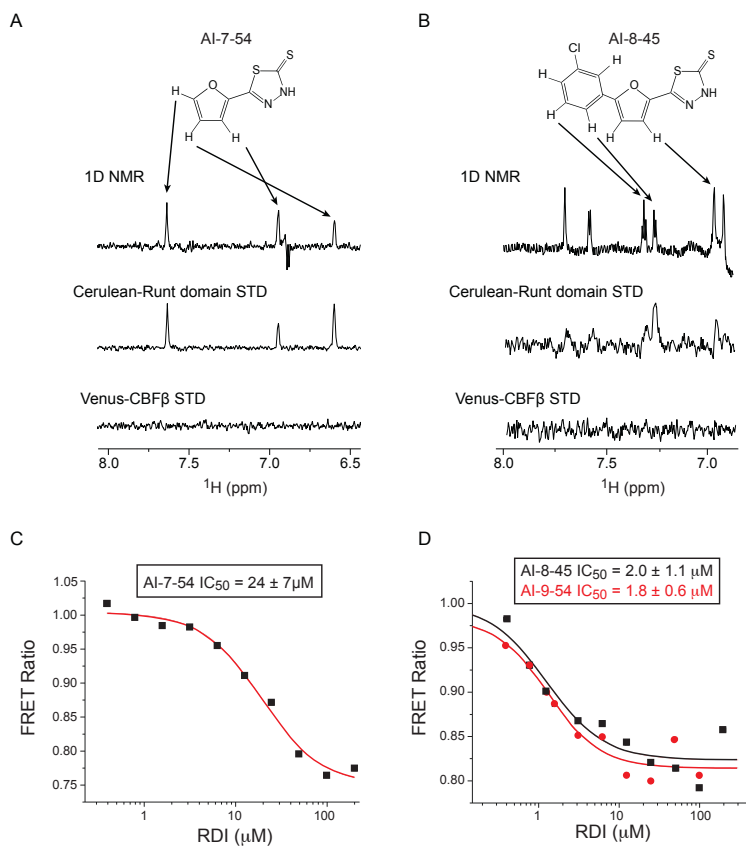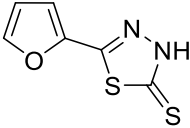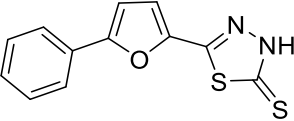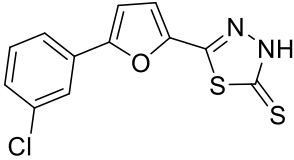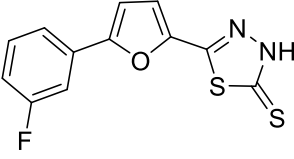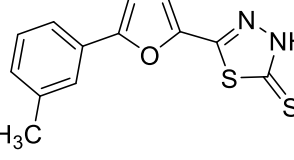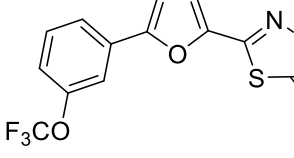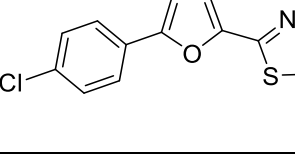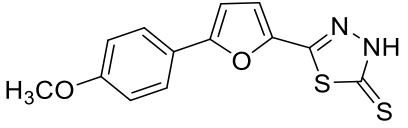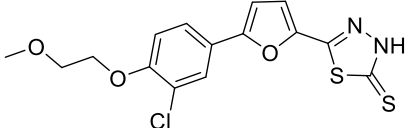
Table 1. Structures and FRET IC$_{50}$ values for selected inhibitors

The numbers in parentheses under compound number refer to the compounds as they appear in Figure 2.

Compound name	Compound Structure	FRET IC$_{50}$ (μM)
AI-7-54 (3)		24 ± 7
AI-8-153 (6e)		13 ± 1.9
AI-8-45 (7f)		2.0 ± 1.1
AI-9-13 (7c)		6.2 ± 0.5
AI-9-24 (7b)		3.7 ± 1.6
AI-9-27 (7l)		9.5 ± 1.4
AI-8-117 (7g)		3.0 ± 0.3

41

AI-9-23 **(7e)**		17 ± 3.9
AI-9-54 **(7m)**		1.8 ± 0.6

Development of pro-drug for improved solubility

To address the somewhat limited solubility of these compounds and facilitate their ability to be employed *in vivo*, we tested a pro-drug approach by masking different functional groups: alkylcarbonyloxymethyl for the thione functionality, and *N*-Mannich bases for thioamide (Figure 4A). The use of N-Mannich base of a thioamide as a pro-drug was demonstrated previously to improve the solubility as well as enhance oral bioavailability (168) . We synthesized two classes of compounds and evaluated them for aqueous solubility. We found that the N-Mannich base compound AI-9-59 had greater solubility than the alkylcarbonyloxymethyl (243 µM versus 1 µM). AI-9-59 also showed improved solubility over the lead compound AI-8-45. The pro-drug undergoes a non-enzymatic cleavage at both acidic and basic pH, releasing the amine, amide, and formaldehyde. Consistent with previous studies, pharmacokinetics analysis after administration of AI-9-54 and the pro-drug AI-9-59 showed that the pro-drug reached a higher concentration and had an enhanced lifetime in plasma (Figure 4).

Figure 4. Pharmacokinetics data for AI-9-54 and the AI-9-59 prodrug in mice.

A.   Structure of AI-9-54 and the prodrug AI-9-59.

B.   Plasma concentration data as a function of time.

C.   Chart showing pharmacokinetic parameters calculated from fit of the data in B.

	AI-9-54	AI-9-59
Half life (min)	64.0	178.6
AUC (0-inf) (μmol.min/L)	17.0	8.4
Mean Residence Time (min)	57.2	74.6
Volume of Distribution (mL)	28.3	193.9
Clearance (mL/min)	0.31	0.8
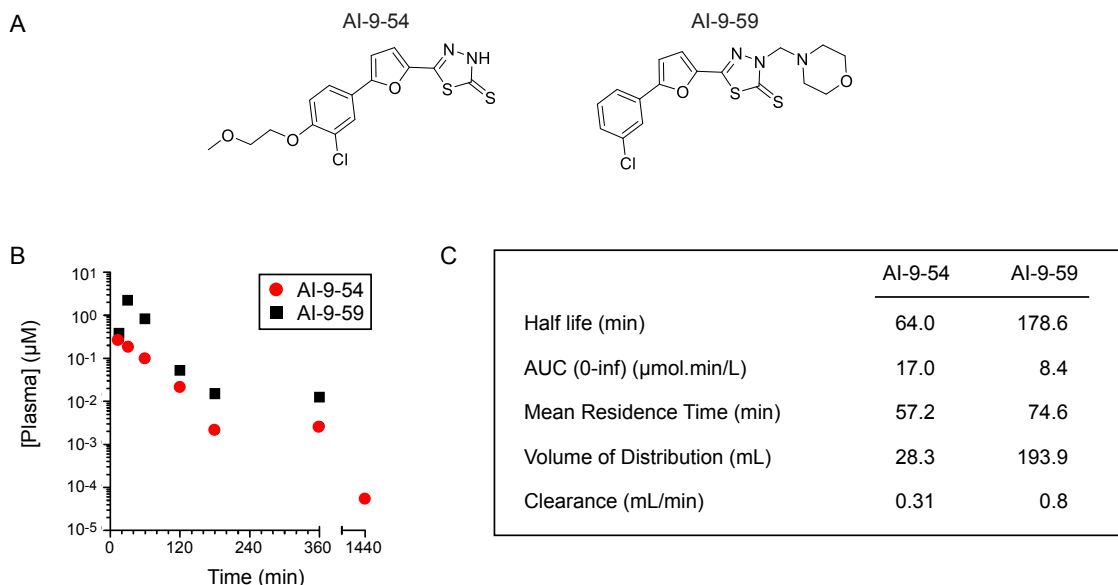
Runt domain inhibitors (RDIs) induce growth arrest

Recent studies showed that Runx1 is required for the maintenance of leukemia cells expressing AML1-ETO, MLL-AF9, and T-ALL cells (145-147). We used an MTT cell viability assay to determine whether the RDIs inhibited the growth of leukemia cells that are either positive or negative for AML1-ETO expression. The RDIs AI-8-45 and AI-9-45 significantly reduced the growth of Kasumi-1 cells, a human AML cell line that harbors t(8;21), after 48 hours in culture (Figure 5A). In contrast, AI-7-54, the structurally similar but weaker potency inhibitor had no effect on Kasumi-1 cells, indicating that the effects are due to specific targeting of the RD-CBFβ interaction. We also tested the efficacy of AI-8-45 and AI-9-54 in murine and human T-ALL cell lines including 720 (derived from a

43

Tcf12$^{+/-}$ mouse expressing a *Tal1* transgene under the control of the *Lck* promoter (159), Jurkat, and 8946 (murine T-ALL induced with doxycycline-repressible *MYC* transgene (160)). AI-8-45 significantly reduced the growth of all three T-ALL cell lines, and to an even greater extent of the 720 T-ALL line than of Kasumi-1 cells, indicating that the RDIs have activity in non-t(8;21) leukemia (Figure 5B-D). AI-9-54 reduced the growth of two of the three T-ALL cell lines (720 and 8946, but not Jurkat). In contrast, the growth of K562, a human CML cell line positive for BCR-ABL, was not inhibited by RDIs at 48 hours (Figure 5E).

We assessed whether the reduction in cell growth was accompanied by increased apoptosis. After 48 hours in culture, Kasumi-1 cells treated with AI-8-45 and AI-9-54, but not the less active compound AI-7-54, showed a statistically significant and dose-dependent increase in the percentage of DAPI-positive dead cells (Figure 5F). This was accompanied by an increase in the level of cleaved caspase-3 (Figure 5G). Taken together, these results showed that RDIs cause growth arrest, leading to caspase-3 mediated apoptosis in leukemia cells *in vitro*.

Figure 5. Runt inhibitors reduce cell growth and induce apoptosis in leukemia cells.

A-E.   RDIs AI-8-45 (8-45) and AI-9-54 (9-54) inhibit proliferation of the AML cell line Kasumi-1 and the T-ALL lines 720, Jurkat (8-45 only), and 8946, but not K562 as detected by MTT cell viability assay. AI-7-54 (7-54) is the negative control, and staurosporine (Stauro) is a positive control. Data represent mean values for triplicates ± standard deviation (SD) (two independent experiments). *P* values were calculated by one-way ANOVA (staurosporine-treated cells were not included in the ANOVA analysis). Dunnett's Multiple Comparison test was performed using DMSO treated cells as the comparator (#); horizontal lines above columns indicate significant differences from DMSO treated cells (*P* ≤ 0.05).

F.   RDIs reduce the percentage of live (DAPI negative) Kasumi-1 cells as measured by flow cytometry. Data represents mean values of two independent experiments; statistical analysis as in A-E.

G.   RDI treatment results in increased caspase-3 cleavage in 720 T-ALL cells (48 hrs).
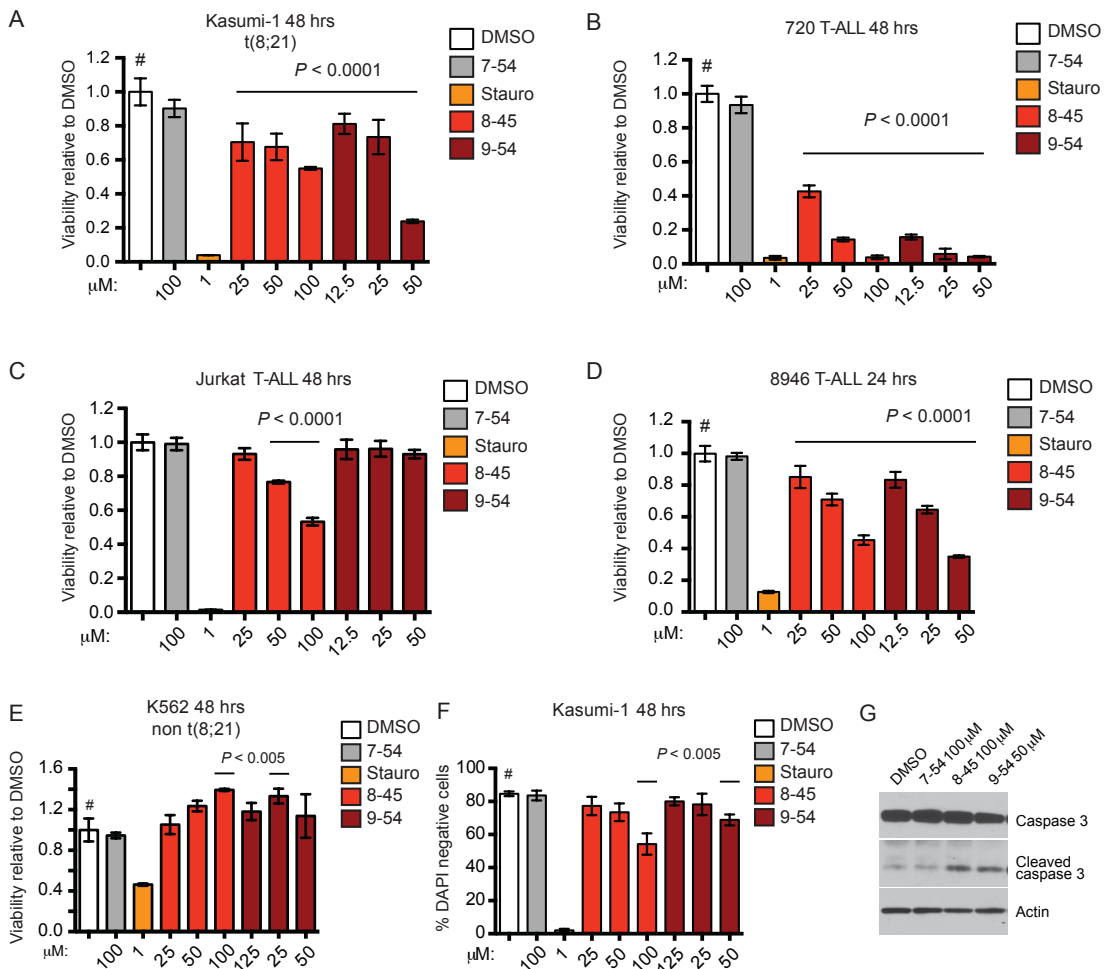
In vivo FACS/FRET assay in 293T cells

We adapted an *in vivo* fluorescence activated cell sorting (FACS) /FRET assay to assess whether our inhibitors could both enter cells and inhibit their target. HEK293 cells were transfected with Cerulean-Runt domain (C-RD) and Venus-CBFβ (V-CBFβ) or Venus-CBFβ with two mutations (G61A/N104A) that reduce binding to the Runt domain by 500 fold (V-CBFβ$_{mut}$). The cells were cultured in the presence of RDIs or vehicle (0.2% DMSO vol/vol) for 6 hours, and cells that are expressing both Cerulean and Venus were further analyzed for FRET signal. We determined that both of our lead compounds AI-8-45 and AI-9-54 exhibited auto-fluorescence that interfered strongly with the Cerulean signal (Figure 6). To bypass the interference from auto-fluorescence, we adjusted our gating strategy to include cells that are expressing high level of both Cerulean and Venus (Figure 6). Analysis of the mean fluorescence intensity of the FRET signal revealed that both AI-8-45 and AI-9-54, but not weakly active compound AI-7-54, significantly reduced FRET activity, nearly to the level of Venus-CBFβ$_{mut}$ that has 500-fold reduction in its ability to interact with the Runt domain (Figure 7). The data demonstrates that the RDIs severely disrupt CBFβ-Runt interaction.

Figure 6. FACS/FRET analysis strategy for assessing the efficacy the Runt domain inhibitors.

HEK293 cells were transfected with Cerulean-Runt alone (C-RD), Venus-CBFβ alone (V-CBFβ), or both Cerulean-Runt and Venus-CBFβ (C-RD + V-CBFβ). The cells were cultured in the presence of RDIs or vehicle (0.2% DMSO vol/vol) for 6 hours, and FRET activity analyzed by flow cytometry. The presence of Runt domain inhibitors (RDIs) induced auto-fluorescence that caused the population to up-shift in the Cerulean signal from its original position (denoted by solid and dotted boxes, respectively). To avoid the interference from auto-fluorescence, only cells that are expressing high level of both Cerulean and Venus were gated (denoted with the oval) and analyzed for mean fluorescence intensity of the FRET signal.
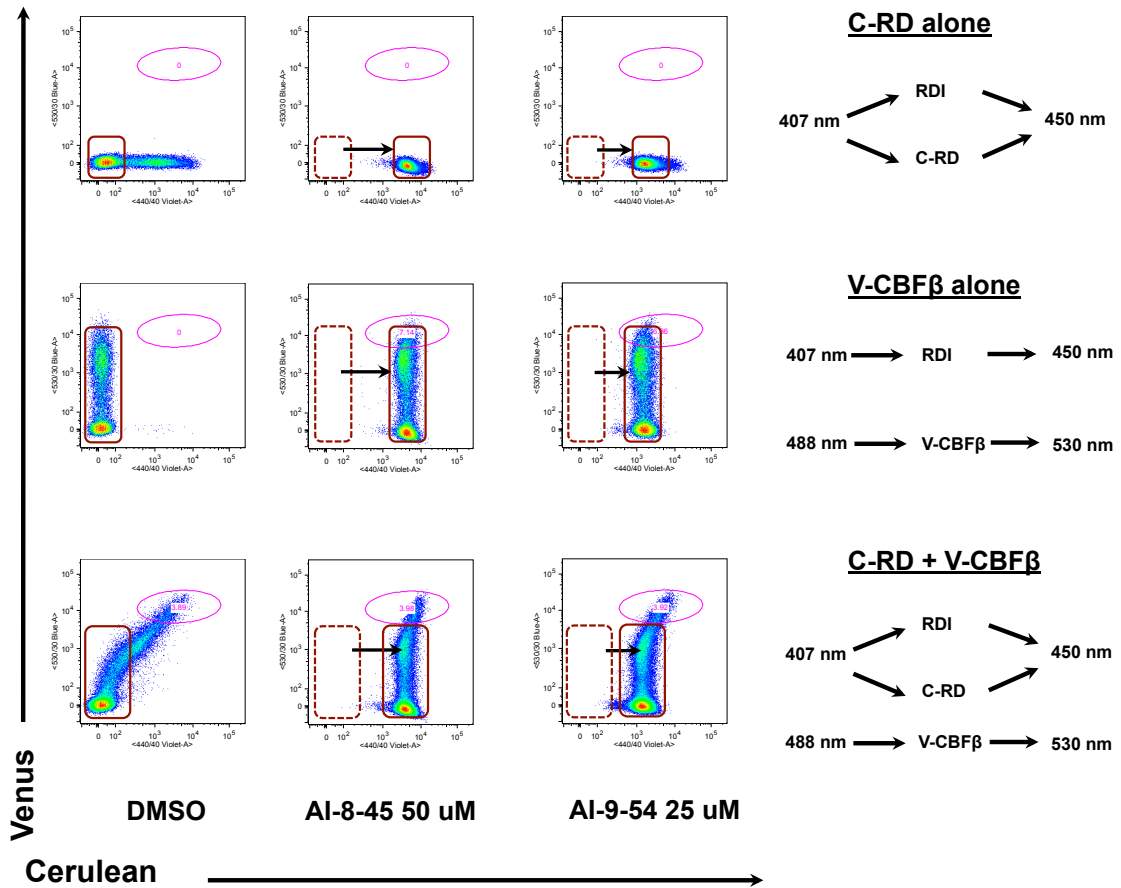
Figure 7. FACS/FRET analysis of the Runt domain inhibitors.

HEK293 cells were transfected with Cerulean-Runt domain (C-RD) and Venus-CBFβ (V-CBFβ) or Venus-CBFβ with two mutations (G61A/N104A) that reduce binding to the Runt domain by 500-fold (V-CBFβ$_{mut}$). The cells were cultured in the presence of RDIs or vehicle (0.2% DMSO vol/vol) for 6 hours, and cells that are expressing both Cerulean and Venus were further analyzed for FRET signal. Data represents mean fluorescence intensity of the FRET signal values for duplicates ± SD, n= three experiments. Significance was determined by one-way ANOVA, and Dunnett's Multiple Comparison test was performed using DMSO treated cells as the comparator; asterisks above columns indicate significant differences from DMSO treated cells ($P < 0.001$).
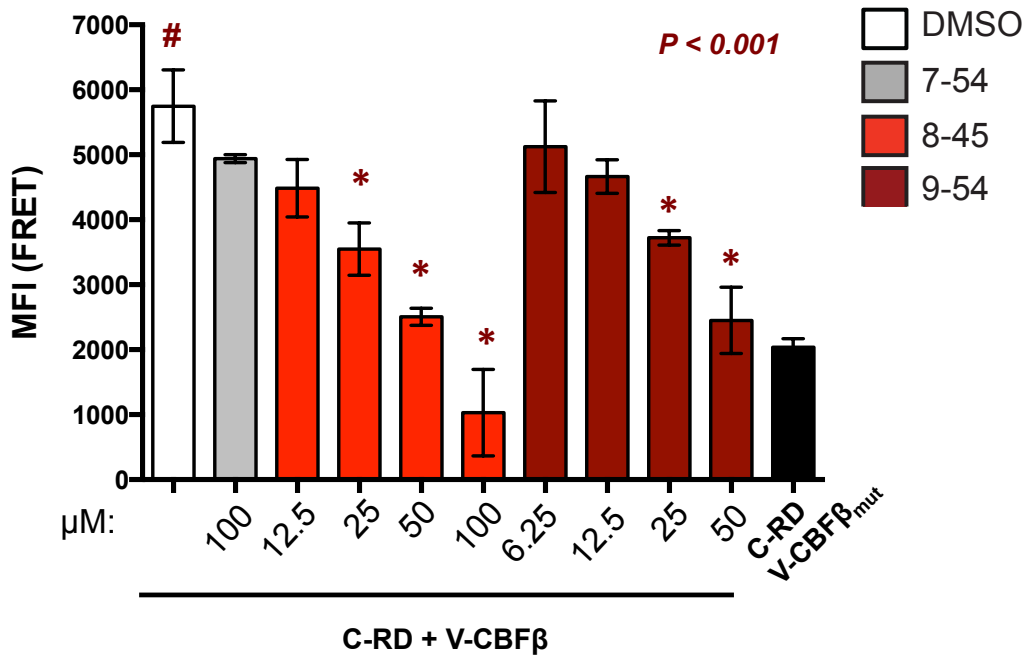
Runt domain inhibitor (RDI) effect on clonogenic potential

We assessed the activity of RD:CBFβ inhibitors on the clonogenic potential of murine AML cells. The AML cells were isolated from a secondary recipient of spleen cells transplanted from a primary recipient that had received fetal liver cells transduced with retroviruses expressing AML1-ETO9a and NRas^{G12D} (169). AML1-ETO9a is a shortened form of AML1-ETO lacking the C-terminal MYND domain, and is more potent at inducing leukemia than full length AML1-ETO (142). The active compounds AI-8-45 and AI-9-54, but not the control compound AI-7-54 significantly reduced colony formation of the AML1-ETO9a + NRas^{G12D} AML cells (Figure 8A). Neither AI-8-45 nor AI-9-54 had any effect on colony formation by normal mouse bone marrow cells (Figure 8A). These data demonstrate that the RDIs reduce the clonogenic potential of AMLs transformed with the AML1-ETO fusion protein, but do not affect normal bone marrow progenitors at the same concentrations, indicating that a therapeutic window is available.

We also determined the effect of RDIs on the clonogenic potential of primary human t(8;21) AML. AI-8-45 and AI-9-54 significantly reduced the colony numbers of five t(8;21) positive human AML samples, but not that of normal bone marrow mononuclear cells (BM-MNCs) (Figure 8B). The control compound AI-7-54 had no effect on colony numbers in either the primary AML samples or normal bone marrow cells. We also examined the effect of AI-8-45 and AI-9-54 on colony formation by AML cells that do not harbor the t(8;21). The RDIs reduced the progenitor activity of some but not all human AML cell samples, indicating that they may have efficacy in a subset of AML not associated with Runx1 mutations (Figure 8C).

Figure 8. Effect of Runt inhibitors on colony formation by normal and leukemic mouse bone marrow cells, and in human AML samples.

A.   Various concentrations of compound were added to methylcellulose cultures containing 20,000 wild type bone marrow cells or 20,000 leukemic mouse cells transformed with AE9a and NRas^{G12D}. All compounds were dissolved in DMSO (final concentration 0.2%). Colonies were counted 7 days after plating. Shown is a representative experiment (n=3 per compound concentration, two experiments). Error bars represent SD. Significance relative to DMSO was determined by one-way ANOVA and Dunnett's multiple-comparison test as in Figure 5.

B-C.   Various concentrations of compound were added to methylcellulose cultures containing bone marrow mononuclear cells (MNC) or primary AML samples. Colonies were counted 14 days after plating. Shown is a representative experiment (n=3 per compound concentration, two experiments). Significance relative to DMSO treatment was determined by one-way ANOVA and Dunnett's multiple-comparison test as in Figure 5.

51
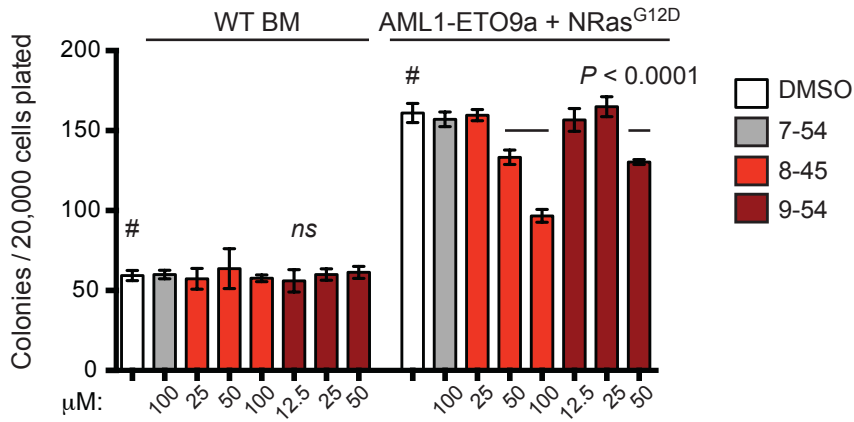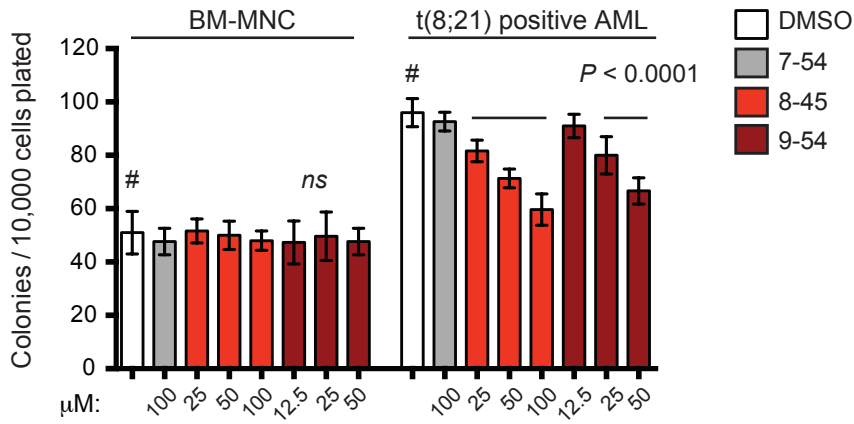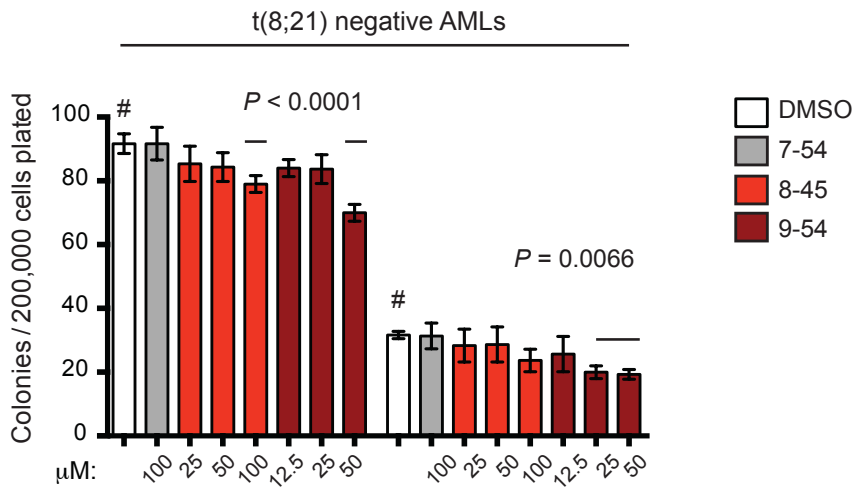
Molecular pathways affected by Runt domain inhibitors (RDIs)

To gain a better understanding of the mechanism of action of the RDIs we performed global gene expression analysis of the highly responsive 720 T-ALL cells following treatment. 720 T-ALL cells were treated with RDIs and harvested 8 hours later, before they underwent apoptosis, and expression was analyzed using microarrays. Overall, we detected only modest changes in expression levels after short-term inhibitor treatment (Figure 9A and Table 2). Pathway analysis revealed that genes involved in lipid and sterol biosynthesis, and in ribosome biogenesis to be among the most significantly down-regulated (Figure 9B). Both of these processes are regulated by RUNX proteins, and therefore are likely to reflect on-target effects (101, 152, 170). We confirmed the microarray data for several genes, including *Deptor*, which encodes an mTOR inhibitor; *Cdkn1a*, encoding the cell cycle inhibitor p21; *Dhcr24* (encoding for 24-dehydrocholesterol reductase); as well as known Runx1 targets, *Cebpa* and *Csf1r* (encoding a transcription factor and cytokine receptor, respectively) (171, 172) by qPCR. The expression of all five genes was affected by treatment with AI-8-45 and AI-9-45, but not by the control compound AI-7-54 (Figure 9C,D), validating the microarray data for these genes.

Figure 9. Microarray analysis of gene expression changes induced by RDIs.

A. Hierarchical clustering of 87 transcript IDs (78 genes) differentially expressed (False Discovery Rate 5%) among 720 T-ALL cells treated for 8 hrs with AI-7-54 (100 μM), AI-8-45 (100 μM), or AI-9-54 (50 μM). Red represents genes up-regulated relative to mean expression level in AI-7-54 treated cells; blue represents genes down-regulated relative to mean expression level in AI-7-54 treated cells.

B. KEGG pathways down-regulated following RDI treatment from functional annotation clustering.

C. Relative expression of genes in 720 T-ALL cells treated with RDIs for 8 hours, measured by qPCR. Data represents mean values for triplicates ± SD, n= two experiments. Significance relative to DMSO treatment was determined by one-way ANOVA. Dunnett's Multiple Comparison test was performed using DMSO treated cells as the comparator (#); horizontal lines above columns indicate significant differences from DMSO treated cells ($P \leq 0.05$).

D. Relative expression of Runx1-regulated differentiation genes, as in panel C.

53
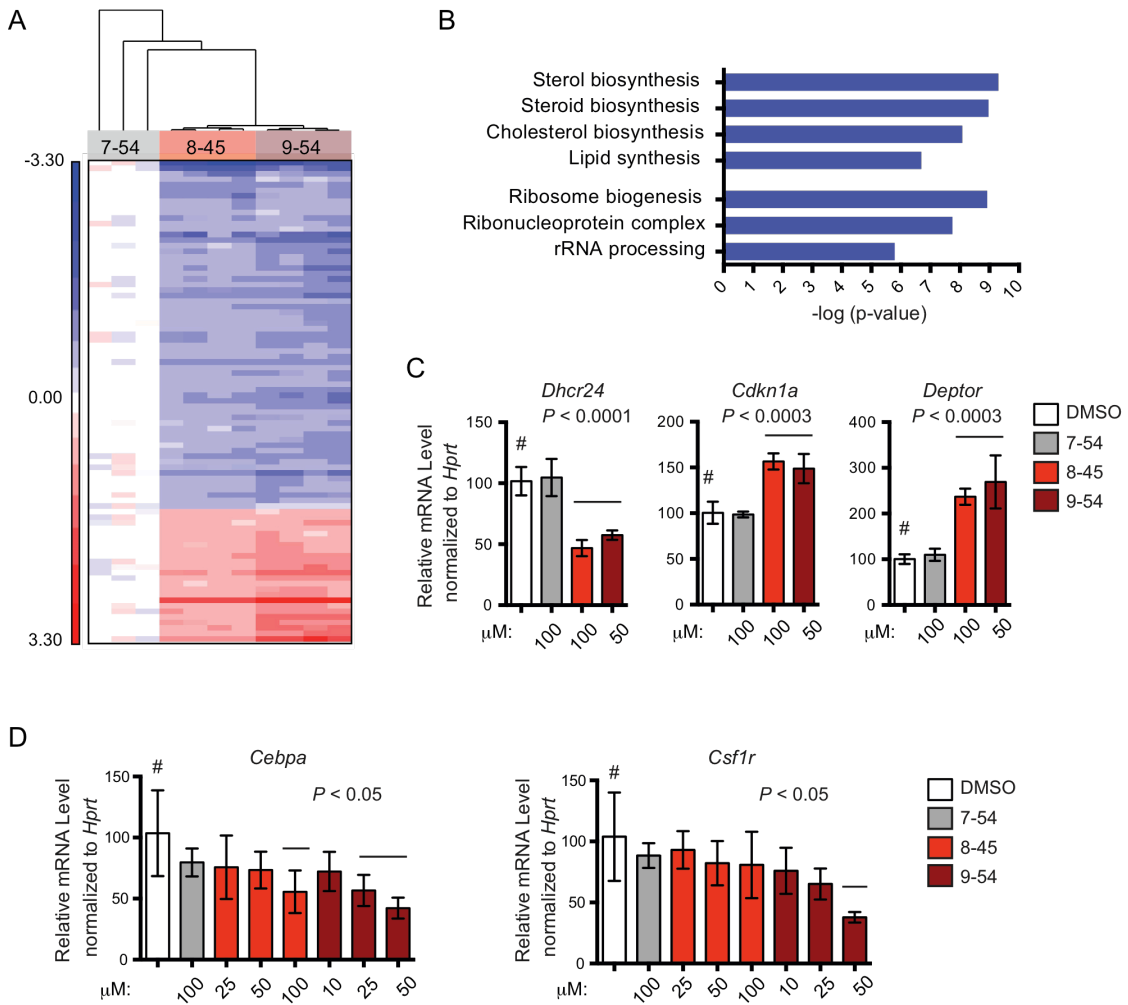
Table 2. A list of 87 unique transcript IDs that are differentially expressed as shown in Figure 9A.

Transcript ID	Gene Symbol	FDR corrected p-value (one-way ANOVA)	Fold-Change in Expression (8-45 vs. 7-54)	Fold-Change in Expression (9-54 vs. 7-54)
17324745	**Bex6**	0.00158259	-7.33049	-4.59099
17344126	**Hspa1b**	0.00208463	-3.85817	-2.78074
17257593		0.0140458	-2.48142	-2.89427
17365098	**Scd1**	0.0114199	-2.19999	-1.83458
17311807	**Sqle**	0.000316021	-2.09513	-2.44847
17445308	**Cyp51**	0.00141668	-2.04547	-1.87648
17234552	**Lss**	0.0026575	-2.00389	-1.81637
17509629	**Sc4mol**	0.000572807	-2.00125	-2.08763
17349549	**Mir1949**	0.000114828	-1.98977	-2.94092
17280836	**Gm889**	0.00470562	-1.94203	-2.03616
17307623	**Blk**	0.00305562	-1.92455	-2.5523
17307588	**Fdft1**	0.00148624	-1.91859	-1.97777
17406921		0.00213029	-1.88603	-1.68628
17344122		0.0020357	-1.87296	-2.29642
17456772	**Fam40b**	0.0169496	-1.84721	-1.80436
17344120	**Snord52**	0.00120916	-1.81659	-2.23537
17548102	**Cycs**	0.00208463	-1.80698	-2.05337
17548541	**Cycs**	0.00208463	-1.80698	-2.05337
17429632	**Mfsd2a**	0.00292244	-1.79145	-2.03065
17515315	**Ldlr**	0.00214274	-1.78586	-2.01483
17239755		0.00378979	-1.78358	-2.32985
17379871	**1500012F01 Rik**	0.00952348	-1.78219	-2.19481
17347448	**Cyp1b1**	0.000851483	-1.74606	-1.67507
17550454		0.00104124	-1.7441	-2.40136
17406908	**Fdps**	0.00281772	-1.71251	-1.61226
17416325	**Dhcr24**	0.000460707	-1.69904	-1.84433
17290173	**Hmgcs1**	0.0194626	-1.66754	-1.61855
17218653	**Gas5**	0.00284469	-1.6535	-1.71731
17291854	**Rpp40**	0.00159662	-1.6511	-1.81983
17523158	**Ccr8**	0.0105598	-1.64633	-1.74329
17535434	**Nsdhl**	0.0210565	-1.62866	-1.8
17440812	**Ung**	0.00141668	-1.62221	-1.89276

17222800	**Slc39a10**	0.00548836	-1.61642	-1.91869
17295233	**Hmgcr**	0.00037293	-1.61557	-1.65871
17285056	**Idi1**	0.000316021	-1.61548	-1.83259
17229466	**Hsd17b7**	0.00180875	-1.6134	-1.77216
17223863	**Idh1**	0.00654201	-1.60528	-1.55718
17435584	**Insig1**	0.00596369	-1.60416	-1.39698
17364725	**Rrp12**	0.00367186	-1.59873	-1.87371
17421694	**Srm**	0.000354355	-1.5965	-1.96059
17305980	**Ccnb1ip1**	0.000851483	-1.59228	-1.75214
17518314		0.00216582	-1.58966	-2.02006
17362050	**Rps6ka4**	0.0095345	-1.57325	-1.47591
17345696	**Bysl**	0.00423671	-1.57092	-1.67243
17550390		0.00225426	-1.57007	-1.67173
17353358	**Stard4**	0.0122649	-1.56525	-1.47024
17344132	**Hspa1a**	0.0493048	-1.56121	-1.32975
17442719	**Aacs**	0.00082026	-1.5585	-1.67379
17301247	**Pinx1**	0.0023485	-1.55258	-1.71709
17472903	**Pthlh**	0.000851483	-1.5512	-2.04757
17376096	**Polr1b**	0.00195718	-1.54927	-1.76023
17490599	**Rps11**	0.00931748	-1.54753	-1.78074
17480636	**Lipt2**	0.000759223	-1.54596	-1.58125
17279190	**Trmt61a**	0.0095652	-1.54222	-1.70026
17437072	**Lyar**	0.000460707	-1.53944	-1.68586
17319405	**Snord43**	0.0010542	-1.51936	-1.87934
17394063	**Ada**	0.0050235	-1.51748	-1.75846
17276520	**Mthfd1**	0.000446191	-1.51489	-1.89582
17263673	**Shmt1**	0.000851483	-1.51387	-1.8391
17435978	**Cad**	0.00011807	-1.51309	-1.71437
17530669	**Acy1**	0.00732517	-1.50854	-1.61375
17463108	**Nop2**	0.000468005	-1.50599	-1.67526
17408483	**Ptgfrn**	0.0014939	-1.50166	-1.93036
17526929	**1110032A03 Rik**	0.000721408	1.50259	1.65712
17285834	**Hist1h2bg**	0.0186052	1.51234	1.60026
17391521	**AI847159**	0.0107837	1.5188	1.56051
17241660	**Arid5b**	0.00796933	1.53632	1.77653
17307354	**Atp8a2**	0.0156396	1.54025	1.69427
17225413	**Col6a3**	0.000199369	1.54863	1.79992
17288876	**Arrdc3**	0.00017328	1.5539	2.7608
17289602	**Adamts6**	0.0392261	1.56898	1.5612

17408940	2010016I18R ik	0.00547947	1.56985	1.99763
17537118	P2ry10	0.00267586	1.57185	1.931
17295295	5330416C01 Rik	0.00547947	1.57232	2.09707
17288859	A830082K12 Rik	0.00109846	1.58813	1.93409
17303754	Gm20140	0.00715448	1.59205	1.61842
17294547	Nr2f1	0.000851483	1.63396	1.83083
17547877	Deptor	0.00277628	1.64108	1.88287
17335770	Abcg1	0.000603849	1.64666	1.53691
17478301	Nav2	0.00215804	1.65932	2.11262
17450461	Gbp4	0.00383816	1.7043	2.10835
17336052	Zfp563	0.000153365	1.72516	2.34173
17445525	Rundc3b	0.000108158	1.73525	2.49975
17405458	Gpr171	0.000169931	1.77936	2.57798
17550428		0.00102227	1.88884	2.75584
17434555	Abcb1b	0.000120667	2.14534	4.36667
17537936	Tceal1	8.87E-06	3.80708	6.02176

Discussion

Based on an initial hit from a virtual screening approach, we developed tool compounds that bind to the Runt domain and are low µM inhibitors of the CBFβ-Runt domain interaction. We also developed a pro-drug based on this structural scaffold that enhances the solubility of the inhibitor and should facilitate its use *in vivo*. Frye recently outlined the key properties of a high quality chemical probe (173), including a clear molecular profile of activity, mechanism of action, identity of active species, and proven utility. The RDIs meet all of these criteria. Furthermore, the inclusion of a weakly active control compound in all the biological evaluations provides high confidence that the observed activities derive from on-target activity rather than other activities of this class of molecules. As the Runt domain is highly conserved and CBFβ binds all three RUNX proteins, it is important to keep in mind that the effect of the RDIs likely reflects inhibition of CBFβ binding to all RUNX proteins in a particular cell type. Recently, it has been reported that the benzodiazepine Ro5-3335 is also an inhibitor of CBFβ-Runx (174), with *in vivo* activity consistent with predicted on-target effects. However direct binding of Ro5-3335 to RUNX or CBFβ was not well documented, thus the biochemical direct target of Ro5-3335 remains to be established.

Based on our finding that the Runt domain's interaction with CBFβ is critical for t(8;21) positive leukemia (132) as well as several recent reports that normal Runx1 function is required for the maintenance of some leukemias (145-147), we hypothesized that molecules targeting the RD:CBFβ interaction might achieve therapeutic efficacy against multiple leukemias. Indeed, we showed that the RDIs induced growth arrest and apoptosis not only in t(8;21) leukemia cells but also in a subset of non t(8;21) leukemia cells. Interestingly, the RDIs showed marked efficacy against the T-ALL cell lines that

57

overexpress *Tal1.* RUNX1 was shown to form an auto-regulatory loop with TAL1 and GATA3 in *TAL1* overexpressing T-ALL cells, and knocking down RUNX1 inhibited cell growth and induced apoptosis (175). In addition, RUNX1 was recently shown to be part of a complex that forms at a super enhancer created by somatic mutations in T-ALL (176). Thus RUNX1 appears to serve as a key member of an interconnected auto-regulatory loop involved in reinforcing and stabilizing the malignant cell state. In contrast, *BCR-ABL* positive K562 cells were minimally affected by the RDIs, as were multiple human primary AML cells.

RUNX proteins have now been implicated in numerous developmental pathways. Their role in leukemia is well established. In addition, there is emerging evidence for roles in various epithelial cancers. The tool compounds we have developed provide reagents to study the function of RUNX proteins in various settings. The advantage of such small molecule tools, unlike genetic approaches, is the rapid inhibition of the target, the ability to monitor time-dependent effects, and the opportunity to withdraw inhibitor and monitor the return to the previous state. Therefore, these compounds could be very useful reagents for studying the effects of core binding factor loss in specific processes or developmental stages. For all these reasons, the RDIs provide a unique tool for studying RUNX protein function.

Appendix:

Luciferase reporter assay

   We employed a previously characterized luciferase reporter system in which the firefly luciferase gene is driven by the enhancer element of T cell receptor beta chain (TBRβ). First, we showed Runx1 activated the luciferase reporter in a dose dependent manner, whereas the mutant Runx1 with reduced DNA binding had no effect on the luciferase activity (Figure 10A). We showed that treatment with the Runt domain inhibitor AI-8-45 inhibited the Runx1 dependent activation of target promoter transcription, while DMSO and inactive control AI-7-54 had no effect (Figure 10B). The luciferase activity was not affected by our other lead compound AI-9-54. These data demonstrate that the Runt domain inhibitor AI-8-45 reduced the RUNX1 dependent activation of target gene transcription.

Figure 10. Runt domain inhibitor reduced luciferase activity of Runx1 in transient co-transfection experiments.

A. P19 cells were transfected with the TCRβ-LUC as well as various concentrations of Runx1 or Runx1 R174Q, the mutant Runx1 with reduced DNA binding. The fold activation was calculated as the luciferase activity induced by Runx1 relative to the empty expression vector pcDNA3.1. Significance relative to DMSO treatment was determined by one-way ANOVA and Dunnett's multiple-comparison test.

B. Various concentrations of the Runt domain inhibitors, weakly active control AI-7-54 or DMSO were added to the TCRβ-LUC system as described in 9A. The fold activation was calculated as the luciferase activity induced by Runx1 relative to the empty expression vector pcDNA3.1. Significance relative to DMSO treatment was determined by one-way ANOVA and Dunnett's multiple-comparison test.
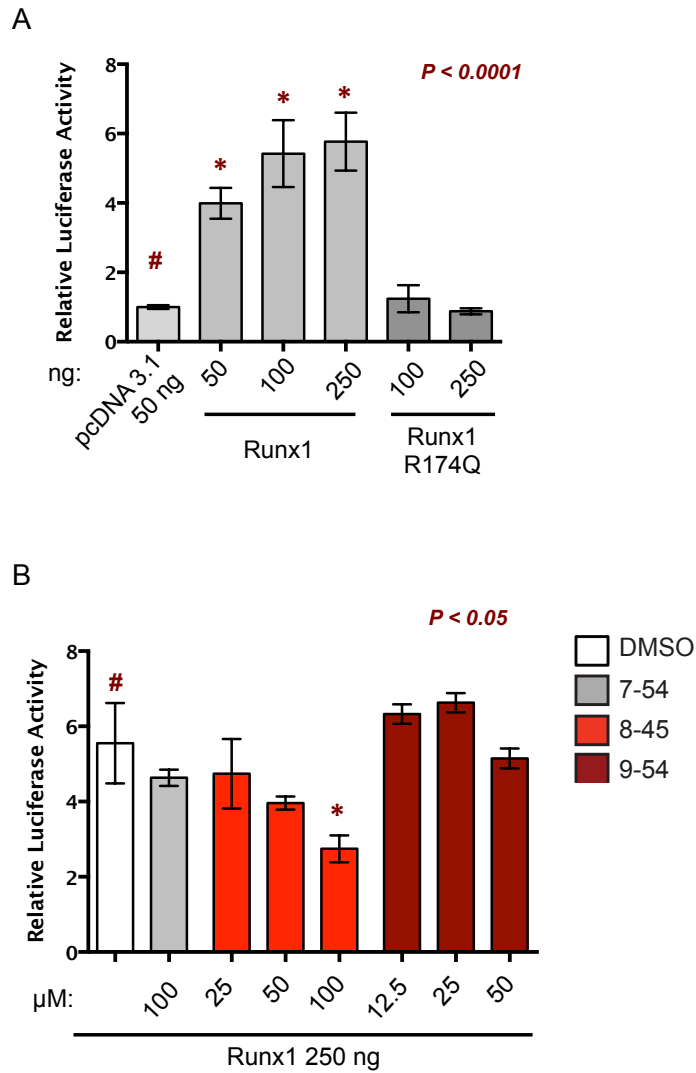
Co-immunoprecipitation of Runx1 and CBFβ

We conducted a co-immunoprecipitation experiment to assess whether our lead compounds could disrupt CBFβ's interaction with RUNX1. We transfected 720 T-ALL cells with FLAG-CBFβ or FLAG-CBFβ$_{G61A/N104A}$ that has 500-fold reduction in its ability to interact with the Runt domain, and conducted immunoprecipitation in the nuclear extract using antibodies against FLAG. By Western Blot, we were unable to detect any significant reduction in the relative level of RUNX1 that were bound to CBFβ in cells that are cultured in the presence of the Runt domain inhibitors compared to DMSO or weakly active control AI-7-54 (Figure 11). Therefore, we were unable to demonstrate that the Runt domain inhibitors reduced the level of RUNX1 bound to CBFβ.

Figure 11. Effect of the Runt domain inhibitors on CBFβ-RUNX1 binding at 16 hours in 720 T-ALL cells, measured by co-immunoprecipitation.

720 T-ALL cells were transfected with FLAG-CBFβ or FLAG-CBFβ$_{G61A/N104A}$ that has 500-fold reduction in its ability to interact with the Runt domain. GFP positive cells were sorted to purify successfully transduced cells. 5 x 10^7 ~ 1 x 10^8 cells were cultured in the presence of RDIs or DMSO (0.2% DMSO vol/vol) for 16 hours, and proteins from the nuclear fraction harvested for immunoprecipitation using antibodies against FLAG. Proteins of interest were visualized by Western Blot.
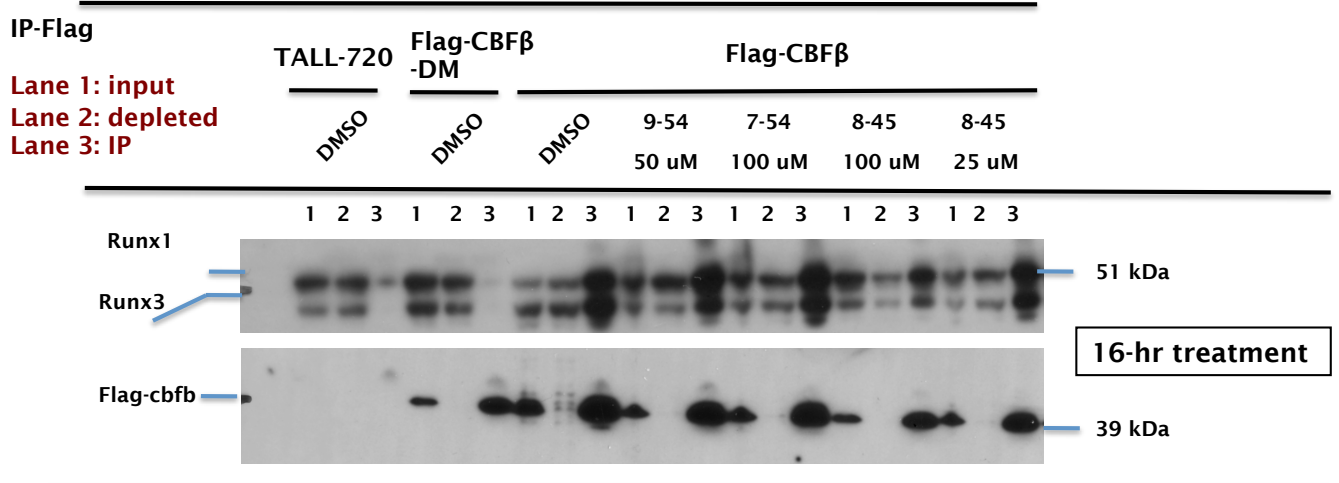
Validation of gene expression affected by RDIs in FDC-P1 cells.

We validated our finding from the microarray analysis in the FDC-P1 cells. FDC-P1 cells were cultured with RDIs or DMSO, mRNA harvested 12 hours later, and gene expressions determined by RT-PCR. Similar to our finding in 720 T-ALL cells, the expression of *Dhcr24* and *Cdkn1a* are affected following exposure to AI-8-45 and AI-9-45, but not by the weakly active control AI-7-54 (Figure 12). However, expression of mTOR inhibitor *Deptor* was not affected by treatment with the Runt domain inhibitors. Therefore, we demonstrated the similarity of RDI-induced changes in gene expressions in two different cell lines. The finding further support that this is due to on-target effects of our inhibitors.

Figure 12. Relative expression of genes in FDC-P1 cells.
FDC-PI cells were treated with RDIs for 16 hours, measured by qPCR. Data represents mean values for triplicates ± SD, n= two experiments. Significance relative to DMSO treatment was determined by one-way ANOVA. Dunnett's Multiple Comparison test was performed using DMSO treated cells as the comparator; asterisks above columns indicate significant differences from DMSO treated cells ($P \leq 0.05$).
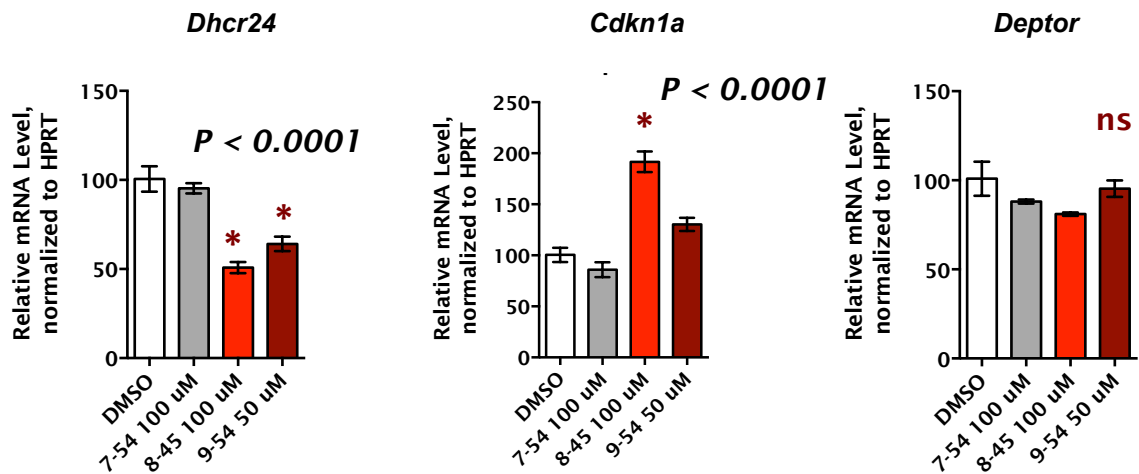
Supplemental Methods

Virtual screening

The coordinates of the RUNX1 Runt domain (1EAN) were obtained from the PDB. The hydrogen atoms were added in InsightII/Builder (Accelrys) program (*Insight 2005 Molecular Modelling Program Package*; Molecular Simulations Inc., San Diego) using the protonation states of protein residues at pH = 7.0. The computer program LUDI/InsightII (154) was applied for virtual screening of CAP (Chemicals Available for Purchase, 78,000 compounds) library to the CBFβ binding interface on the Runt domain structure. Compounds from CAP library were docked and ranked by the scoring function (Energy Estimate 1) implemented in the LUDI program (155). The values of the most important LUDI parameters used for virtual screening searches were as follows: Min Separation = 3; Link, Lipo and H-Bond Weights were set to 1.0; Aliphatic_Aromatic and Reject Bifurcated parameters were turned off; No_Unpaired_Polar, Electrostatic_Check and Invert parameters were turned on; Es Dist = 2.5Å; Max RMS = 0.8 Å; Number of Rotatable Bonds: two at a time, Radius of Search was 10Å. The 500 best scored hits (compounds with the predicted binding affinity < 300 μM as evaluated by LUDI's empirical scoring function) were subjected to visual inspection of their potential interactions with the Runt domain. Compounds with diverse scaffolds and involved in at least two hydrogen bonds with the Runt domain were selected for experimental evaluation.

Chemical synthesis

Commercially obtained reagents were used as received. Progress of reactions was monitored by TLC performed on Analtech 250micron silica gel GF plates visualized with 254 nm UV light and also by mass spectrometry using a Waters single-quadrupole LCMS. All compounds were purified on Biotage Isolera Four Flash Chromatography system, using SNAP cartridges. All final compounds were also purified by HPLC. Melting points were determined on a Mel-Temp manual melting point apparatus with a Fluke 51II thermocouple. ^{1}H and ^{13}C NMR spectra were recorded on a Bruker NMR spectrometer at 600 MHz in CDCl$_3$ and DMSO-d_6, with TMS as internal standard. Chemical shift values are reported in ppm units. Mass spectra were recorded on a Micromass AutoSpec Ultima Magnetic sector mass spectrometer in both positive and negative ESI mode at the University of Michigan Department of Chemistry mass spec facility.

The compounds **4a-4d, 5a-f** and **6a-b** were prepared as described previously (177-179).

5-(thiophen-2-yl)-1,3,4-thiadiazole-2(3H)-thione **(4a)** CAS Registry Number 41526-33-4

5-phenyl-1,3,4-thiadiazole-2(3H)-thione **(4b)** CAS Registry Number 5585-19-3

5-(6-methylpyridin-2-yl)-1,3,4-thiadiazole-2(3H)-thione (**4c**) CAS Registry Number 1093390-88-5

5-(pyrazin-2-yl)-1,3,4-thiadiazole-2(3H)-thione (**4d**) CAS Registry Number 37545-34-9

5-(2-fluorophenyl)-1,3,4-thiadiazole-2(3H)-thione (**5a**) CAS Registry Number 108413-60-1

5-(3-fluorophenyl)-1,3,4-thiadiazole-2(3H)-thione (**5b**) CAS Registry Number 276254-76-3

5-(4-fluorophenyl)-1,3,4-thiadiazole-2(3H)-thione (**5c**) CAS Registry Number 108413-72-5

5-(o-tolyl)-1,3,4-thiadiazole-2(3H)-thione (**5d**) CAS Registry Number 76779-96-9

5-(2-methoxyphenyl)-1,3,4-thiadiazole-2(3H)-thione (**5e**) CAS Registry Number 108413-63-4

5-(4-fluoro-2-methylphenyl)-1,3,4-thiadiazole-2(3H)-thione (**5f**) CAS Registry Number 1093390-85-2

2-(2-fluorophenyl)-5-(methylthio)-1,3,4-thiadiazole (**6a**) CAS Registry Number 276254-77-4

5-(benzofuran-2-yl)-1,3,4-thiadiazole-2(3H)-thione (**6b**) CAS Registry Number 130967-94-1

5-(5-(3-chlorophenyl)-1,3,4-oxadiazol-2-yl)-1,3,4-thiadiazole-2(3H)-thione (6d)

The title compound prepared as described previously (180)**.**

^{1}H-NMR (300 MHz, DMSO): δ 7.66-7.71 (1H, dd, *J*=6.00 Hz, *J*=9.00 Hz), 7.77-7.80 (1H, d, *J*=9.00 Hz), 8.04-8.07 (2H, d, 9.00 Hz); ^{13}C-NMR (600 MHz, DMSO): δ 125.08, 126.50, 127.17, 132.38, 133.32, 134.90, 144.66, 157.08, 164.33, and 189.13

General Synthetic procedure for the Key Intermediates in Scheme 5

The compounds, methyl 5-aryl furan-2-carboxylates in step 1 and 5-arylfuran-2-carbohydrazides in step 2 of **Scheme 5,** were prepared as described previously (181-183).
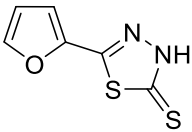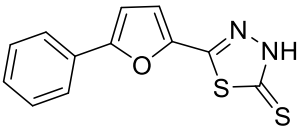
General procedure for the synthesis of Potassium 2-(5-arylfuran-2-carbonyl) hydrazine carbodithioate: To a solution of potassium hydroxide in ethanol (0.5M) was added 2-carbohydrazide fallowed by carbon disulfide. The resulting solution was allowed to stir overnight at room temperature. The precipitate was diluted with ether, filtered, washed with ether (3X), dried and used in the next step without further purification.
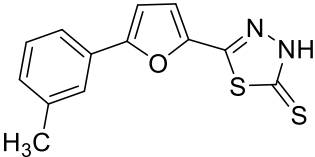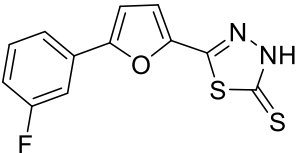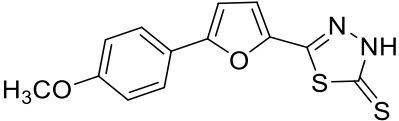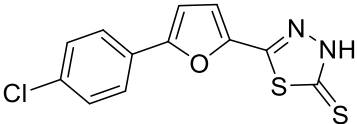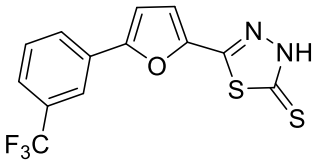
General procedure for the synthesis of 5-(5-(aryl) furan-2-yl)-1, 3, 4-thiadiazole- 2 (3H) - thione
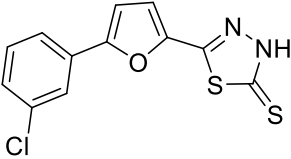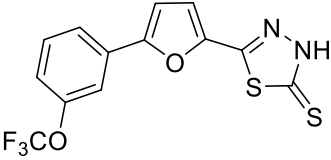
Potassium hydrazine carbodithioate (1 mmol) was added to concentrated sulfuric acid (1mL) at -10°C under argon and stirred at the same temperature for 30 min. The reaction mixture was warmed to 0°C and stirred at that temperature for 2h. The cold reaction mixture was poured over crushed ice, the solid thus separated was filtered, washed with water, and dried. The dried compound was stirred with DL-dithiothreitol (DTT) in ethanol for 3h at room temperature. The resulting solution was diluted with water and solid thus separated was filtered, dried and purified by mass directed HPLC using water/acetonitrile as solvent system on a Waters Sun Fire column.
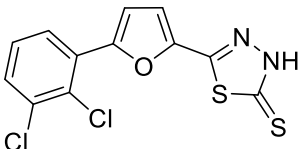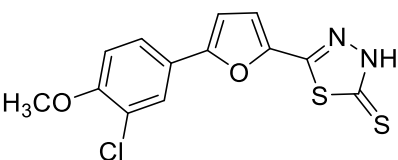
Compound physical properties and spectral data
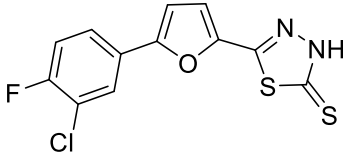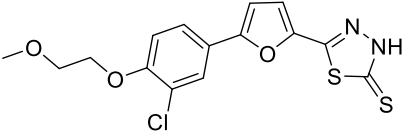
Name	Structure	MP (°C)	^{1}H-NMR (δ in ppm)	^{13}C-NMR (δ in ppm)	HRMS
AI-7-54 (3)		214-215	^{1}H-NMR (800 MHz, DMSO): δ6.76-6.77 (1H, dd, J = 1.76, 3.52 Hz), 7.20-7.21 (1H, d, J = 3.28 Hz), 7.98-7.99 (1H, d, J = 1.36 Hz), 14.78 (1H, s)	^{13}C-NMR (600 MHz, DMSO): δ112.90, 113.22, 143.57, 146.66, 150.64, 187.33	m/z [M+H]$^+$ calcd for $C_6H_4N_2OS_2$; 184.9843; found: 184.9837
AI-8-153 (6c)		237-238	^{1}H-NMR (800 MHz, DMSO): δ7.25-7.26 (1H, d, J = 3.60 Hz), 7.33-7.34 (1H, d, J = 3.68 Hz), 7.40-7.42 (1H, dd, J = 7.36, 7.36 Hz), 7.49-7.51 (2H, dd, J = 7.68, 7.68 Hz), 7.81-7.82 (2H, d, J = 7.76	^{13}C-NMR (600 MHz, DMSO): δ108.88, 115.29, 124.47, 129.29, 129.33, 129.57, 142.78, 150.37, 156.01, 187.26	m/z [M-H]$^-$ calcd for $C_{12}H_8N_2OS_2$; 259.0005; found: 259.0005
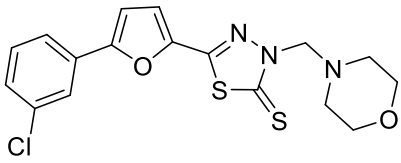
			Hz), 14.10 (1H, s)		
AI-9-24 (7a)		176-178	¹H-NMR (800 MHz, DMSO): δ2.38 (3H, s), 7.22-7.23 (2H, m), 7.32-7.33 (1H, d, *J* = 2.48 Hz), 7.37-7.39 (1H, dd, *J* = 7.64, 7.64 Hz), 7.61-7.62 (1H, d, *J* = 7.76 Hz), 7.64 (1H, s), 14.80 (1H, s)	¹³C-NMR (800 MHz, DMSO): δ21.46, 109.03, 115.46, 121.89, 125.04, 129.23, 129.50, 130.08, 138.90, 142.88, 150.60, 156.23, 187.15	m/z [M-H]⁻ calcd for $C_{13}H_{10}N_2OS_2$; 273.0162; found: 273.0163
AI-9-13 (7b)		222-225	¹H-NMR (600 MHz, DMSO): δ7.23-7.26 (1H, m), 7.34-7.36 (2H, m), 7.53-7.56 (1H, m), 7.65-7.67 (2H, m), 14.81 (1H, s)	¹³C-NMR (600 MHz, DMSO): δ110.43, 111.29, 115.24, 115.96, 120.70, 131.48, 143.27, 150.58, 154.54, 162.34, 163.52, 187.26	m/z [M-H]⁻ calcd for $C_{12}H_7FN_2OS_2$; 276.9911; found: 276.9913
AI-9-23 (7c)		211-212	¹H-NMR (800 MHz, DMSO): δ3.80	¹C-NMR (800 MHz, DMSO): δ55.77,	m/z [M-H]⁻ calcd for $C_{13}H_{10}N_2O_2S_2$; 289.0111; found: 289.0112
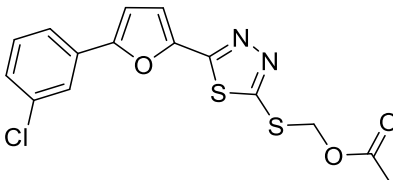
			(3H, s), 7.04-7.05 (3H, m), 7.25-7.26 (1H, d, *J* = 3.68 Hz), 7.73-7.74 (2H, d, *J* = 8.88 Hz), 14.84 (1H, s)	107.41, 115.07, 115.66, 122.02, 126.35, 142.09, 150.82, 156.40, 160.26, 187.00	
AI-8-117 (7d)		>250	^{1}H-NMR (800 MHz, DMSO): δ7.24-7.25 (1H, d, *J* = 3.68 Hz), 7.30-7.31 (1H, d, *J* = 3.28 Hz), 7.54-7.55 (2H, d, *J* = 8.64 Hz), 7.81-7.82 (2H, d, *J* = 8.56 Hz), 14.84 (1H, s)	^{13}C-NMR (800 MHz, DMSO): δ109.76, 115.48, 126.26, 127.97, 129.55, 133.66, 143.02, 150.53, 154.88, 187.16	m/z [M-H]$^-$ calcd for $C_{12}H_7ClN_2OS_2$; 292.9616; found: 292.9615
AI-9-28 (7e)		223-228	^{1}H-NMR (800 MHz, DMSO): δ7.37-7.38 (1H, d, *J* = 3.68 Hz), 7.49-7.50 (1H, d, *J* = 3.68 Hz), 7.73-7.77	^{13}C-NMR (600 MHz, DMSO): δ110.80, 115.38, 120.98, 123.50, 125.54, 128.35, 130.27, 130.58,	m/z [M-H]$^-$ calcd for $C_{13}H_7F_3N_2OS_2$; 326.9879; found: 326.9881

			(2H, m), 8.12-8.13 (2H, m), 14.86 (1H, s)	130.82, 143.68, 150.33, 154.31, 187.37	
AI-8-45 (7f)		220-222	^{1}H-NMR (800 MHz, DMSO): δ7.35-7.36 (1H, d, J = 3.68 Hz), 7.38-7.39 (1H, d, J = 3.68 Hz), 7.46-7.47 (1H, ddd, J = 0.88, 2.00, 7.96 Hz), 7.52-7.54 (1H, dd, J = 7.88, 7.88 Hz), 7.78-7.79 (1H, dt, J = 1.24, 7.76 Hz), 7.89-7.90 (1H, dd, J = 1.80, 1.80 Hz), 14.80 (1H, s)	^{13}C-NMR (600 MHz, DMSO): δ110.30, 115.15, 123.04, 124.03, 128.90, 131.11, 131.53, 134.34, 143.46, 150.34, 154.37, 187.32	m/z [M+H]$^+$ calcd for C$_{12}$H$_7$ClN$_2$OS$_2$; 294.9767; found: 294.9761
AI-9-27 (7g)		226-227	^{1}H-NMR (600 MHz, DMSO): δ7.34-7.35 (1H, d, J = 3.66 Hz), 7.39-7.41 (2H, m), 7.62-7.65 (1H, dd,	^{13}C-NMR (600 MHz, DMSO): δ110.73, 115.27, 117.13, 119.54, 121.38, 123.51, 131.29,	m/z [M-H]$^-$ calcd for C$_{13}$H$_7$F$_3$N$_2$O$_2$S$_2$; 342.9828; found: 342.9830

70

			$J = 8.04$, 8.04 Hz), 7.78 (1H, s), 7.84-7.86 (1H, d, $J = 7.38$ Hz), 14.83 (1H, s)	131.64, 143.61, 149.33, 150.37, 154.15, 187.36	
AI-8-57 (7h)		202-204	^{1}H-NMR (800 MHz, DMSO): δ7.39-7.40 (1H, d, $J = 3.86$ Hz), 7.42-7.43 (1H, d, $J = 3.76$ Hz), 7.52-7.54 (1H, dd, $J = 7.96$, 7.96 Hz), 7.73-7.74 (1H, dd, $J = 1.44$, 8.00 Hz), 7.87-7.88 (1H, dd, $J = 1.44$, 7.92 Hz), 14.88 (1H, s)	^{13}C-NMR (600 MHz, DMSO): δ114.67, 114.76, 127.83, 128.39, 129.17, 129.91, 130.95, 133.67, 143.63, 150.22, 151.53, 187.55	m/z [M+H]$^+$ calcd for $C_{12}H_6Cl_2N_2OS_2$; 327.9299; found: 327.9293
AI-8-103 (7i)		212-214	^{1}H-NMR (600 MHz, DMSO): δ3.91 (3H, s), 7.21-7.22 (1H, d, $J = 3.66$ Hz), 7.28-7.29 (1H, d, $J = 8.10$	^{13}C-NMR (600 MHz, DMSO): δ56.67, 108.46, 113.61, 115.49, 122.10, 123.01, 124.89, 125.87,	m/z [M-H]$^-$ calcd for $C_{13}H_9ClN_2O_2S_2$; 322.9721; found: 322.9720

			Hz), 7.30-7.31 (1H, d, J = 3.66 Hz), 7.76-7.77 (1H, dd, J = 2.07, 8.61 Hz), 7.89-7.90 (1H, d, J = 2.16 Hz), 14.77 (1H, s)	142.57, 154.54, 155.31, 187.05	
AI-8-89 (7j)		>250	^{1}H-NMR (800 MHz, DMSO): δ7.34-7.35 (1H, d, J = 3.76 Hz), 7.35-7.36 (1H, d, J = 3.68 Hz), 7.55-7.57 (1H, m), 7.82-7.84 (1H, m), 8.06-8.07 (1H, m), 14.84 (1H, s)	^{13}C-NMR (600 MHz, DMSO): δ110.08, 115.17, 118.32, 121.08, 125.35, 126.53, 127.39, 143.63, 150.65, 153.44, 156.96, 158.53, 187.13	m/z [M-H]$^{-}$ calcd for $C_{12}H_6ClFN_2OS_2$; 310.9521; found: 310.9520
AI-9-54 (7k)		175-177	^{1}H-NMR (800 MHz, DMSO): δ3.36 (3H, s), 3.72-3.73 (2H, t), 4.26-4.27 (2H, t), 7.22-7.23 (1H, d, J = 3.60	^{13}C-NMR (600 MHz, DMSO): δ58.68, 68.88, 70.47, 108.39, 114.47, 115.21, 122.35, 122.88,	m/z [M-H]$^{-}$ calcd for $C_{15}H_{13}ClN_2O_3S_2$; 366.9983; found: 366.9986

			Hz), 7.28-7.29 (1H, d, J = 8.80 Hz), 7.31-7.32 (1H, d, J = 3.12 Hz), 7.73-7.74 (1H, dd, J = 2.20, 8.60 Hz), 7.89-7.90 (1H, d, J = 2.24 Hz), 14.80 (1H, s)	124.83, 125.89, 142.71, 150.43, 154.69, 154.83, 187.07	
AI-9-59		134-135	^{1}H-NMR (600 MHz, DMSO): δ2.77-2.78 (4H, t), 3.57-3.59 (4H, t), 5.24 (2H, s), 7.35-7.36 (1H, d, J = 3.30 Hz), 7.37-7.38 (1H, d, J = 3.54 Hz), 7.44-7.46 (1H, dd, J = 1.11, 8.07 Hz), 7.50-7.53 (1H, dd, J = 7.92, 7.92 Hz), 7.76-7.77 (1H, d, J = 7.80	^{13}C-NMR (600 MHz, DMSO): δ50.76, 66.56, 70.80, 110.53, 115.81, 123.20, 124.27, 129.06, 131.16, 131.55, 134.14, 143.49, 154.61, 186.58	293 as neg. ion $C_{17}H_{16}ClN_3O_2S_2$

			Hz), 7.87 (1H, dd, *J* = 1.68, 1.68 Hz)		
AI-9-63		85-87	^{1}H-NMR (800 MHz, CDCl$_3$): δ2.19 (3H, s), 5.81 (2H, s), 6.88-6.89 (1H, d, *J* = 3.60 Hz), 7.29-7.30 (1H, d, *J* = 3.44 Hz), 7.34-7.36 (1H, ddd, *J* = 0.96, 2.04, 7.96 Hz), 7.39-7.41 (1H, dd, *J* = 8.04, 8.04 Hz), 7.64-7.65 (1H, dt, *J* = 1.24, 7.76 Hz), 7.75-7.76 (1H, dd, *J* = 1.88, 1.88 Hz)	^{13}C-NMR (800 MHz, CDCl$_3$): δ20.90, 65.44, 108.75, 113.79, 122.43, 124.32, 128.64, 130.24, 130.97, 135.04, 144.91, 155.04, 159.57, 161.57, 170.22	

Pharmacokinetics

Test Compound Formulation

All dosing solutions were formulated in-house and passed through 0.22-micron sterile filters prior to use. Solutions were stable over two weeks at 25°C as assessed by HPLC. Detailed procedures for each compound are provided below.

AI-9-54

A dosing nanosuspension was prepared at 19.15 mg/mL in 0.05% Tween 80 in 0.9% NaCl. Briefly, 46 mg AI-9-54 and 460 mg yttrium stabilized zirconia grinding media (0.5 mm; Inframat Advanced Materials LLC, Manchester, CT, USA) were added to a 5 mL PTFE bottle and shaken on a Wig-L-Bug mixer (DENTSPLY, York, PA,USA) until the mean square particle size was less than 0.5 µM (Brookhaven zetaPALS analyzer, Brookhaven Instruments Corporation, Holtsville, NY, USA).

AI-9-59

A dosing solution 25 mg/mL in 0.2 M Captisol (Ligand Pharmacueticals, La Jolla, CA, USA) was prepared with the *in situ* formed hydrochloride salt of AI-9-59.

Pilot Pharmacokinetic Studies

The University of Kansas Institutional Animal Care and Use Committee approved this study and appropriate guidelines for the use of animals were observed during all aspects of the study. Prior to the study, mice were fasted at least three hours and water was available *ad libitum*. Animals were housed on a 12-hour light/dark cycle at 72-74°C and 30-50% relative humidity.

For IP dosing 24-28 gm male C57BL/6 mice (Harlan Laboratories, USA) were manually restrained and injected in the peritoneal cavity midway between the sternum and pubis and slightly off the midline of the mouse. A 1-cc syringe with a 27-gauge needle was used for each injection. Blood was collected from the animals according to scheduled time points. Animals were anesthetized with isoflurane and blood drawn via cardiac puncture. Blood was immediately transferred to 1.5 mL heparinized microcentrifuge tubes and centrifuged at 4000 rpm for ten minutes. Plasma was then transferred to clean tubes and frozen. Due to exsanguination, the animals did not wake from the anesthesia and death was insured while under anesthesia by thoracotomy. This method is consistent with the recommendations of the AVMA Guidelines on Euthanasia for use of exsanguination as a means of euthanasia.

Noncompartmental pharmacokinetic analysis of the test compound plasma concentration-time data was conducted using PK Solutions 2.0 (Summit Research Services, Montrose, CO, USA).

Bioanalysis

Materials – Methyl-t-butyl ether (MtBE) and HPLC grade acetonitrile (ACN) were obtained from Fisher (NJ, USA). Trifluoroacetic acid (TFA) and formic acids was from Fluka (St. Louis, MO, USA). Dimethylsulfoxide (DMSO) was obtained from Sigma (St. Louis, MO, USA) and was Hybri-Max grade.

General Equipment - A VX-2500 multi-tube vortexer from VWR (West Chester, PA, USA) and an accuSpin Micro 17 centrifuge from Fisher (NJ, USA) were used in the sample preparation. Solvent evaporation was carried out on a CentriVap concentrator from Labconco (Kansas City, MO, USA) with a Büchi V-800 vacuum controller

(Switzerland). Samples were analyzed on an Applied Biosystems 3200 QTRAP (Grand Island, NY, USA) operated in negative ion mode with a Shimadzu SCL-10A vp controller, SIL-20AC autosampler, LC-20AD pumps and CTO-20A column oven (Kyoto, Japan).

AI-9-54 – An LC/MS/MS method was developed for AI-9-54 using external standards. LC/MS chromatography conditions included a Zorbax SB C18 2.1 x 50 mm at 45°C with a mobile phase flow rate of 0.20 mL/min. The gradient elution consisted of solvents A and B with A) 10 mM ammonium acetate pH 8.0, and B) acetonitrile. The gradient consisted of 10-95% B in four minutes, 95% B for two minutes, 95-10% B in 0.5 minutes, and 10% B for three minutes. Samples were held at 8°C and 2 µL were injected. The retention time of AI-9-54 is 3.0 minutes.

Mass spectrometry conditions consisted of a curtain gas of 14 xx, a temperature of 650°C, GS1 & GS2 of 50 and 45 xx, respectively. Monitored AI-9-54 transitions were 367.127/58.000, DP = -45, EP = -3.3, CEP = -16, CE = -48, CXP = -8. Two sets of standards and samples, a high concentration and a low concentration range were run. Extraction of plasma samples was conducted on 50 µL of the respective samples using 0.2 mL of MtBE after adding 10 µL of AI-9-54 spiking solution (10X), vortexing, and allowing the sample sit at room temperature for five min. The two-phase mixture was vortexed for five min then centrifuged at 12,000 rpm for five min. 190 µL of the MtBE layer was transferred to clean tubes and evaporated to dryness. The resulting residue was reconstituted in 100 µL of 50/50 ACN/H2O and vortexed followed by centrifugation at 12,000 rpm for five min. 90 µL of the supernatant was transferred to autosampler vials with polypropylene inserts and analyzed.

The validation sets consisted of blank plasma and a standard curve with the range of 25, 50, 100, 250, 500, and 1000 ng/mL AI-9-54 (r > 0.9933).

AI-9-59 - An LC/MS/MS method was developed for AI-9-59 using external standards. LC/MS chromatography conditions included a Zorbax SB C18, 5 µm, 2.1 x 50 mm at 50°C with a mobile phase flow rate of 0.20 mL/min. The gradient elution consisted of solvents A and B with A) 10 mM ammonium acetate pH 8.0, and B) acetonitrile. The gradient consisted of 5-95% B in three minutes, 95% B for 1.5 minutes, 95-5% B in 0.5 minutes, and 5% B for 3.5 minutes. Samples were held at 8°C and 5 µL were injected. The retention time of AI-9-59 is 4.3 minutes.

Mass spectrometry conditions consisted of a curtain gas of 12 xx, a temperature of 650°C and GS1 & GS2 of 30 xx. Monitored AI-9-59 transitions were 292.94/89.1, DP = -40, EP = -4, CEP = -12, CE = -19, CXP = -2. Two sets of standards and samples, a high concentration and a low concentration range were run. Following the addition of 50 µL of external standard, the standards prepared in plasma and samples were charged with acetonitrile, vortexed, centrifuged and the supernatant transferred to clean tubes, which were then dried under vacuum. The standards and samples were reconstituted in 50 µL 50/50 acetonitrile/water, vortexed, centrifuged, and the supernatant transferred to autosampler vials for analysis. The validation sets consisted of blank plasma and a standard curve with the range of 2, 5, 10, 20 50, 100 and 200 ng/mL AI-9-59 (r > 0.9993).

MTT Cell Proliferation Assay

A 12 mM stock solution of MTT (3-(4, 5-dimethylthiazolyl-2)-2, 5-diphenyltetrazolium bromide) (Invitrogen) was prepared by dissolving 5 mg MTT in 1 mL of sterile PBS. 10 µl of the MTT stock solution was added to each well of the 96-well culture plate, and incubated at 37°C for 4 hours. The plate was centrifuged at 300 g for 5 minutes, the media removed, and 100 µl of DMSO (Sigma-Aldrich) was added to solubilize the resulting reagent formazan and incubated at room temperature for 10 minutes. The plate was then analyzed by measuring absorbance at 540 nm wavelength in a SpectraMax plate reader (Molecular Devices). Data are plotted as percentage of viable cells relative to DMSO.

Gene expression analysis (microarray)

RNA for microarray was isolated with the RNeasy Kit (QIAGEN). Total RNA quantity and integrity were verified using Bioanalyzer (Agilent Technologies), and amplified using Ambion WT Expression Kit (Applied Biosystems). Microarray experiments were performed on GeneChip Mouse Gene 2.0 ST Array (Affymetrix) at the University of Pennsylvania Molecular Profiling Facility, according to the manufacturer's instructions.

Affymetrix probe intensity (cel) files were analyzed using Partek Genomics Suite (v6.6, Partek, Inc., St. Louis, MO). The data was normalized using Robust Multichip Average Algorithm (RMA), and technical controls were excluded to leave 34,365 transcript IDs available for statistical analysis. A one-way ANOVA followed by 3 pairwise comparisons (t-tests) were performed across the samples, each yielding a p-value for each transcript ID. The p-values were further corrected using the Benjamini-Hochberg procedure for false discovery rate (FDR). Fold-change in expression level for each transcript ID was calculated for the 3 pairwise comparisons.

To identify genes that are differentially expressed following treatment, the data was filtered to retain transcript IDs that demonstrated a false discovery rate of 5% and have a mean fold change of at least 1.5, up or down in AI-7-54 vs AI-8-45 treated cells. 87 IDs (78 unique genes) met these cutoffs. Hierarchical clustering was performed using Pearson correlation and average linkage. The colors red and blue are used to indicate the log-2 intensity of each gene relative to the mean of AI-7-54 treatment.

Chapter II: Characterization of the Runt domain inhibitor's *in vivo* efficacy by mouse leukemia models

Zaw Min Oo[1], Anuradha Illendula[2], Roger A. Rajewski[3], Nancy A. Speck[1], and John H. Bushweller[2]

[1]Abramson Family Cancer Research Institute and Department of Cell and Molecular Biology, University of Pennsylvania, Philadelphia, Pennsylvania, USA, 19104

[2]Department of Molecular Physiology and Biological Physics, University of Virginia, Charlottesville, Virginia, USA, 22908

All figures within this chapter were contributed primarily by Zaw Min Oo.

AML1-ETO9; NRAS[G12D] cells were generated by Dr. Scott W. Lowe.

The text of this chapter was written primarily by Zaw Min Oo.

Introduction

In the previous chapter, we established that the Runt domain inhibitors demonstrated good efficacy in mouse t(8;21) leukemia bone marrow cells and in human patient samples of both t(8;21) and non t(8;21) leukemias. In addition, the RDIs did not affect normal bone marrow progenitors at the same concentrations, indicating that a therapeutic window is available. Furthermore, our inclusion of a structurally related and weakly active compound as a control strongly support that the efficacies we observed were due to on target inhibition of RUNX proteins functions.

Beyond the *in vitro* efficacies described above, we wished to demonstrate the inhibitors' *in vivo* efficacies in order to establish clinical applicability. To this end, we have developed a pro-drug AI-9-59 that has improved solubility and pharmacokinetic properties. We also needed to adopt a mouse model that reproduces the characteristics of the t(8;21) AML. Numerous studies have demonstrated that full-length AML1-ETO is not capable of initiation leukemia on its own (184-188). The chimeric transcription factor was shown to cooperate with activating mutations in the receptor tyrosine kinases (189-192), including activated form of platelet-derived growth factor receptor-β (TEL-PDGFβR) (121) and RAS (193) in t(8;21) AML.

In our previous effort to examine the contribution of various protein-protein interactions towards AML1-ETO's leukemogenic capability, we generated a mouse model of t(8;21) leukemia through retroviral expression of AML1-ETO and TEL-PDGFβR in mouse bone marrow cells (132). In this model, the transduced bone marrow cells were transplanted into lethally irradiated primary recipients, all of whom developed a completely penetrant lethal leukemia and succumbed to disease within 4 weeks. While this model was useful for studying the role of each of AML1-ETO's interaction partners

towards leukemogenesis, it did not faithfully recapitulate the human disease, as the t(5;12) that generates TEL- PDGFβR and the t(8;21) were rarely found together in AML patients (194). Furthermore in this retrovirus-mediated model, TEL-PDGFβR independently generated a chronic myeloproliferative disorder (CMPD). As a result, the presence of mixed diseases makes this model a less optimal model for studying the *in vivo* efficacy of the Runt domain inhibitors.

More recently, a similar mouse model of t(8;21) AML using retroviral expression was reported. In this model, MSCV-based retroviral constructs with GFP and luciferase markers were used to co-express AML1-ETO9a and NRAS^{G12D} in fetal liver cells that are embryonic day 13.5-15 old (169). AML1-ETO9a is a form of AML1-ETO lacking the C-terminal MYND domain, and is more potent at inducing leukemia than full length AML1-ETO (142). The infected fetal liver cells were transplanted into lethally irradiated recipient mice, which were monitored for development of leukemia. Mice reconstituted with one million AML1-ETO9a + NRAS^{G12D} fetal liver cells had a mean survival of 84 days. End point analysis showed that the bone marrow of the recipient mice contain immature blasts that could be immuno-phenotyped as c-Kit$^+$, Mac-1$^-$, Gr-1$^-$, CD3e$^-$, and CD19$^-$. The blast cells were also positive for GFP and the luciferase markers, validating the cooperation between AML1-ETO9a and NRAS^{G12D} in generating leukemia. The leukemia cells could be transplanted into secondary recipients to reproduce the same disease.

Additionally, the GFP and luciferase markers allowed for studying leukemia burden in the recipients by flow cytometry and bioluminescent imaging. The AML1-ETO9a + NRAS^{G12D} leukemia cells were also responsive to standard chemotherapy (cytarabine combined with doxorubicin) used to treat AML in human patients (169). Under combination chemotherapy, the leukemia regressed and lead to complete

remission. Therefore, this represents a well-characterized model of t(8;21) AML suitable for our *in vivo* studies for determining the single agent efficacy of the Runt domain inhibitor pro-drug, as well as potential synergy of the pro-drug in combination with chemotherapy.

Another possible mouse model involved the engraftment of human AML cells in immuno-compromised NSG (NOD/LtSz-scid IL2Rγc null) mice (195). The NSG mice allowed robust engraftment of primary human AML samples. Out of 35 patient AML samples transplanted into NSG mice, 13 samples achieved high (>10%) engraftment based on the percentage of human AML cells in NSG bone marrow. Additionally, the high-engrafting AML samples could be serially transplanted into secondary and tertiary NSG recipient mice. One distinct benefit of the xenograft model is that we will be treating leukemia cells immediately derived from human patient samples, and thus the model is appropriate for establishing direct clinical relevance; despite the fact that none of the serially engraftable samples are t(8;21) positive. Based on our *in vitro* data which showed that the Runt domain inhibitors reduced growth and induced apoptosis in non t(8;21) leukemia cells, we believe the xenograft model would allow us to interrogate the efficacy of the Runt domain inhibitor beyond CBF leukemias through human AML samples.

Based on the models described above, we selected the AML1-ETO9a + NRAS^{G12D} model, as it represents a well-characterized model that is genetically relevant to our *in vivo* studies. We set out to determine whether the Runt domain inhibitors could reduce the leukemia burden or extend the survival in the mice transplanted with leukemia cells.

Materials and Methods

Mice

All mouse procedures were approved by the University of Pennsylvania University Animals Resource Center (ULAR) and Institutional Animal Care and Use Committees (IACUC) of the University of Pennsylvania.

Transplant

B6.SJL (CD45.1) mice were used as transplant recipients. Bone marrow chimeras were established by injecting donor bone marrow cells from C57BL6/J background (CD45.2) along with 2×10^5 bone marrow cells from C57BL6/J crossed to B6.SJL (competitor CD45.1/CD45.2) into lethally irradiated recipients (two doses of 450 cGy each, 4 hours apart).

Xenograft in NSG mice

2 million 720 T-ALL cells were injected subcutaneously into right flank of NSG (NOD/LtSz-scid IL2Rγc null) mice. The tumors were allowed to grow to a size of 250 mm^3 after which the mice received DMSO or 50 mg/kg AI-9-59 ip injections.

Flow cytometry

Flow cytometry analyses were performed on BD LSRII (BD Bioscience, San Jose CA). For peripheral blood analysis erythrocytes were lysed in RBC Lysis Buffer (Sigma). The following monoclonal antibodies (BD Bioscience and/or eBioscience, San Diego CA) were used for staining: FITC-CD16/32 (2.4G2), APC-CD34 (RAM34), APC-Cy7-cKit (2B8), PE-Flt3 (A2F10), PE-Cy7-Sca1 (D7), APC-CD45.1 (A20), FITC CD45.2 (104),

PE-Cy7-Mac1 (M1/70), PerCP-Cy5.5-Gr1 (RB6-8C5), APC-CD3e (145-2C11), PE-CD19 (1D3). Dead cells were stained with DAPI.

Data analyses for flow cytometry were carried out using FlowJo (Treestar Inc, Ashland OR).

Pilot study for efficacy of RDI in AML1-ETO^{9a} + NRAS^{G12D} mouse model

In order to examine the potential *in vivo* efficacies of the Runt domain inhibitor pro-drug, we conducted a pilot experiment using the AML1-ETO9a and NRAS^{G12D} mouse transplant model of t(8;21) AML (169). We obtained AML1-ETO9a and NRAS^{G12D} bone marrow leukemia cells harvested from the primary recipients and transplanted into lethally irradiated hosts at 250,000 AML cells per mouse. Our results showed all the recipients succumbed to leukemia within four weeks. Flow cytometry analysis showed high percentage of GFP positive AML cells in the peripheral blood. We observed high percentage of GFP positive cells in spleen and bone marrow. The GFP positive cells were also positive for c-Kit, a surface marker associated with progenitor cells, and were negative for various hematopoietic lineage markers including granulocyte makers Gr-1 and Mac-1, B lymphocyte marker CD19, and T lymphocyte marker CD3e (Figure 1). Thus we showed that AML1-ETO9a and NRAS^{G12D} expressing cells were serially transplantable and gave a consistent phenotype, and we confirmed that the GFP positive cells are myeloid leukemia cells in accordance with the Bethesda proposals for classification of nonlymphoid hematopoietic neoplasms in mice (196).

Figure 1. Flow cytometry analysis of peripheral blood from mice transplanted with *AML1-ETO^9a* + *NRAS^G12D* bone marrow cells.

A-B. Peripheral blood (PB) of the mice transplanted with 250,000 *AML1-ETO^9a* + *NRAS^G12D* bone marrow cells showed engraftment of GFP positive cells that showed higher c-Kit expression.

C-D. Lineage analysis of GFP positive and GFP negative PB cells using myeloid (Mac1 and Gr1) and lymphoid (CD3e and CD19) markers.
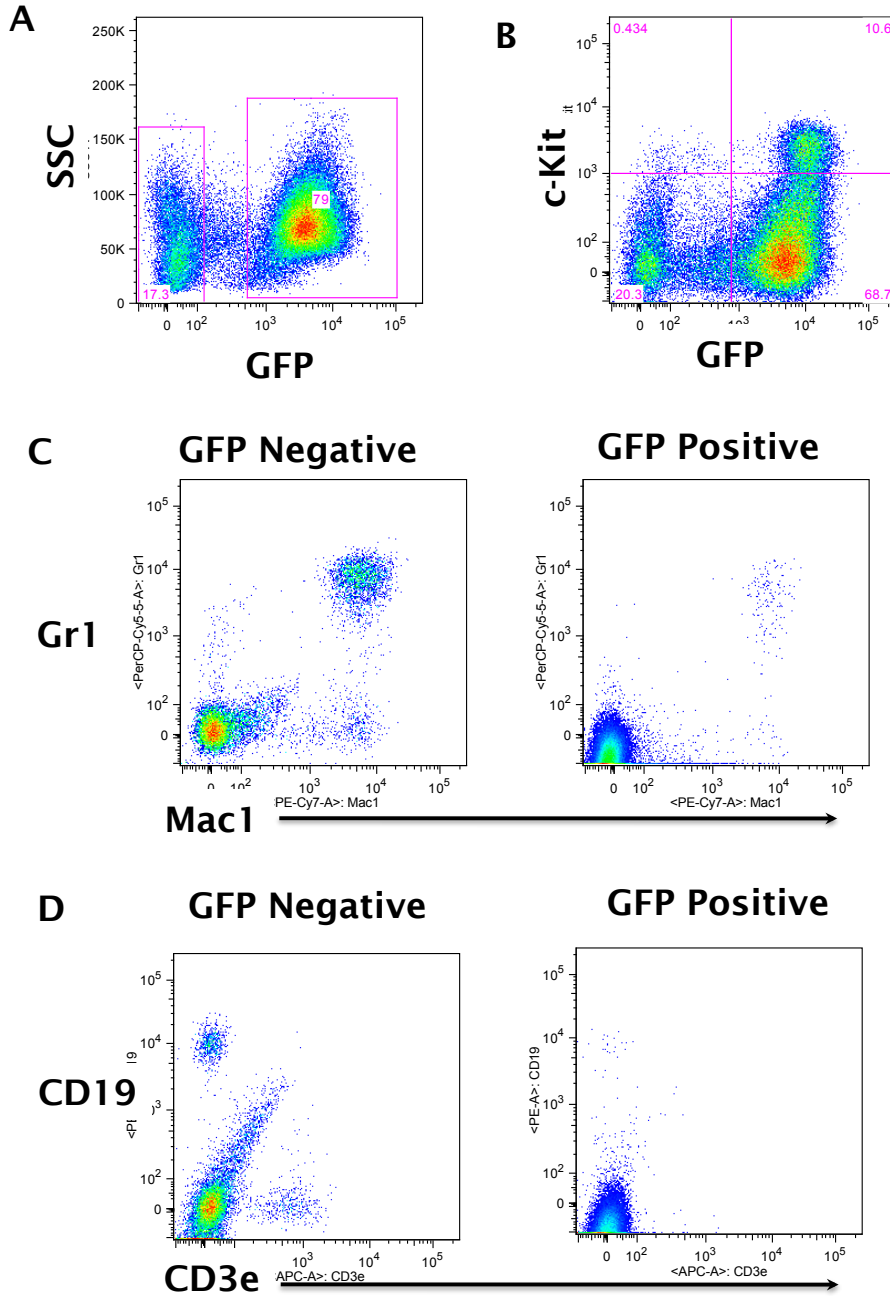
We isolated splenocytes and bone marrow cells from these recipients and transplanted into irradiated host at 250,000 cells per mice. Five days post-transplant, we began daily intraperitoneal injections of 50 µl vehicle (DMSO) or 100 mg/kg AI-9-59 (dissolved in DMSO). After four doses, mice that received 100 mg/kg AI-9-59 showed signs of toxicity including lethargy and weight loss, at which point we stopped the injections and monitored the mice for recovery. Eight out of ten mice that received the 100 mg/kg injections died within one week due to toxicity (Figure 2). Therefore we determined that the dosage of 100 mg/kg was toxic to the mice, as they did not tolerate beyond four doses.

Figure 2. Assessing *in vivo* efficacy of the pro-drug for the Runt domain inhibitors.
Kaplan-Meier survival analysis of mice transplanted with 250,000 AML1-ETO9a + NRAS^{G12D} mouse AML cells, and injected with DMSO (vehicle) or four doses of AI-9-59 100 mg/kg intraperitoneal injections daily. P-value was determined by Mantel-Cox test (n=10 for AI-9-59 100 mg/kg and n=5 for DMSO).
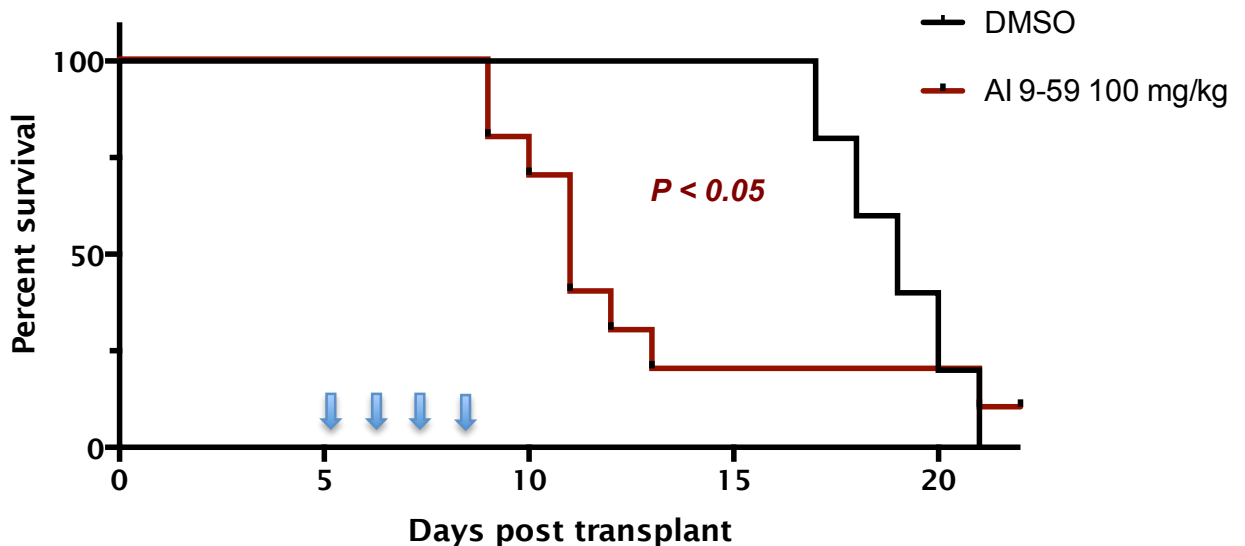
In order to continue the study, the DMSO control group was split into two groups of five mice each: one group received daily IP injection of 50 µl DMSO and the other received a lower dose of 25 mg/kg AI-9-59 (Figure 3A). The mice tolerated daily injections of 25 mg/kg AI-9-59. Kaplan-Meier analysis showed a small but statistically significant improvement in the survival of mice that received AI-9-59, compared to mice that received vehicle control (Figure 3B). FACS analysis of the peripheral blood revealed a trend towards reduction in the percentage of GFP-positive leukemia cells in the mice that received AI-9-59 (Figure 3C). These data suggested the pro-drug AI-9-59 could reduce the growth of mouse leukemia cells expressing AML1-ETO[9a] and NRAS[G12D] *in vivo* and extend the survival in a mouse model of t(8;21) AML.

Figure 3. Assessing *in vivo* efficacy of the pro-drug for the Runt domain inhibitors.

A. Revised schematics for assessing *in vivo* efficacy of the pro-drug. The mice from the DMSO control group were equally divided into a control (DMSO) and a lower dose of 25 mg/kg IP injections, and studied for survival.

B. Kaplan-Meier survival analysis of mice as described in A. P-value was determined by Mantel-Cox test (n=5 per group). The three remaining mice from the 25 mg/kg group was sacrificed at Day 22 as recommended by the veterinarian.

C. FACS analysis of the peripheral blood at Day 19 post-transplant (n=2 for DMSO and n= 4 for 25 mg/kg).

A
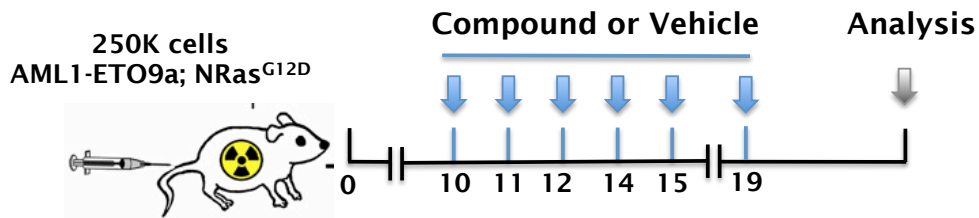
B
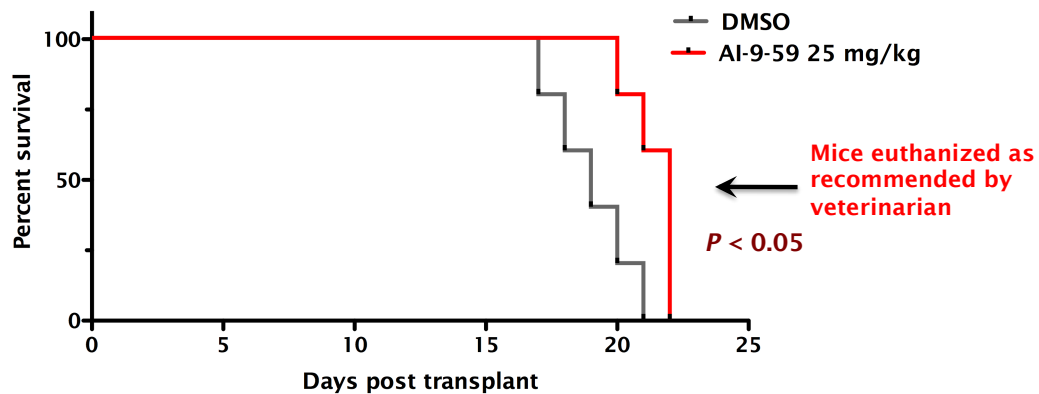
C
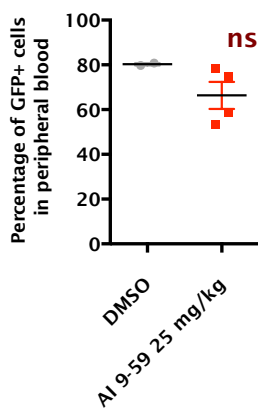
Efficacy of RDI in AML1-ETO^{9a} + NRAS^{G12D} mouse model

Based on the preliminary results obtained from the pilot study, we conducted a second experiment in which we engrafted 250,000 AML1-ETO^{9a} + NRAS^{G12D} leukemia cells per recipient using a larger cohort of 40 mice. Five days post-transplant, we began the intraperitoneal injections of 50 µl of DMSO, 25 mg/kg, or 50 mg/kg AI-9-59. In order to minimize toxicity from the drug, the mice were given three consecutive daily IP injections followed by one-day rest. Eighteen days post-transplant, the mice from the DMSO group started to show signs of leukemia related sickness, at which point all the animals were sacrificed and tissues collected for histology and analysis.

FACS analysis of the peripheral blood and bone marrow of the mice showed no significant change in the percentage of GFP positive leukemia cells (Figure 4A,B), suggesting that AI-9-59 did not affect the growth of t(8;21) leukemia cells *in vivo*. We also did not detect any significant difference in the relative spleen weight, although mice that received 50 mg/kg injections exhibited a trend towards smaller relative spleen size (Figure 4C). Therefore based on the parameters of the analysis, we did not detect any significant efficacy in the ability of the pro-drug to reduce the growth of t(8;21) leukemia cells expressing AML1-ETO^{9a} and NRAS^{G12D}.

Figure 4. Efficacy of RDI in AML1-ETO[9a]; NRAS[G12D] mouse model.

A-B. Percentage of GFP positive leukemia cells in the peripheral blood cells (A) and bone marrow cells (B) harvested from mice transplanted with 250,000 AML1-ETO[9a]; NRAS[G12D] mouse leukemia cells, and treated with DMSO, 25 or 50 mg/kg AI-9-59. (n= 9 for DMSO, n=13 for 25 mg/kg, and n= 10 for 50 mg/kg). Significance relative to DMSO treatment was determined by one-way ANOVA followed by Dunnett's Multiple Comparison.

C. Spleen weight relative to body weight of mice transplanted with 250,000 AML1-ETO[9a]; NRAS[G12D] mouse leukemia cells, and treated with DMSO, 25 or 50 mg/kg AI-9-59 (n= 9 for DMSO, n=13 for 25 mg/kg, and n= 10 for 50 mg/kg). Significance relative to DMSO treatment was determined by one-way ANOVA followed by Dunnett's Multiple Comparison.
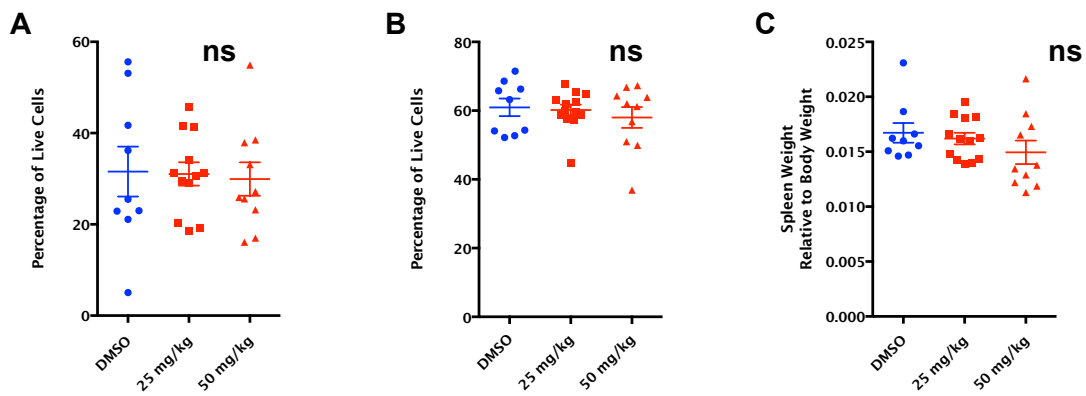
Efficacy of RDI in NSG engrafted 720 T-ALL model

We employed a xenograft model in which the murine T-ALL cell line 720 was engrafted subcutaneously into immune-compromised NSG mice. First, we determined the maximum tolerated dose of the pro-drug in NSG mice by giving 50 mg/kg or 75 mg/kg AI-9-59 injections. The NSG mice did not tolerate daily injections of 75 mg/kg beyond four doses (Figure 5), but tolerated a 50 mg/kg dosing regimen in which three consecutive daily IP injections are followed by one-day rest for a total of nine injections. Therefore we proceeded with 50 mg/kg IP injections for *in vivo* study.

Figure 5. Determining the maximum tolerated dose of NSG mice to the pro-drug AI-9-59.
Kaplan-Meier survival analysis of mice injected with 50 µl of 50 mg/kg or 75 mg/kg AI-9-59 daily (n=5 for each group). Mice from the 75 mg/kg group received a total of four i.p. injections, and the experiment was terminated for 50 mg/kg group at Day 16, after we determined that the mice tolerated our dosing regimen.
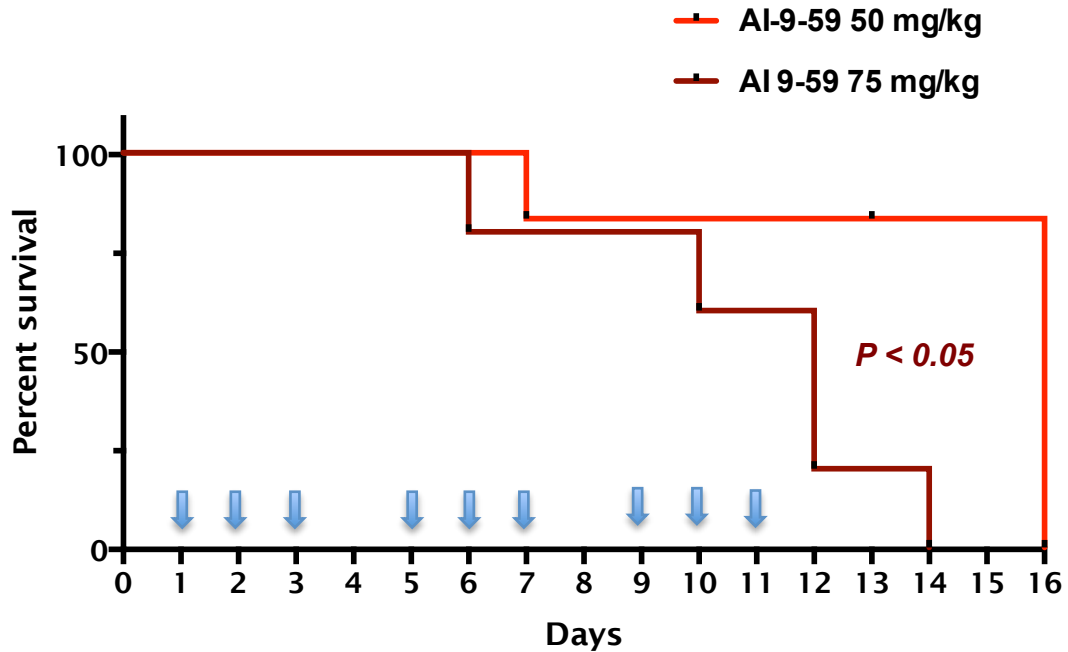
We injected two million 720 T-ALL cells subcutaneously into NSG mice, and allowed the tumors to engraft and grow to the size of approximately 250 mm^3. The mice were then treated with 50 µl DMSO or 50 mg/kg of AI-9-59. Tumor measurements were taken every two days to assess the effect of the pro-drug on tumor growth. Overall, we did not detect any difference in tumor growth (Figure 6A). The mice that received 50 mg/kg injections of AI-9-59 showed signs of drug-related toxicity including weight loss (Figure 6B), and reduction in spleen size (Figure 6C).

Figure 6. End point analysis of NSG mice engrafted with 720 T-ALL cells and treated with DMSO or 50 mg/kg AI-9-59.

A. Relative tumor growth of NSG treated with 50 µl of 50 mg/kg or DMSO. Linear regression analysis showed no significant difference in the rate of tumor growth (n=10 per group). Error bars represent S.D.

B. Change in body weight of mice before the treatment and 9 days post-treatment (n=10 per group). Significance relative to DMSO treatment was determined by two-tailed student t-test. Error bars represent S.D.

C. Change in relative spleen weight of mice post-treatment (n=10 per group). Significance relative to DMSO treatment was determined by two-tailed student t-test. Error bars represent S.D.
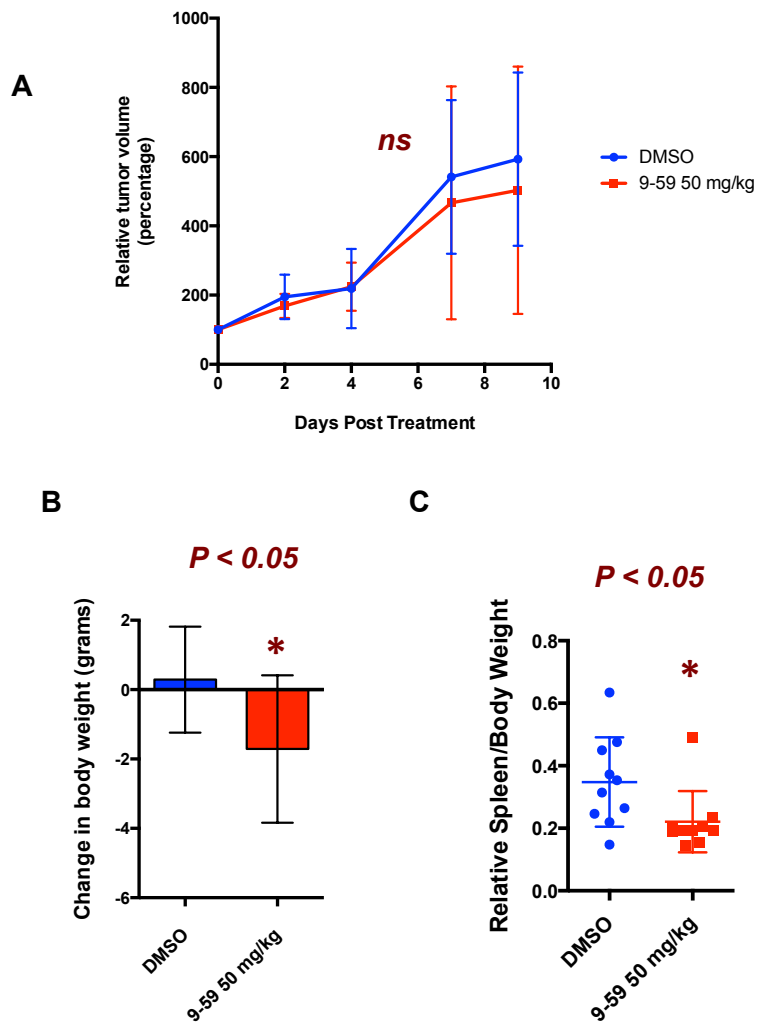
FACS analysis of hematopoietic lineages in the peripheral blood showed that AI-9-59 had no effect on the percentage distribution of the granulocyte (Figure 8A) and B-lymphocyte (Figure 8B) populations. Analysis of the bone marrow progenitor populations showed that the pro-drug AI-9-59 did not significantly affect the distribution of LK, LSK or LKS- progenitor populations (Figure 8C-E). Further analysis of the LKS- cells by surface markers CD34 and CD16/32 revealed that AI-9-59 treatment induced a small but significant increase in the granulocyte-macrophage progenitors (GMPs) but not in the common myeloid progenitors (CMPs) nor in the megakaryocyte-erythrocyte progenitors (MEPs) (Figure 8F-H) populations.

In addition, we continued to observe symptoms of toxicity including unkempt coat due to decreased grooming, lethargy, and rapid weight loss. Moreover, in mice that received AI-9-59, we observed signs of gastro-intestinal toxicity including dilation of small and large intestines as well as abnormal accumulations of food and gas in the gastrointestinal tract. Taken together, our findings showed that the pro-drug AI-9-59 had toxic effects on mice but did not reduce the growth of leukemia cells in mouse models.

Figure 7. Flow cytometry analysis of peripheral blood and bone marrow cells from NSG mice engrafted with 720 T-ALL cells and treated with DMSO or 50 mg/kg AI-9-59.

A. Schematic representing the gating strategy for the FACS analysis of the peripheral blood.

B. A schematic representing the gating strategy for the FACS analysis of the bone marrow.
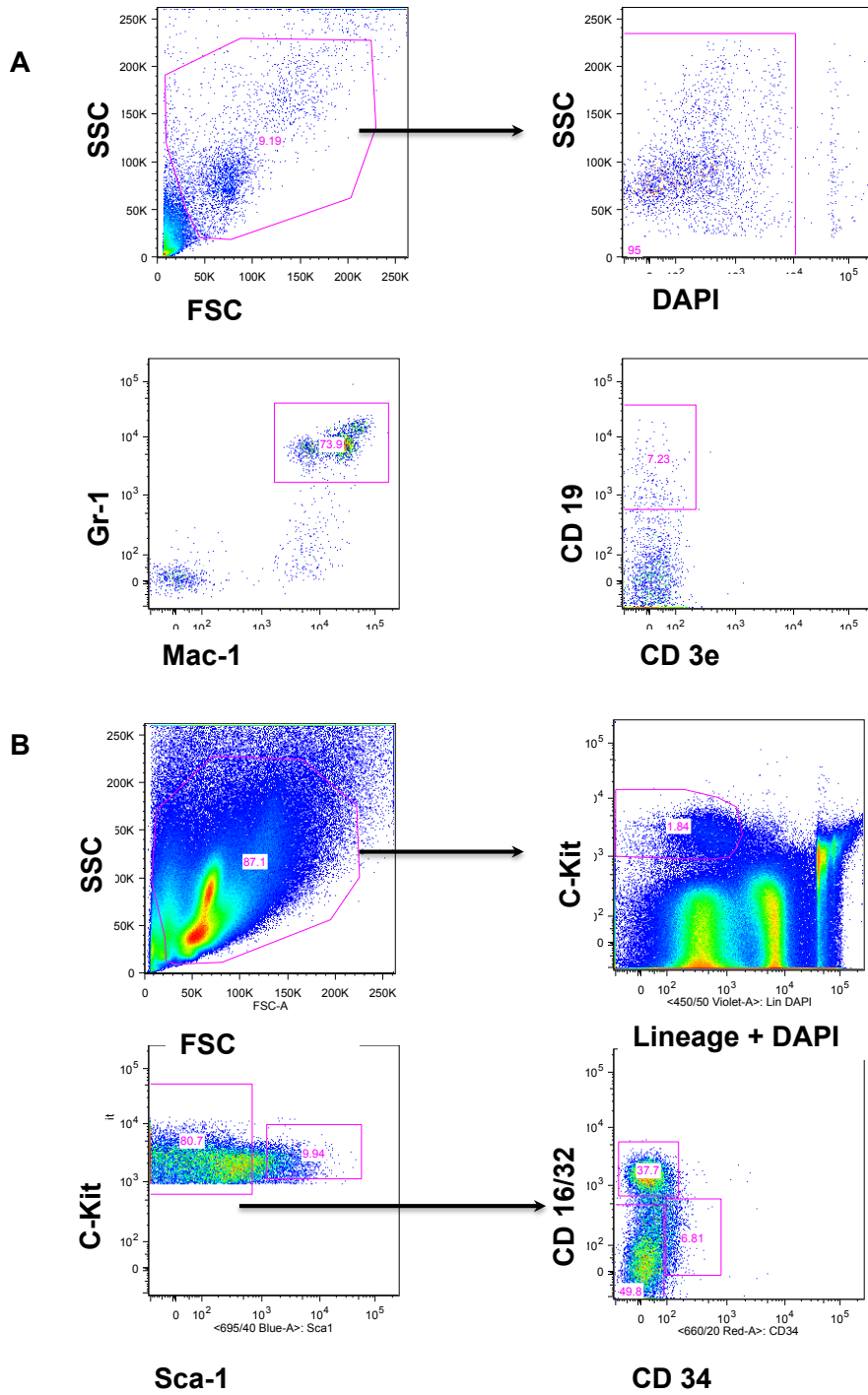
Figure 8. Toxicity analysis of peripheral blood and bone marrow cells from NSG mice engrafted with 720 T-ALL cells and treated with DMSO or 50 mg/kg AI-9-59.

The specific populations are represented as mean percentage of total live cell (n=10 per group). Error bars represents the S.D. Significance relative to DMSO treatment was determined by two-tailed student t-test in all comparisons.

A-B. Percentage of Gr-1 and Mac-1 positive granulocyte population (A) and CD19 positive B lymphocyte population (B) in the peripheral blood of NSG mice treated with DMSO or 50 mg/kg AI-9-59. n=10 per group in all comparisons and the specific populations are represented as mean percentage of total live cells. Error bars represent the S.D. Significance relative to DMSO treatment was determined by two-tailed student t-test in all comparisons.

C-E. Percentage of bone marrow progenitor population in NSG mice treated with DMSO or 50 mg/kg AI-9-59: (C) lineage negative c-Kit positive (LK) population, (D) lineage negative c-Kit positive and Sca-1 positive (LSK) population, and (E) lineage negative c-Kit positive and Sca-1 negative (LKS-) population.

F-H. Percentage of each progenitor compartment in LKS- progenitor cells from NSG mice treated with DMSO or 50 mg/kg AI-9-59: (F) common myeloid progenitors [CMP: LKS- CD34(+) CD16/32(-)], (G) megakaryocyte/erythroid progenitors [MEP: LKS- CD34(-) CD16/32(-)], and (H) granulocyte/monocyte progenitors [GMP: LKS- CD34(+) CD16/32(+)] populations.
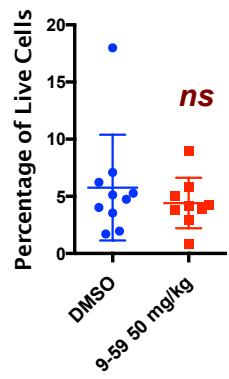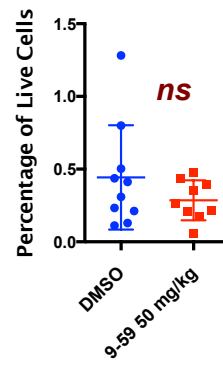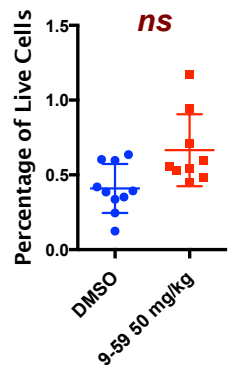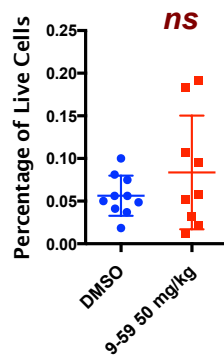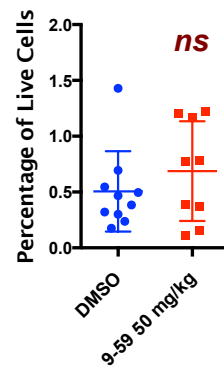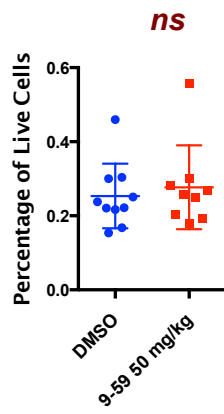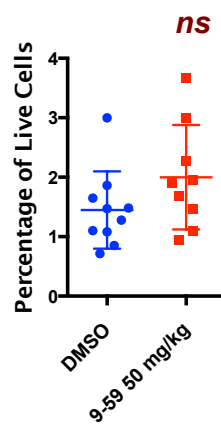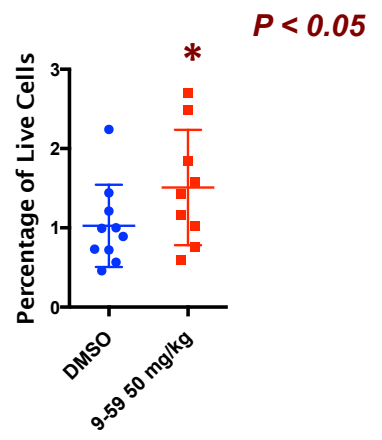
Discussion

Based on our findings that the Runt domain inhibitors reduce growth of multiple leukemia cell lines and diminish the clonogenic potential in t(8;21) AML patient samples, we developed a pro-drug AI-9-59 with improved solubility and pharmacokinetic properties to study the potential *in vivo* efficacies of AI-9-59 in mouse models. In our pilot experiment, we determined that daily injections of AI-9-59 at 100 mg/kg was toxic to mice by the fourth dose, and observed a small but statistically significant improvement in the survival of mice that received 25 mg/kg AI-9-59. However in subsequent experiments using two different mouse models, we did not detect any inhibitory effect of AI-9-59 on the growth of leukemia cells. Therefore our data suggested that the pro-drug AI-9-59 was toxic to the mice but had no on-target anti-leukemic effects.

To further assess whether AI-9-59 had any effect on hematopoietic cells, we used flow cytometry to analyze the bone marrow cells of mice that had been xenografted subcutaneously with T-ALL cells, and treated with 50 mg/kg AI-9-59. FACS analysis revealed no perturbation in the distribution of different hematopoietic lineages, or in the frequency of hematopoietic progenitors LK and LSK populations in the bone marrow of mice treated with AI-9-59. On the other hand, we observed a small but significant increase in the frequency of granulocyte macrophage progenitors (GMPs) in mice that received AI-9-59 at 50 mg/kg. Interestingly, deletion of Runx1 was previously reported to induce a three-fold expansion in GMPs but not in other progenitors (94). Therefore the expansion in GMP population we observed could be the result of AI-9-59's on-target inhibition of Runx1 functions in hematopoietic progenitors.

Our efforts towards studying the potential efficacy of the pro-drug were further hampered by the fact that AI-9-59 was toxic to mice at concentrations above 50 mg/kg.

The observed signs of toxicity included lethargy and weight loss. The rapid weight loss after four doses suggested that the toxicity could be gastrointestinal. Indeed, in the mice that received AI-9-59 we observed signs of gastrointestinal toxicity including dilation of small and large intestines, and abnormal accumulations of food and gas in gastrointestinal tract. These symptoms were strikingly similar to symptoms described in a mouse model of chronic intestinal pseudo-obstruction (CIPO) using smooth muscle specific inactivation of the SRF gene (197). Coincidentally, Runx1 levels were reported to be significantly reduced in a subset of CIPO patients (198). Furthermore, another member of the core binding factors Runx3 is known to play an important role in the gastrointestinal development and gastric cancer. Runx3 null mice exhibited gastrointestinal hyperplasia due to stimulated proliferation and suppressed apoptosis in epithelial cells (87). All the data suggest the possibility the CIPO-like phenotypes observed in treated mice could be attributed to AI-9-59's on-target repression of RUNX functions in the gastrointestinal track.

The lack of growth inhibitory effect on leukemia cells also raised the possibility that the concentration of AI-9-59 necessary to inhibit RUNX functions in leukemia cells exceeded the maximum tolerated dose in mice. In other words, the lack of efficacy on the growth of leukemia cells could be attributed to low level of AI-9-59 in the serum. In order to determine the on-target effect of the pro-drug on leukemia cells, I propose a future experiment in which we would treat the transplanted mice with DMSO or the pro-drug AI-9-59 at 50 mg/kg. After the completion of treatment regimen of 9 total doses, we would isolate the leukemia bone marrow cells based on GFP as a marker, isolate mRNA and conduct RT-PCR to compare the expression of known Runx1 target genes as well as the expression of genes identified from our microarray analysis. We could also harvest cells from the small and large intestines of mice treated with AI-9-59 to assess

the expression of Runx1 and Runx3, in order to determine whether the GI toxicity is RUNX-related.

Furthermore, DMSO was reported to induce apoptosis and *in vivo* toxicity in mice at concentrations lower than 10% vol/vol, and a concentration of less than 1% DMSO vol/vol was recommended to dissolve compounds to avoid potential solvent toxicity (199). Therefore for future studies, we should explore alternative solubilizing strategies for dissolving the pro-drug.

For future development of the Runt domain inhibitor pro-drugs, a detailed toxicology and pharmacokinetic studies would need to be conducted prior to determining the *in vivo* efficacy of the compound. Additionally, the effects on normal mouse hematopoietic cells will also need to be assessed through methods such as clinical blood counts and gene expression profiling of bone marrow cells harvested from treated mice.

Chapter III: Conditional expression of AML1-ETO in hematopoietic cells

Zaw Min Oo[1], Xiongwei Cai[1], and Nancy A. Speck[1]

[1]Abramson Family Cancer Research Institute and Department of Cell and Molecular Biology, University of Pennsylvania, Philadelphia, Pennsylvania, USA, 19104

All figures within this chapter were contributed primarily by Zaw Min Oo.

AML1-ETO knock in mouse strain was generated by Dr. James R Downing.

NRAS^{G12D} knock in mouse strain was generated by Dr. Tyler Jacks.

The text of this chapter was written primarily by Zaw Min Oo.

Introduction

The 8;21 translocation t(8;21)(q22;q22) is one of the most common genetic aberrations in *de novo* AML, occurring in 10% of adult and 12% of pediatric AMLs (96, 106, 107). The translocation fuses the N-terminal 177 amino acids of Runx1 (also known as AML1, encoded by *RUNX1*) to ETO (eight twenty-one, encoded by *RUNX1T1*), generating the chimeric protein AML1-ETO. Although AML1-ETO is known to be an essential causative agent for t(8;21) AML, exactly how it affects hematopoietic stem and progenitor populations remains poorly understood. The chimeric protein was known to occupy a subset of RUNX1 target genes (200) and blocks differentiation at an early myeloid progenitor stage (201). Through its ETO moiety, AML1-ETO is able to recruit co-repressor proteins including N-CoR (115), and AML1-ETO expression is associated with a repressive chromatin structure characterized by reduced levels of histone H3 acetylation (202). Therefore, the chimeric protein was thought to act as a dominant negative inhibitor of Runx1 functions (124), although recent findings are starting to challenge this simplistic model (203, 204). Specifically, Mx1-Cre mediated Runx1 deficient cells exhibit much more severe lineage defects than cells expressing AML1-ETO (125, 205-207). Furthermore, patients with inactivating Runx1 mutations exhibit much severe phenotypes compared to t(8;21) AML patients.

Numerous studies have demonstrated that full-length AML1-ETO is not capable of initiating leukemia on its own (184-188). The requirement of additional cooperating mutations commonly in the receptor tyrosine kinases (189-192) for leukemogenesis suggested that AML1-ETO induces a pre-leukemic state in hematopoetic cells. Therefore a detailed mouse model study of how AML1-ETO affects hematopoietic stem and progenitor cells (HSPCs) is needed. The understanding of the cellular processes

104

underlying AML1-ETO mediated transformation of HSPCs would allow us to identify novel therapeutic targets for improving the treatment of t(8;21) leukemia.

In an effort to better understand effects of Runx1 deficiency on HSCs and progenitors, we used Vav1-Cre to specifically delete Runx1 in hematopoietic cells and study the effects systematically (101). We propose to employ the same Vav1-cre mediated excision strategy to examine the impact of a conditionally activated AML1-ETO allele (125) on the hematopoietic stem and progenitor cells and their properties. In combination with the data from Vav1-Cre mediated Runx1 deletion, our finding from AML1-ETO expression may help explain how t(8;21) and Runx1 deficiency each gives rise to clinically distinct hematological malignancies.

Materials and Methods

Mice

All mouse procedures were approved by the University of Pennsylvania University Animals Resource Center (ULAR) and Institutional Animal Care and Use Committees (IACUC) of the University of Pennsylvania.

The conditional AML1-ETO knock-in mice and NRAS^{G12D} mice were bred and maintained as previously described (125, 208).

Transplant

F1 progeny of C57BL6/J (Ly5.2) females crossed to B6.SJL-*Ptprc^{a}Pepc^b/*BoyJ males were used as transplant recipients. All donor cells were Ly5.2 (CD45.2$^+$). Bone marrow chimeras were established by injecting donor bone marrow cells along with 2×10^5 B6.SJL (competitor CD45.1/Ly5.1) marrow cells into lethally-irradiated (split dose 900 cGy 3 hours apart) recipients. Engraftment was scored as ≥1% donor derived cells.

Cell purification and flow cytometry

Flow cytometry analyses were performed on BD LSRII (BD Bioscience, San Jose CA). Subsequent data analyses were carried out using Flowjo (Treestar Inc, Ashland OR). Lineage depletion of bone marrow was achieved using the MACS Lineage Cell Depletion Kit, MidiMACS LS Separation units, and the QuadroMACS Multistand (Miltenyi) according to the manufacturer's instructions. In some cases erythrocytes were lysed in an RBC Lysis Buffer (eBioscience, San Diego, CA) prior to lineage depletion.

The following monoclonal antibodies (BD Bioscience and/or eBioscience, San Diego CA) were used for staining: FITC-CD16/32 (2.4G2), APC-CD34 (RAM34), APC-Cy7-cKit (2B8), PE-Flt3 (A2F10), PE-Cy7-Sca1 (D7), APC-CD45.1 (A20), FITC CD45.2 (104), PE-Cy7-Mac1 (M1/70), PerCP-Cy5.5-Gr1 (RB6-8C5), APC-CD3e (145-2C11), PE-CD19 (1D3). Dead cells were stained with DAPI.

Data analyses for flow cytometry were carried out using FlowJo (Treestar Inc, Ashland OR).

CFU-C Assay

Mouse bone marrow cells were thawed and cultured in RPMI 1640 with 10% FBS for two hours. Live cells were washed and recovered, and subsequently plated in in Methocult GF M3434 (Stem Cell Technologies) and incubated in 5% CO_2 at 37°C for 7 days. All classes of myeloid and/or erythroid colonies consisting of at least 40 cells were counted according to manufacturer's recommendations.

Lineage analysis of bone marrow cells from Vav1-Cre; AML1-ETO mice

To characterize the effect of AML1-ETO expression on HSCs and committed progenitors, we used Vav1-Cre to conditionally activate AML1-ETO expression in hematopoietic cells. Flow cytometry analysis of bone marrow cells isolated from 6-8 week old Vav1-Cre; AML1-ETO mice revealed a slightly lower percentage of CD19^{+} B-lymphocytes compared to littermate controls. We detected no significant difference in the percentage of Gr-1^{+} Mac-1^{+} granulocytes as well as in the CD3e^{+} T lymphocyte populations (Figure 1 A-B).

Figure 1. Lineage analysis of bone marrow cells from Vav1-Cre; AML1-ETO and WT mice.
A. Schematic representing the gating strategy for the FACS analysis.
B. Comparisons of granulocytes, B-lymphocytes, and T-lymphocytes populations in the bone marrow of Vav1-Cre; AML1-ETO mice and littermate controls (n=8 per group). Error bars represents the S.D. Significance relative to WT was determined by two-tailed student t-test in all comparisons.
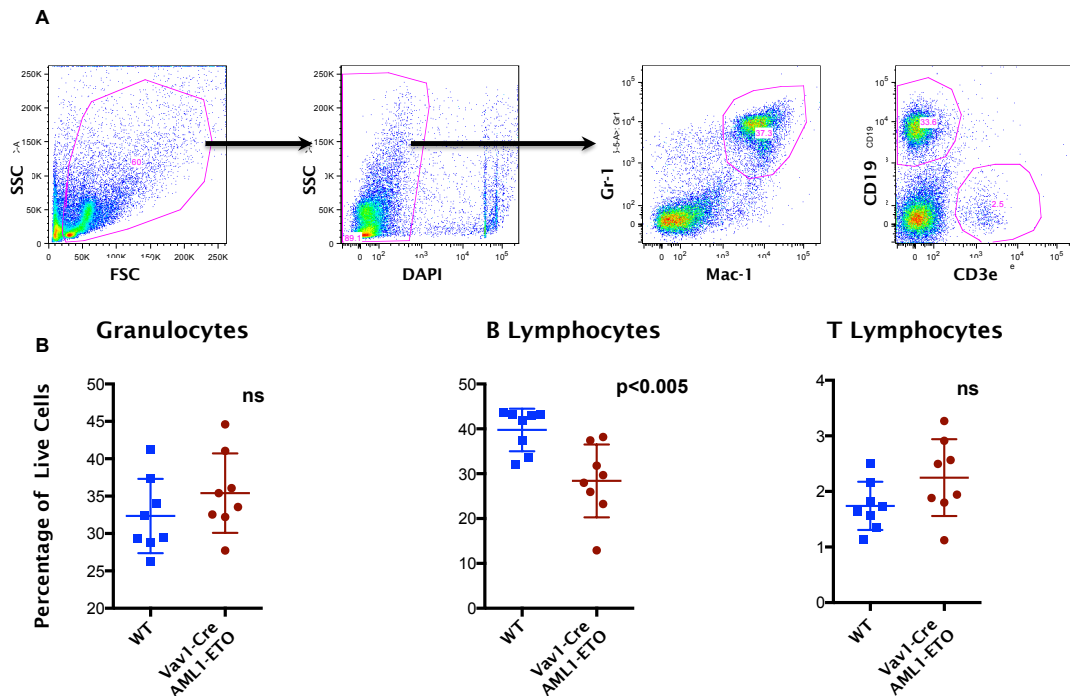
Phenotypic HSC analysis of bone marrow cells from Vav1-Cre; AML1-ETO mice

AML1-ETO expressing BM cells contain a higher percentage of the lineage$^-$ Sca-1$^+$ cKit$^+$ progenitor populations. Further analysis of the LSK cells by staining for CD34 and Flt3 revealed a significant increase in the short-term HSCs (ST-HSCs) population defined as LSK CD34$^-$ Flk2$^+$, but not in the long-term HSCs (LT-HSCs) LSK CD34$^-$ Flk2$^-$ population (Figure 2 A-B).

Figure 2. Phenotypic HSC analysis of bone marrow cells from Vav1-Cre; AML1-ETO and WT mice.

A. Schematic representing the gating strategy for the FACS analysis.

B. Comparisons of LSK,ST-HSC, and LT-HSC populations in the bone marrow of Vav1-Cre; AML1-ETO and WT mice. n=8 per group. Error bars represents the S.D. Significance relative to WT was determined by two-tailed student t-test in all comparisons.
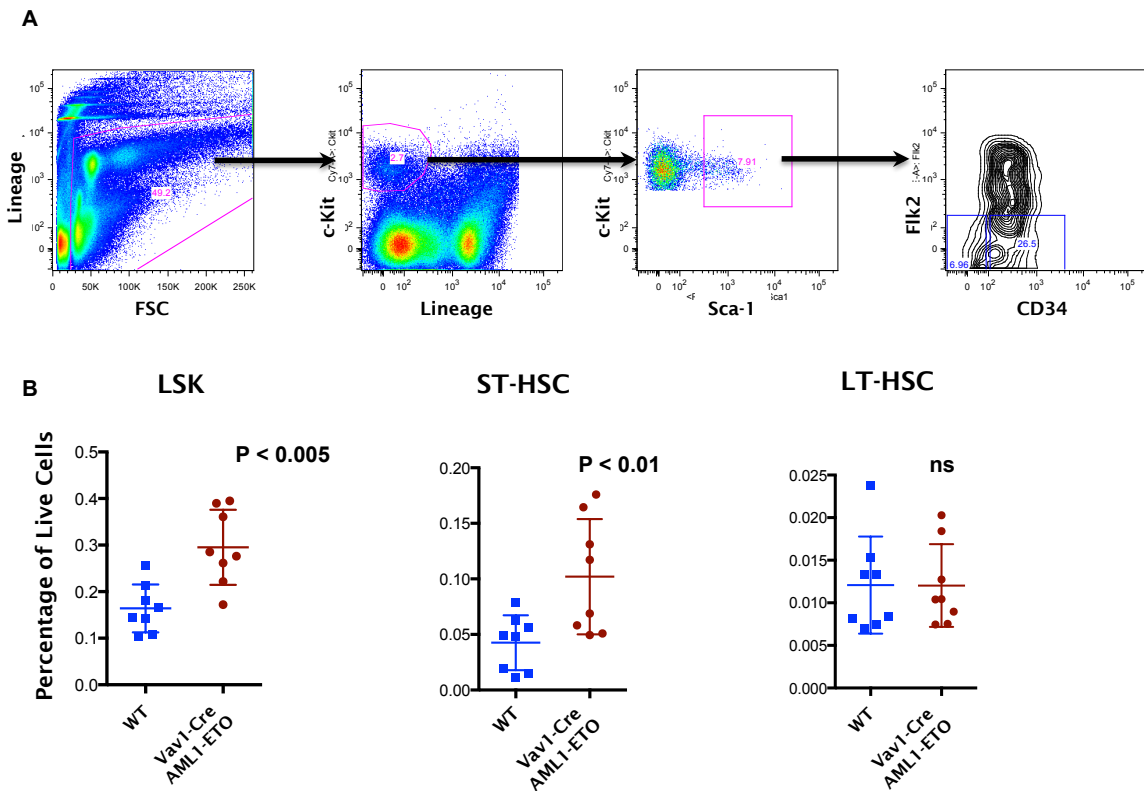
Analysis of functional HSC frequency in AML1-ETO mice

In order to determine the functional capability and the frequency of hematopoietic stem cells in the bone marrow of mice expressing AML1-ETO, we conducted a competitive repopulation assay. Peripheral blood FACS analysis revealed that AML1-ETO expressing donor bone marrow cells had a significant reduction in their ability to reconstitute CD3e positive^{+} T lymphocytes and Gr-1^{+} and Mac-1^{+} granulocyte populations in the irradiated host (Figure 3 B). We also determined that AML1-ETO expressing bone marrow cells contained a lower frequency of functional hematopoietic stem cells (Figure 4).

Figure 3. Competitive limited dilution transplant to assess the frequency of functional HSCs in AML1-ETO expressing mice.

A. Schematic of the competitive limited dilution transplant. Bone marrow from 6-8 week old *AML1-ETO*;Vav1-Cre mice was injected along with 2×10^5 Ly5.1$^+$ adult bone marrow cells into irradiated Ly5.1/5.2 recipients. Contribution of Ly5.2$^+$ cells to peripheral blood was assessed. Recipients with ≥1% donor-derived cells at ≥16 weeks were deemed reconstituted.

B. Flow cytometry analysis of peripheral blood from recipient mice transplanted with various numbers of Vav1-Cre; AML1-ETO bone marrow cells or WT control cells. Contribution of Ly5.2$^+$ (CD45.2$^+$) cells to various lineage compartments of the peripheral blood was assessed at three months post-transplant.

111
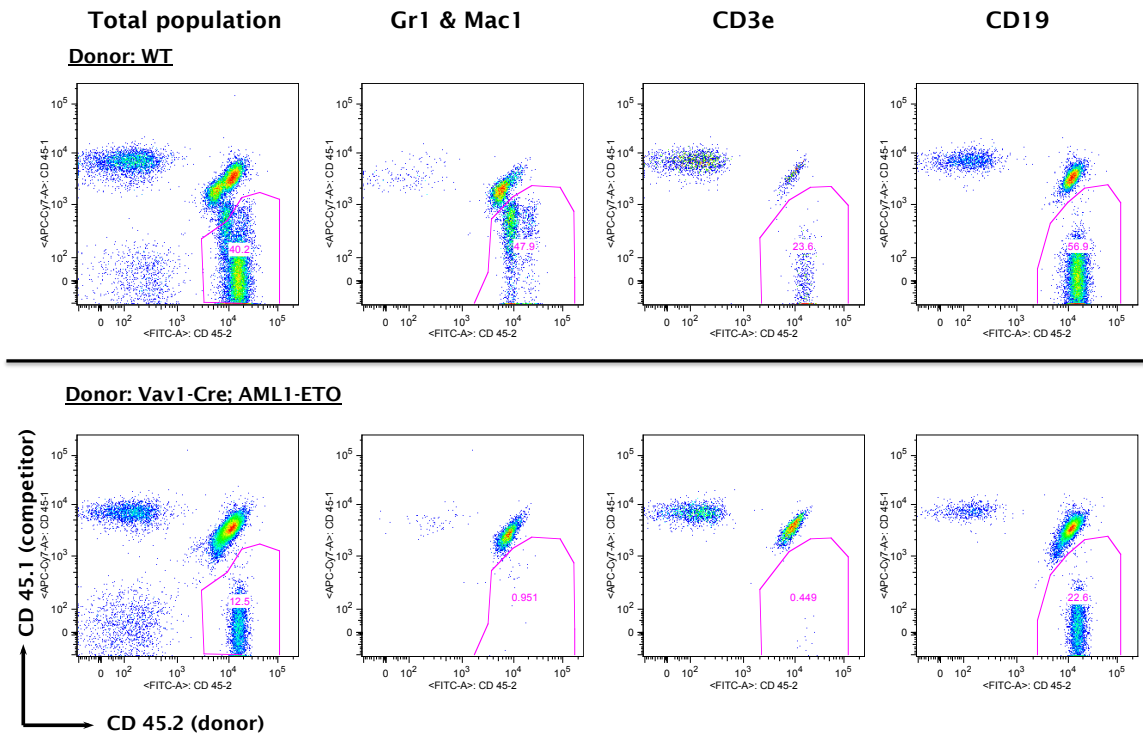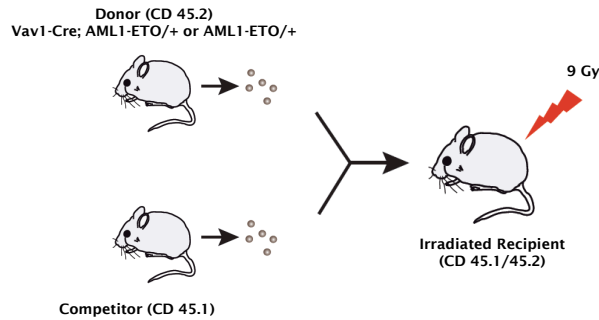
Figure 4. Expression of AML1-ETO leads to lower functional HSCs.

Bone marrow from 6-8 week old AML1-ETO;Vav1-Cre mice was injected along with 2×10^5 Ly5.1$^+$ adult bone marrow cells into irradiated Ly5.1/5.2 recipients. Contribution of Ly5.2$^+$ cells to peripheral blood was assessed. Recipients with ≥1% donor-derived cells at ≥16 weeks were deemed reconstituted.
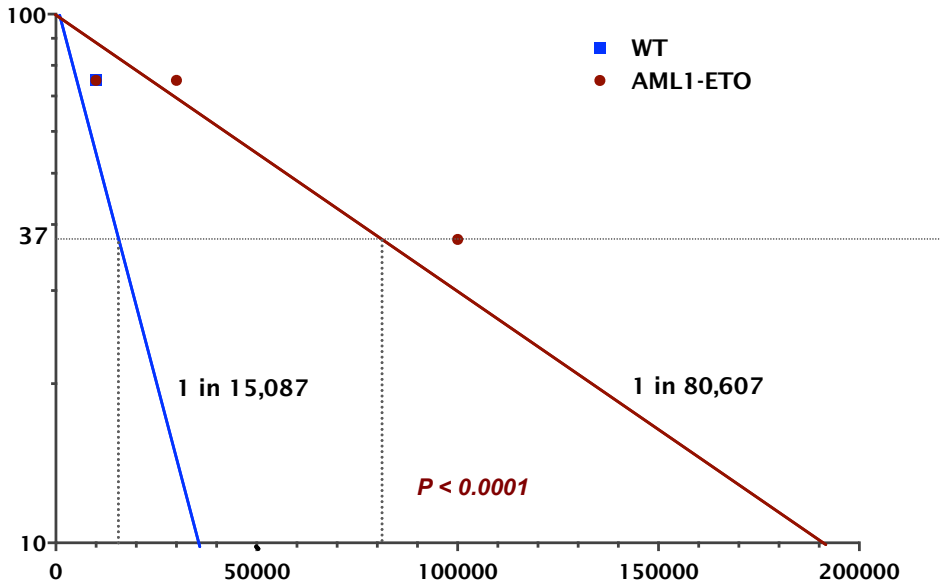
Co-expression of AML1-ETO and activated NRAS (NRAS^{G12D}) in hematopoietic compartments

We examined whether the conditional expression of AML1-ETO could cooperate with activated NRAS to give leukemia. We crossed AML1-ETO to NRAS^{G12D} background. Mice expressing both AML1-ETO and NRAS^{G12D} developed hematological disease around 6 months old. The disease could be successfully transplanted into lethally irradiated secondary recipients, and FACS analysis of the peripheral blood showed the malignant cells to have expanded Gr1$^+$ Mac1$^+$ granulocyte population but negative for T- and B-lymphocyte makers (Figure 5A). FACS analysis of also revealed an increase in the percentage of Lin$^-$ c-Kit$^+$ (LK) progenitors in bone marrow and spleens of mice transplanted with Vav1-Cre; AML1-ETO; NRAS^{G12D} cells (Figure 5B).

Figure 5. Co-expression of AML1-ETO and activated NRAS (NRAS^{G12D}) in hematopoietic compartments leads to development of hematological disorder.

A. FACS analysis of peripheral blood of mice transplanted with malignant cells from Vav1-Cre; AML1-ETO; NRAS^{G12D} primary mouse.

B. FACS analysis of bone marrow and spleen cells of mice transplanted with malignant cells from Vav1-Cre; AML1-ETO; NRAS^{G12D} primary mouse.
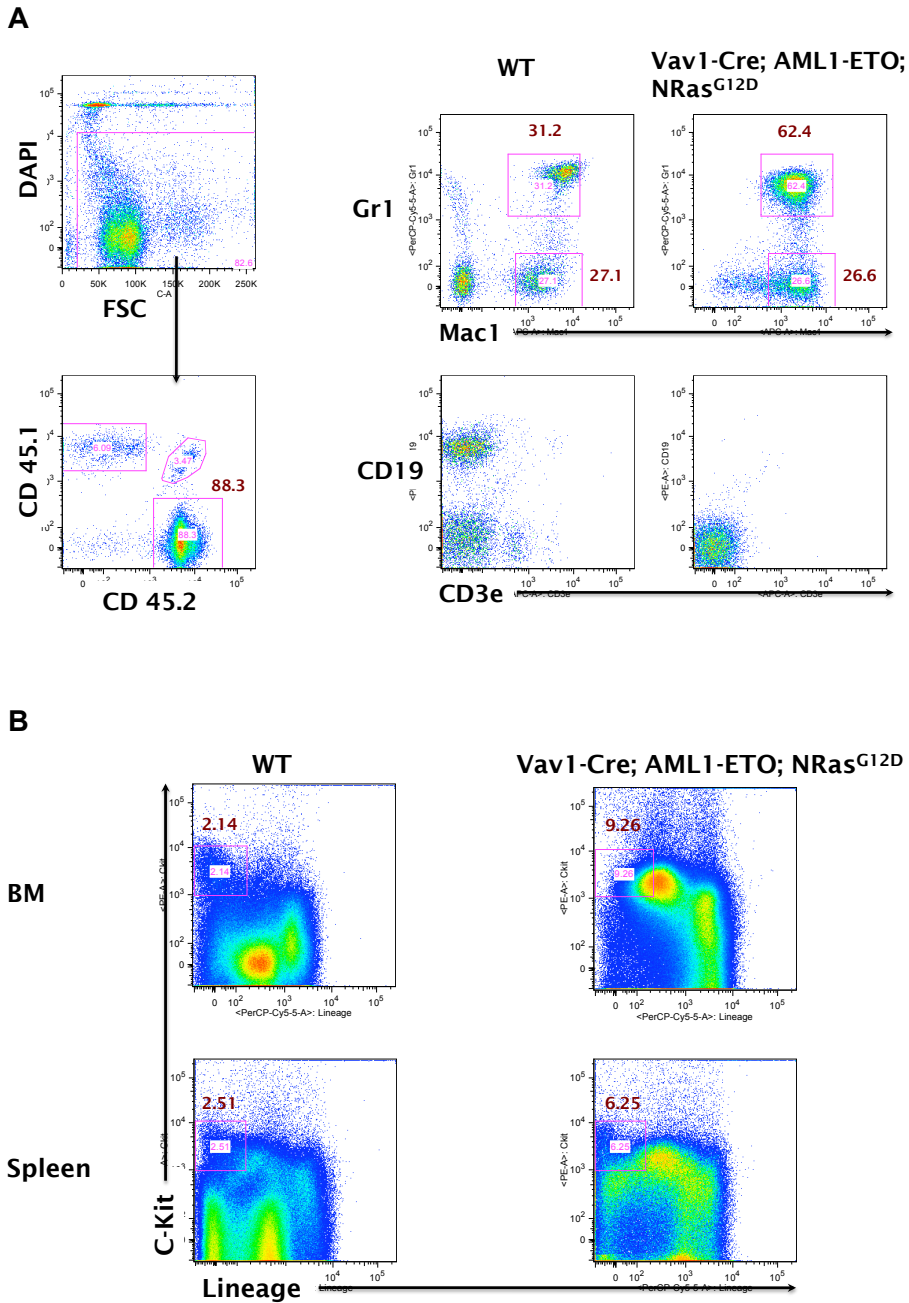
RDIs reduced progenitor activity in Vav1-Cre; AML1-ETO; NRAS^{G12D} bone marrow cells

We used CFU-C assays to assess whether the malignant bone marrow cells expressing AML1-ETO and NRAS^{G12D} through Vav1-Cre were sensitive to RDIs. The active compounds AI-8-45 and AI-9-54, but not the control compound AI-7-54 significantly reduced colony formation of the Vav1-Cre; AML1-ETO*;* NRAS^{G12D} malignant bone marrow cells (Figure 6). Similar to our previous study, neither AI-8-45 nor AI-9-54 had any effect on colony formation by normal mouse bone marrow cells.

Figure 6. Malignant hematopoietic cells from Vav1-Cre; AML1-ETO; NRAS^{G12D} are senstitive to RDIs.

Various concentrations of compounds were added to methylcellulose cultures containing 20,000 wild type bone marrow cells or 20,000 Vav1-Cre; AML1-ETO; NRAS^{G12D} malignant mouse bone marrow. All compounds were dissolved in DMSO (final concentration 0.2%). Colonies were counted 7 days after plating. Error bars represent SD. Significance relative to DMSO was determined by one-way ANOVA and Dunnett's multiple-comparison.
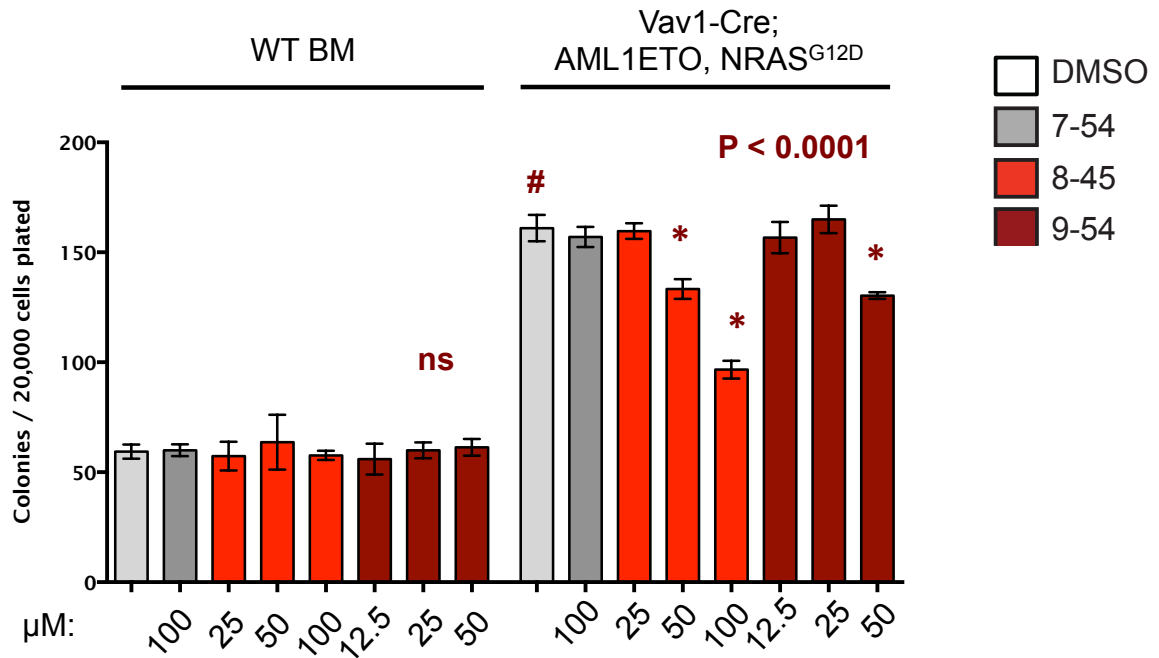
Discussion

From our study using Vav1-Cre to conditionally induce AML1-ETO expression in hematopoietic cells, we determined that expression of AML1-ETO led to a small reduction in the frequency of B lymphocytes marked by CD19, but not in the frequency of T lymphocytes and granulocytes in the bone marrow. Similar to our finding, another study used a doxycycline-inducible expression of AML1-ETO and also found reduction in the frequency of B200[+] B lymphocytes in the bone marrow (209). The study proceeded to demonstrate that DOX-inducible expression of AML1-ETO did not significantly affect hematopoietic stem and progenitor cells, but specifically expanded the GMP population. The expansion in the GMP population seemed to be biologically significant, as the study proceeded to demonstrate that prolonged expression of AML1-ETO led to a myeloproliferative disease (MPD) –like leukemia, and that the leukemic GMP acquired leukemia stem cell properties.

We have previously reported that the frequency of phenotypic HSCs as defined by immuno-phenotyping did not necessarily correlate with the actual number of functional HSCs (97), which are defined by their ability to reconstitute hematopoiesis in irradiated hosts in bone marrow transplantation assays. Indeed, our transplantation experiments revealed that AML1-ETO expressing bone marrow cells contained five-fold fewer functional hematopoietic stem cells (HSCs). Furthermore, the AM1-ETO expressing cells were defective in their ability to generate granulocytes and T lymphocytes.

In addition, we showed that conditional expression of AML1-ETO and NRAS[G12D] induced a malignant state marked by abnormal expansion of Mac1^{+} Gr1^{+} myeloid cells, and that the disease could be transplanted into secondary recipients. One caveat of this

study is that we did not confirm the conditional expression of AML1-ETO and NRAS^{G12D} beyond simple PCR genotyping. Therefore, it is unknown whether the malignant state was caused by activation of single or both transgene. However, we detected by CFU-C assay that the malignant bone marrow cells were sensitive to the Runt domain inhibitors that we described in the previous chapters.

Closing Remarks And Future Directions

This thesis project was aimed at developing and characterizing a novel class of targeted therapy for leukemia. The goal of targeted therapy is to translate our understanding of the molecular programs associated with the pathology of disease into treatments with a markedly improved therapeutic index. In the field of leukemia, the majority of such studies have focused on targeting components of receptor signaling pathways. One major success story is the small molecule imatinib, which acts by targeting the ATP binding pocket of the ABL kinase to block the tyrosine kinase activity of BCR-ABL in chronic myelogenous leukemia (CML) (210, 211). The development of imatinib represented a major improvement in CML treatment, and several tyrosine kinase inhibitors (TKIs) have emerged as important therapeutic agents for a variety of human malignancies. However the application of this approach in leukemias that harbor more complex genetic alterations has been less successful (212).

Many cancers either directly involve transcription factors, or indirectly modulate transcription factor activity; and a variety of transcription factors have been identified as driving agents promoting tumorigenesis and cancer progression (1). Therefore, inhibition of protein-protein interactions involving transcription factors has a high therapeutic potential (2). One recent success story is the development of Nutlin family of small molecules (6). Nutlin inhibits the interaction of MDM2 with p53, leading to stabilization of p53 level and enhanced p53 mediated apoptosis (10-13). Additionally, several small molecule inhibitors targeting the transcription factors such as Notch1 and STAT3 have reported (213, 214). These results demonstrate that targeting transcription factors with small molecules is feasible and provide validation for our proposal to develop inhibitors of the Runt domain:CBFβ interaction for treatment of leukemia cells.

117

Through our functional characterization of the Runt domain:CBFβ complex, we identified amino acid residues on the Runt domain that contribute to major binding energy of the RD:CBFβ interaction. By mutating these residues on the RD of AML1-ETO, we demonstrated that the interaction with CBFβ is required for AML1-ETO's ability to transform hematopoietic cells and induce leukemia in mice. Therefore, we established the RD:CBFβ interface as an interface suitable for targeting with small molecules. Additionally, recent studies have provided strong experimental evidence that normal CBF functions are required for the maintenance of leukemic stem cell functions in a certain subset of leukemia, including t(8;21), inv(16), and MLL-AF9 leukemia (145, 146). These findings suggest that these leukemias may be particularly sensitive to perturbations in CBF activity output and further support our rationale for developing small molecules targeting the RD:CBFβ interface.

Indeed, here we describe the development of a novel class of small molecule inhibitors that binds to the Runt domain of RUNX proteins and inhibits their interaction with CBFβ. These Runt domain inhibitors reduced growth of multiple leukemia cell lines, and decreased the clonogenic potential of t(8;21) patient samples while having little effect on normal bone marrow cells. The inhibitors showed clear effects on the expression of well-characterized RUNX1 target genes. Analysis of genome-wide changes in gene expression identified RUNX regulated pathways to be significantly affected by the inhibitors.

Based on our *in vitro* findings, we developed a pro-drug AI-9-59 with improved solubility and pharmacokinetic properties, and set out to study the potential *in vivo* efficacies of AI-9-59 in mouse leukemia models. However, we did not detect any inhibitory effects of AI-959 against the growth of leukemia cells in two different mouse models. This suggests that the pro-drug we have developed had no *in vivo* efficacy.

Our efforts towards studying the potential efficacy of the pro-drug were further hampered by the fact that AI-9-59 was toxic to mice at concentrations above 50 mg/kg. The gastrointestinal toxicity in the mice that received AI-9-59 was strikingly similar to symptoms described in a mouse model of chronic intestinal pseudo-obstruction (CIPO) (197). Coincidentally, Runx1 levels were significantly reduced in a subset of CIPO patients (198). Furthermore, another member of the core binding factors Runx3 is known to play an important role in gastrointestinal epithelial cells (87). Therefore, the CIPO-like phenotypes observed in AI-9-59 treated mice could be attributed to on-target repression of RUNX functions in the gastrointestinal track. Flow cytometry analysis also revealed that AI-9-59 induced a small but significant increase in the frequency of granulocyte macrophage progenitors (GMPs). Interestingly, deletion of Runx1 was previously reported to induce expansion in the GMPs (94), suggesting that the expansion in GMP population could be the result of AI-9-59's on-target inhibition of Runx1 functions. Together, the data suggested the possibility that the plasma level of AI-9-59 was too low to significantly affect growth of leukemia cells, but high enough to suppress RUNX functions in the intestines. This lack of selectivity against leukemia cells could be due to the nature of the RDI that we developed: the drug was interfering with RD:CBFβ interaction in both AML1-ETO and the wild type core binding factors.

In order to establish the on-target effect of the pro-drug on leukemia cells, I propose future experiments in which we would treat the transplanted mice with DMSO or the pro-drug AI-9-59 at 50 mg/kg. After the completion of treatment regimen of 9 total doses, we would isolate the leukemia bone marrow cells based on GFP marker, isolate mRNA and conduct RT-PCR to compare the expression of known Runx1 target genes as well as the expression of genes identified from our microarray analysis. We could also harvest cells from the small and large intestines of mice treated with AI-9-59 to

assess the expression of Runx1 and Runx3, in order to determine whether the GI toxicity is RUNX-related.

For future development of the Runt domain inhibitor pro-drugs, a detailed toxicology and pharmacokinetic studies would need to be conducted prior to determining the *in vivo* efficacy of the compounds. We will also need to assess the effects inhibitors have on normal mouse blood cells by using clinical blood counts (CBCs). This will provide critical data on potential side effects involving the blood cell lineages. We will examine the effects of the compounds on hematopoietic progenitors using gene expression profiling. Furthermore, DMSO was reported to induce apoptosis and *in vivo* toxicity in mice at concentrations lower than 10% vol/vol, and a concentration of less than 1% DMSO vol/vol was recommended to dissolve compounds to avoid potential solvent toxicity (199). Therefore for future studies, we should explore alternative solubilizing strategies.

In order to minimize the side effects of treatment, we propose to develop selective inhibitors of AML1-ETO. Our study of the HHR domain of AML1-ETO showed that it mediates tetramer formation. Therefore, we could exploit the oligomeric nature of AML1-ETO by developing homodimeric inhibitors to achieve specificity towards AML1-ETO. The development of a homodimeric inhibitor against inv(16) represents one successful example (50). The monomeric version of the compound binds to CBFβ and disrupts interaction with Runx1, and the homodimeric inhibitor was developed by connecting two monomeric compounds through polyethylene glycol based linkers. This improved IC_{50} by 60-fold and enhanced the compound's specificity for CBFβ-SMMHC, the oncogenic transcription factor in inv(16) AML. We could adopt the same strategy to develop homodimeric version of RDIs, which should achieve both improvement in IC_{50} as well as in selectivity for AML1-ETO. Additionally, we could develop heterodimeric

inhibitors of AML1-ETO. In fact, we have screened for small molecules that bind to the nearby eTAFH domain and further optimized eTAFH domain inhibitors. It is our hypothesis that both the homodimer and heterodimer compounds will achieve greater selectivity for AML1-ETO and thereby provide a mechanism to selectively inhibit AML1-ETO while minimally affecting normal core binding factor function.

In addition to assessing our inhibitors' single agent efficacies, we will explore the potential of our inhibitors to synergize with other drugs such as imatinib, cytosine arabinoside, or vitamin D analogs. All of these drugs are well characterized in preclinical mouse leukemia models, thus dosing schedules are readily available.

RUNX proteins have now been implicated in numerous developmental pathways. In addition to their well-established role in leukemia, there is emerging evidence for their involvement in epithelial cancers. Although we were unable to demonstrate *in vivo* efficacy, the RDIs we have developed are still useful as tool compounds to study the function of RUNX proteins in various settings. The advantage of such small molecule tools, unlike genetic approaches, is the rapid inhibition of the target, the ability to monitor time-dependent effects, and the opportunity to withdraw inhibitor and monitor the return to the previous state. Therefore, these compounds could be very useful reagents for studying the effects of core binding factor loss in specific processes or developmental stages. For all these reasons, the RDIs provide a unique tool for studying RUNX protein function.

BIBLIOGRAPHY

1.   Colburn NH, Kensler TW. Targeting Transcription Factors for Cancer Prevention—the Case of Nrf2. Cancer Prevention Research. 2008;1(3):153-5.

2.   Arndt H-D. Small Molecule Modulators of Transcription. Angewandte Chemie International Edition. 2006;45(28):4552-60.

3.   Clackson T, Wells JA. A hot spot of binding energy in a hormone-receptor interface. Science. 1995;267:383-6.

4.   Thanos CD, DeLano WL, Wells JA. Hot-spot mimicry of a cytokine receptor by a small molecule. Proceedings of the National Academy of Sciences. 2006;103(42):15422-7.

5.   Moreira IS, Fernandes PA, Ramos MJ. Hot spots—A review of the protein–protein interface determinant amino-acid residues. Proteins: Structure, Function, and Bioinformatics. 2007;68(4):803-12.

6.   Chène P. Inhibiting the p53–MDM2 interaction: an important target for cancer therapy. Nat Rev Cancer. 2003;3(2):102-9.

7.   Soussi T, Wiman KG. Shaping Genetic Alterations in Human Cancer: The p53 Mutation Paradigm. Cancer cell. 2007;12(4):303-12.

8.   Muller PAJ, Vousden KH. p53 mutations in cancer. Nat Cell Biol. 2013;15(1):2-8.

9.   Poyurovsky MV, Katz C, Laptenko O, Beckerman R, Lokshin M, Ahn J, et al. The C terminus of p53 binds the N-terminal domain of MDM2. Nat Struct Mol Biol. 2010;17(8):982-9.

10.   Vassilev LT, Vu BT, Graves B, Carvajal D, Podlaski F, Filipovic Z, et al. In Vivo Activation of the p53 Pathway by Small-Molecule Antagonists of MDM2. Science. 2004;303(5659):844-8.

11.   Shangary S, Qin D, McEachern D, Liu M, Miller RS, Qiu S, et al. Temporal activation of p53 by a specific MDM2 inhibitor is selectively toxic to tumors and leads to complete tumor growth inhibition. Proceedings of the National Academy of Sciences. 2008;105(10):3933-8.

12.   Tovar C, Rosinski J, Filipovic Z, Higgins B, Kolinsky K, Hilton H, et al. Small-molecule MDM2 antagonists reveal aberrant p53 signaling in cancer: Implications for therapy. Proceedings of the National Academy of Sciences of the United States of America. 2006;103(6):1888-93.

13.   Efeyan A, Ortega-Molina A, Velasco-Miguel S, Herranz D, Vassilev LT, Serrano M. Induction of p53-Dependent Senescence by the MDM2 Antagonist Nutlin-3a in Mouse Cells of Fibroblast Origin. Cancer Research. 2007;67(15):7350-7.

14.   Berg T. Inhibition of transcription factors with small organic molecules. Current Opinion in Chemical Biology. 2008;12(4):464-71.

15.   Becker S, Groner B, Muller CW. Three-dimensional structure of the Stat3[beta] homodimer bound to DNA. Nature. 1998;394(6689):145-51.

16.   Song H, Wang R, Wang S, Lin J. A low-molecular-weight compound discovered through virtual database screening inhibits Stat3 function in breast cancer cells. Proceedings of the National Academy of Sciences of the United States of America. 2005;102(13):4700-5.

17.   Siddiquee K, Zhang S, Guida WC, Blaskovich MA, Greedy B, Lawrence HR, et al. Selective chemical probe inhibitor of Stat3, identified through structure-based virtual screening, induces antitumor activity. Proceedings of the National Academy of Sciences. 2007;104(18):7391-6.

18.   Ci W, Polo JM, Melnick A. B-cell lymphoma 6 and the molecular pathogenesis of diffuse large B-cell lymphoma. Current opinion in hematology. 2008;15(4):381-90.

19.   Phan RT, Dalla-Favera R. The BCL6 proto-oncogene suppresses p53 expression in germinal-centre B cells. Nature. 2004;432(7017):635-9.

20.   Ranuncolo SM, Polo JM, Dierov J, Singer M, Kuo T, Greally J, et al. Bcl-6 mediates the germinal center B cell phenotype and lymphomagenesis through transcriptional repression of the DNA-damage sensor ATR. Nat Immunol. 2007;8(7):705-14.

21.   Ranuncolo SM, Polo JM, Melnick A. BCL6 represses CHEK1 and suppresses DNA damage pathways in normal and malignant B-cells. Blood Cells, Molecules, and Diseases. 2008;41(1):95-9.

22.   Baron BW, Anastasi J, Montag A, Huo D, Baron RM, Karrison T, et al. The human BCL6 transgene promotes the development of lymphomas in the mouse. Proceedings of the National Academy of Sciences of the United States of America. 2004;101(39):14198-203.

23.   Cattoretti G, Pasqualucci L, Ballon G, Tam W, Nandula SV, Shen Q, et al. Deregulated BCL6 expression recapitulates the pathogenesis of human diffuse large B cell lymphomas in mice. Cancer cell. 2005;7(5):445-55.

24.   Cerchietti LC, Yang SN, Shaknovich R, Hatzi K, Polo JM, Chadburn A, et al. A peptomimetic inhibitor of BCL6 with potent antilymphoma effects in vitro and in vivo. Blood. 2008;113(15):3397-405.

25.   Polo JM, Dell'Oso T, Ranuncolo SM, Cerchietti L, Beck D, Da Silva GF, et al. Specific peptide interference reveals BCL6 transcriptional and oncogenic mechanisms in B-cell lymphoma cells. Nat Med. 2004;10(12):1329-35.

26.   Stogios P, Downs G, Jauhal J, Nandra S, Prive G. Sequence and structural analysis of BTB domain proteins. Genome Biology. 2005;6(10):R82.

27.   Ahmad KF, Melnick A, Lax S, Bouchard D, Liu J, Kiang C-L, et al. Mechanism of SMRT Corepressor Recruitment by the BCL6 BTB Domain. Molecular Cell. 2003;12(6):1551-64.

28.   Ghetu AF, Corcoran CM, Cerchietti L, Bardwell VJ, Melnick A, Privé GG. Structure of a BCOR corepressor peptide in complex with the BCL6 BTB domain dimer. Molecular cell. 2008;29(3):384-91.

29.   Cerchietti LC, Ghetu AF, Zhu X, Da Silva GF, Shijun Z, Matthews M, et al. A small molecule inhibitor of BCL6 kills DLBCL cells in vitro and in vivo. Cancer cell. 2010;17(4):400-11.

30. Sorensen PH, Chen CS, Smith FO, Arthur DC, Domer PH, Bernstein ID, et al. Molecular rearrangements of the MLL gene are present in most cases of infant acute myeloid leukemia and are strongly correlated with monocytic or myelomonocytic phenotypes. Journal of Clinical Investigation. 1994;93(1):429-37.

31. Huret J-L, Dessen P, Bernheim A. Atlas of Genetics and Cytogenetics in Oncology and Haematology, year 2003. Nucleic Acids Research. 2003;31(1):272-4.

32. Hess JL. MLL: a histone methyltransferase disrupted in leukemia. Trends in Molecular Medicine. 2004;10(10):500-7.

33. Krivtsov AV, Armstrong SA. MLL translocations, histone modifications and leukaemia stem-cell development. Nat Rev Cancer. 2007;7(11):823-33.

34. Ayton PM, Cleary ML. Transformation of myeloid progenitors by MLL oncoproteins is dependent on Hoxa7 and Hoxa9. Genes & Development. 2003;17(18):2298-307.

35. Yokoyama A, Lin M, Naresh A, Kitabayashi I, Cleary ML. A Higher-Order Complex Containing AF4 and ENL Family Proteins with P-TEFb Facilitates Oncogenic and Physiologic MLL-Dependent Transcription. Cancer cell. 2010;17(2):198-212.

36. Chandrasekharappa SC, Teh BT. Functional studies of the MEN1 gene. J Intern Med. 2003;253(6):606-15.

37. Yokoyama A, Wang Z, Wysocka J, Sanyal M, Aufiero DJ, Kitabayashi I, et al. Leukemia Proto-Oncoprotein MLL Forms a SET1-Like Histone Methyltransferase Complex with Menin To Regulate Hox Gene Expression. Molecular and Cellular Biology. 2004;24(13):5639-49.

38. Yokoyama A, Somervaille TC, Smith KS, Rozenblatt-Rosen O, Meyerson M, Cleary ML. The menin tumor suppressor protein is an essential oncogenic cofactor for MLL-associated leukemogenesis. Cell. 2005;123(2):207-18.

39. Shi A, Murai MJ, He S, Lund G, Hartley T, Purohit T, et al. Structural insights into inhibition of the bivalent menin-MLL interaction by small molecules in leukemia. Blood. 2012;120(23):4461-9.

40. Grembecka J, Belcher AM, Hartley T, Cierpicki T. Molecular Basis of the Mixed Lineage Leukemia-Menin Interaction: IMPLICATIONS FOR TARGETING MIXED LINEAGE LEUKEMIAS. Journal of Biological Chemistry. 2010;285(52):40690-8.

41. Grembecka J, He S, Shi A, Purohit T, Muntean AG, Sorenson RJ, et al. Menin-MLL inhibitors reverse oncogenic activity of MLL fusion proteins in leukemia. Nat Chem Biol. 2012;8(3):277-84.

42. Huang J, Gurung B, Wan B, Matkar S, Veniaminova NA, Wan K, et al. The same pocket in menin binds both MLL and JUND but has opposite effects on transcription. Nature. 2012;482(7386):542-6.

43. Liu P, Tarle SA, Hajra A, Claxton DF, Marlton P, Freedman M, et al. Fusion between transcription factor CBFb/PEBP2b and a myosin heavy chain in acute myeloid leukemia. Science. 1993;261:1041-4.

44. Castilla LH, Garrett L, Adya N, Orlic D, Dutra A, Anderson S, et al. Chromosome 16 inversion-generated fusion gene *Cbfb-MYH11* blocks myeloid differentiation and predisposes mice to acute myelomonocytic leukemia. Nature Genet. 1999;23:144-6.

45. Castilla LH, Perrat P, Martinez NJ, Landrette SF, Keys R, Oikemus S, et al. Identification of genes that synergize with Cbfb-MYH11 in the pathogenesis of acute myeloid leukemia. Proceedings of the National Academy of Sciences of the United States of America. 2004;101(14):4924-9.

46. Ravandi F, Burnett AK, Agura ED, Kantarjian HM. Progress in the treatment of acute myeloid leukemia. Cancer. 2007;110(9):1900-10.

47. Kuo YH, Landrette SF, Heilman SA, Perrat PN, Garrett L, Liu PP, et al. Cbf beta-SMMHC induces distinct abnormal myeloid progenitors able to develop acute myeloid leukemia. Cancer cell. 2006;9(1):57-68.

48. Kottaridis PD, Gale RE, Langabeer SE, Frew ME, Bowen DT, Linch DC. Studies of FLT3 mutations in paired presentation and relapse samples from patients with acute myeloid leukemia: implications for the role of FLT3 mutations in leukemogenesis, minimal residual disease detection, and possible therapy with FLT3 inhibitors. Blood. 2002;100(7):2393-8.

49. Lukasik S, Zhang L, Corpora T, Tomanicek S, Li Y, Kundu M, et al. Altered affinity of core binding factor ß-smooth muscle myosin heavy chain protein, product of the inv(16), for Runx1 suggests a mechanism for its dominant negative activity and role in leukemogenesis. Nat Struct Biol. 2002;9:674-9.

50. Illendula A, Pulikkan JA, Zong H, Grembecka J, Xue L, Sen S, et al. Chemical biology. A small-molecule inhibitor of the aberrant transcription factor CBFbeta-SMMHC delays leukemia in mice. Science. 2015;347(6223):779-84.

51. Miyoshi H, Shimizu K, Kozu T, Maseki N, Kaneko Y, Ohki M. t(8;21) breakpoints on chromosome 21 in acute myeloid leukemia are clustered within a limited region of a single gene, *AML1*. Proc Natl Acad Sci USA. 1991;88:10431-4.

52. Kagoshima H, Shigesada K, Satake M, Ito Y, Miyoshi H, Ohki M, et al. The Runt-domain identifies a new family of heteromeric DNA-binding transcriptional regulatory proteins. Trends Genet. 1993;9:338-41.

53. Daga A, Tighe JE, Calabi F. Leukaemia/Drosophila homology. Nature (London). 1992;356:484.

54. Duffy JB, Gergen JP. Sex, segments, and the central nervous system: common genetic mechanisms of cell fate determination. Advances Genet. 1994;31:1-28.

55. Duffy JB, Gergen JP. The Drosophila segmentation gene *runt* acts as a position-specific numerator element necessary for the uniform expression of the sex-determining gene *Sex-lethal*. Genes Dev. 1991;5:2176-87.

56. Canon J, Banerjee U. Runt and Lozenge function in *Drosophila* development. 2000. 2000;Cell and Developmental Biology:327-36.

57. Kamachi Y, Ogawa E, Asano M, Ishida S, Murakami Y, Satake M, et al. Purification of a mouse nuclear factor that binds to both the A and B cores of the polyomavirus enhancer. J Virol. 1990;64:4808-19.

58. Wang S, Speck NA. Purification of core-binding factor, a protein that binds the conserved core site in murine leukemia virus enhancers. Mol Cell Biol. 1992;12:89-102.

59. Ogawa E, Maruyama M, Kagoshima H, Inuzuka M, Lu J, Satake M, et al. PEBP2/PEA2 represents a new family of transcription factor homologous to the products of the Drosophila *runt* and the human *AML1* gene. Proc Natl Acad Sci USA. 1993;90:6859-63.

60. Wang S, Wang Q, Crute BE, Melnikova IN, Keller SR, Speck NA. Cloning and characterization of subunits of the T-cell receptor and murine leukemia virus enhancer core-binding factor. Mol Cell Biol. 1993;13:3324-39.

61. Ogawa E, Inuzuka M, Maruyama M, Satake M, Naito-Fujimoto M, Ito Y, et al. Molecular cloning and characterization of PEBP2b, the heterodimeric partner of a novel Drosophila runt-related DNA binding protein PEBP2a. Virology. 1993;194:314-31.

62. Tahirov TH, Inoue-Bungo T, Morii H, Fujikawa A, Sasaki M, Kimura K, et al. Structural analyses of DNA recognition by the AML1/Runx-1 Runt domain and its allosteric control by CBFb. Cell. 2001;104:755-67.

63. Huang G, Shigesada K, Ito K, Wee HJ, Yokomizo T, Ito Y. Dimerization with PEBP2b protects RUNX1/AML1 from ubiquitin-proteosome-mediated degradation. EMBO J. 2001;15:723-33.

64. North TE, Stacy T, Matheny CJ, Speck NA, de Bruijn MF. Runx1 is expressed in adult mouse hematopoietic stem cells and differentiating myeloid and lymphoid cells, but not in maturing erythroid cells. Stem Cells. 2004;22:158-68.

65. North TE, Gu T-L, Stacy T, Wang Q, Howard L, Binder M, et al. *Cbfa2* is required for the formation of intra-aortic hematopoietic clusters. Development. 1999;126:2563-75.

66. Ottersbach K, Dzierzak E. The murine placenta contains hematopoietic stem cells within the vascular labyrinth region. Dev Cell. 2005;8(3):377-87.

67. Rhodes KE, Gekas C, Wang Y, Lux CT, Francis CS, Chan DN, et al. The emergence of hematopoietic stem cells is initiated in the placental vasculature in the absence of circulation. Cell Stem Cell. 2008;2(3):252-63.

68. Chen MJ, Yokomizo T, Zeigler BM, Dzierzak E, Speck NA. Runx1 is required for the endothelial to haematopoietic cell transition but not thereafter. Nature. 2009;457(7231):889-91.

69. Mukouyama Y, Chiba N, Hara T, Okada H, Ito Y, Kanamuru R, et al. The AML1 transcription factor functions to develop and maintain hematogenic precursor cells in the embryonic aorta-gonad-mesonephros region. Dev Biol. 2000;220:27-36.

70.   Yokomizo T, Ogawa M, Osato M, Kanno T, Yoshida H, Fujimoto T, et al. Requirement of Runx1/AML1/PEBP2aB for the generation of haematopoietic cells from endothelial cells. Genes Cells. 2001;6:13-23.

71.   Kissa K, Herbomel P. Blood stem cells emerge from aortic endothelium by a novel type of cell transition. Nature. 2010;464(7285):112-5.

72.   Eilken HM, Nishikawa S, Schroeder T. Continuous single-cell imaging of blood generation from haemogenic endothelium. Nature. 2009;457(7231):896-900.

73.   Okuda T, van Deursen J, Hiebert SW, Grosveld G, Downing JR. AML1, the target of multiple chromosomal translocations in human leukemia, is essential for normal fetal liver hematopoiesis. Cell. 1996;84:321-30.

74.   Wang Q, Stacy T, Binder M, Marín-Padilla M, Sharpe AH, Speck NA. Disruption of the *Cbfa2* gene causes necrosis and hemorrhaging in the central nervous system and blocks definitive hematopoiesis. Proc Natl Acad Sci USA. 1996;93:3444-9.

75.   Wang Q, Stacy T, Miller JD, Lewis AF, Huang X, Bories J-C, et al. The CBFb subunit is essential for CBFa2 (AML1) function in vivo. Cell. 1996;87:697-708.

76.   Sasaki K, Yagi H, Bronson RT, Tominaga K, Matsunashi T, Deguchi K, et al. Absence of fetal liver hematopoiesis in mice deficient in transcriptional coactivator core binding factor beta. Proc Natl Acad Sci USA. 1996;93:12359-63.

77.   Niki M, Okada H, Takano H, Kuno J, Tani K, Hibino H, et al. Hematopoiesis in the fetal liver is impaired by targeted mutagenesis of a gene encoding a non-DNA binding subunit of the transcription factor, polyomavirus enhancer binding protein 2/core binding factor. Proc Natl Acad Sci USA. 1997;94:5697-702.

78.   Zeigler BM, Sugiyama D, Chen M, Guo Y, Downs KM, Speck NA. The allantois and chorion, when isolated before circulation or chorio-allantoic fusion, have hematopoietic potential. Development. 2006;133(21):4183-92.

79.   Cai Z, de Bruijn MFTR, Ma X, Dortland B, Luteijn T, Downing JR, et al. Haploinsufficiency of AML1/CBFA2 affects the embryonic generation of mouse hematopoietic stem cells. Immunity. 2000;13:423-31.

80.   Okuda T, Takeda K, Fujita Y, Nishimura M, Yagyu S, Yoshida M, et al. Biological characteristics of the leukemia-associated transcriptional factor AML1 disclosed by hematopoietic rescue of AML1-deficient embryonic stem cells by using a knock-in strategy. Mol Cell Biol. 2000;20(1):319-28.

81.   Komori T, Yagi H, Nomura S, Yamaguchi A, Sasaki K, Deguchi K, et al. Targeted disruption of *Cbfa1* results in a complete lack of bone formation owing to maturational arrest of osteoblasts. Cell. 1997;89:755-64.

82.   Otto F, Thornell AP, Crompton T, Denzel A, Gilmour KC, Rosewell IR, et al. *Cbfa1*, a candidate gene for Cleidocranial dysplasia syndrome, is essential for osteoblast differentiation and bone development. Cell. 1997;89:765-72.

83.   Ducy P, Zhang R, Geoffroy V, Ridall AL, Karsenty G. Osf2/Cbfa1: a transcriptional activator of osteoblast differentiation. Cell. 1997;89:747-54.

84.   Ducy P, Starbuck M, Priemel M, Shen J, Pinero G, Geoffroy V, et al. A Cbfa1-dependent genetic pathway controls bone formation beyond embryonic development. Genes Dev. 1999;13:1025-36.

85.   Levanon D, Bettoun D, Harris-Cerruti C, Woolf E, Negreanu V, Eilam R, et al. The Runx3 transcription factor regulates development and survival of TrkC dorsal root ganglia neurons. EMBO J. 2002;21:3454-6.

86.   Woolf E, Xiao C, Fainaru O, Lotem J, Rosen D, Negreanu V, et al. Runx3 and Runx1 are required for CD8 T cell development during thymopoiesis. Proc Natl Acad Sci USA. 2003;100(June 9):7731-6.

87.   Li Q-L, Ito K, Sakakura C, Fukamachi H, Inoue K, Chi X-Z, et al. Causal relationship between the loss of *RUNX3* expression and gastric cancer. Cell. 2002;109:113-24.

88.   Inoue K, Ozaki S, Shiga T, Ito K, Masuda T, Okado N, et al. Runx3 controls the axonal projection of proprioceptive dorsal root ganglion neurons. Nat Neurosci. 2002;5:946-54.

89.   Taniuchi I, Osato M, Egawa T, Sunshine JJ, Bae S-C, Komori T, et al. Differential requirements for Runx proteins in *CD4* repression and epigenetic silencing during T lymphocyte development. Cell. 2002;111:621-33.

90.   Huang B, Qu Z, Ong CW, Tsang YHN, Xiao G, Shapiro D, et al. RUNX3 acts as a tumor suppressor in breast cancer by targeting estrogen receptor [alpha]. Oncogene. 2012;31(4):527-34.

91.   Kim I, Otto F, Zabel B, Mundlos S. Regulation of chondrocyte differentiation by Cbfa1. Mech Dev. 1999;80:159-70.

92.   Inada M, Yasui T, Nomura S, Miyake S, Deguchi K, Himeno M, et al. Maturational disturbance of chondrocytes in Cbfa1-deficient mice. Dev Dyn. 1999;214:279-90.

93.   Fainaru O, Woolf E, Lotem J, Yarmus M, Brenner O, Goldenberg D, et al. Runx3 regulates mouse TGF-beta-mediated dendritic cell function and its absence results in airway inflammation. Embo J. 2004;23(4):969-79.

94.   Growney JD, Shigematsu H, Li Z, Lee BH, Adelsperger J, Rowan R, et al. Loss of Runx1 perturbs adult hematopoiesis and is associated with a myeloproliferative phenotype. Blood. 2005;106:494-504.

95.   Ichikawa M, Asai T, Saito T, Yamamoto G, Seo S, Yamazaki I, et al. AML-1 is required for megakaryocytic maturation and lymphocytic differentiation, but not for maintenance of hematopoietic stem cells in adult hematopoiesis. Nat Med. 2004;10(3):299-304.

96.   Putz G, Rosner A, Nuesslein I, Schmitz N, Buchholz F. AML1 deletion in adult mice causes splenomegaly and lymphomas. Oncogene. 2006;25:929-39.

97.   Cai X, Gaudet JJ, Mangan JK, Chen MJ, De Obaldia ME, Oo Z, et al. Runx1 loss minimally impacts long-term hematopoietic stem cells. PLoS One. 2011;6(12):e28430.

98.   Ichikawa M, Goyama S, Asai T, Kawazu M, Nakagawa M, Takeshita M, et al. AML1/Runx1 negatively regulates quiescent hematopoietic stem cells in adult hematopoiesis. J Immunol. 2008;180(7):4402-8.

99. Jacob B, Osato M, Yamashita N, Wang CQ, Taniuchi I, Littman DR, et al. Stem cell exhaustion due to Runx1 deficiency is prevented by Evi5 activation in leukemogenesis. Blood. 2009;1610-1620.

100. Motoda L, Osato M, Yamashita N, Jacob B, Chen LQ, Yanagida M, et al. Runx1 protects hematopoietic stem/progenitor cells from oncogenic insult. Stem Cells. 2007;25(12):2976-86.

101. Cai X, Gao L, Teng L, Ge J, Oo Z, Kumar AR, et al. Runx1 deficiency decreases ribosome biogenesis and confers stress resistance to hematopoietic stem and progenitor cells. Cell Stem Cell. 2015;http://dx.doi.org/10.1016/j.stem.2015.06.002.

102. Wang CQ, Motoda L, Satake M, Ito Y, Taniuchi I, Tergaonkar V, et al. Runx3 deficiency results in myeloproliferative disorder in aged mice. Blood. 2013;122(4):562-6.

103. Wang Chelsia Q, Krishnan V, Tay Lavina S, Chin Desmond Wai L, Koh Cai P, Chooi Jing Y, et al. Disruption of Runx1 and Runx3 Leads to Bone Marrow Failure and Leukemia Predisposition due to Transcriptional and DNA Repair Defects. Cell Reports. 2014;8(3):767-82.

104. Wang CQ, Chin DWL, Chooi JY, Chng WJ, Taniuchi I, Tergaonkar V, et al. Cbfb deficiency results in differentiation blocks and stem/progenitor cell expansion in hematopoiesis. Leukemia. 2015;29(3):753-7.

105. Tober J, Yzaguirre AD, Piwarzyk E, Speck NA. Distinct temporal requirements for Runx1 in hematopoietic progenitors and stem cells. Development. 2013;140(18):3765-76.

106. Mangan JK, Speck NA. RUNX1 mutations in clonal myeloid disorders: from conventional cytogenetics to next generation sequencing, a story 40 years in the making. Crit Rev Oncog. 2011;16(1-2):77-91.

107. Lam K, Zhang DE. RUNX1 and RUNX1-ETO: roles in hematopoiesis and leukemogenesis. Front Biosci (Landmark Ed). 2012;17:1120-39.

108. Rowley JD. Letter: A new consistent chromosomal abnormality in chronic myelogenous leukaemia identified by quinacrine fluorescence and Giemsa staining. Nature. 1973;243(5405):290-3.

109. Erickson P, Gau J, Chang K-S, Look T, Whisenant E, Raimondi S, et al. Identification of breakpoints in t(8;21) AML and isolation of a fusion transcript with similarity to Drosophila segmentation gene *runt*. Blood. 1992;80:1825-31.

110. Miyoshi H, Kozu T, Shimizu K, Enomoto K, Maseki N, Kaneko Y, et al. The t(8;21) translocation in acute myeloid leukemia results in production of an AML1-MTG8 fusion transcript. EMBO J. 1993;12:2715-21.

111. Nucifora G, Birn DJ, Erickson P, Gao J, LeBeau MM, Drabkin HA, et al. Detection of DNA rearrangement in the AML1 and ETO loci and of an AML1/ETO fusion mRNA in patients with t(8;21). Blood. 1993;81:883.

112. Chang KS, Fan YH, Stass SA, Estey EH, Wang G, Trujillo JM, et al. Expression of AML1-ETO fusion transcripts and detection of minimal residual disease in t(8;21)-positive acute myeloid leukemia. Oncogene. 1993;8(4):983-8.

113. Calabi F, Pannell R, Pavloska G. Gene targeting reveals a crucial role for MTG8 in the gut. Mol Cell Biol. 2001;21(16):5658-66.

114. Amann JM, Chyla BJ, Ellis TC, Martinez A, Moore AC, Franklin JL, et al. Mtgr1 is a transcriptional corepressor that is required for maintenance of the secretory cell lineage in the small intestine. Mol Cell Biol. 2005;25(21):9576-85.

115. Liu Y, Chen W, Gaudet J, Cheney MD, Roudaia L, Cierpicki T, et al. Structural basis for recognition of SMRT/N-CoR by the MYND domain and its contribution to AML1/ETO's activity. Cancer cell. 2007;11(6):483-97.

116. Liu Y, Cheney MD, Gaudet JJ, Chruszcz M, Lukasik SM, Sugiyama D, et al. The tetramer structure of the Nervy homology two domain, NHR2, is critical for AML1/ETO's activity. Cancer cell. 2006;9(4):249-60.

117. Park S, Chen W, Cierpicki T, Tonelli M, Cai X, Speck NA, et al. Structure of the AML1-ETO eTAFH domain-HEB peptide complex and its contribution to AML1-ETO activity. Blood. 2009;113(15):3558-67.

118. Corpora T, Roudaia L, Oo ZM, Chen W, Manuylova E, Cai X, et al. Structure of the AML1-ETO NHR3-PKA(RIIalpha) complex and its contribution to AML1-ETO activity. J Mol Biol. 2010;402(3):560-77.

119. Plevin MJ, Zhang J, Guo C, Roeder RG, Ikura M. The acute myeloid leukemia fusion protein AML1-ETO targets E proteins via a paired amphipathic helix-like TBP-associated factor homology domain. Proc Natl Acad Sci U S A. 2006;103(27):10242-7.

120. Wei Y, Liu S, Lausen J, Woodrell C, Cho S, Biris N, et al. A TAF4-homology domain from the corepressor ETO is a docking platform for positive and negative regulators of transcription. Nat Struct Mol Biol. 2007;14(7):653-61.

121. Grisolano JL, O'Neal J, Cain J, Tomasson MH. An activated receptor tyrosine kinase, TEL/PDGFßR, cooperates with AML1/ETO to induce acute myeloid leukemia in mice. Proc Natl Acad Sci USA. 2003;100:9506-11.

122. Wang YY, Zhao LJ, Wu CF, Liu P, Shi L, Liang Y, et al. C-KIT mutation cooperates with full-length AML1-ETO to induce acute myeloid leukemia in mice. Proc Natl Acad Sci U S A. 2011;108(6):2450-5.

123. Schessl C, Rawat VP, Cusan M, Deshpande A, Kohl TM, Rosten PM, et al. The AML1-ETO fusion gene and the FLT3 length mutation collaborate in inducing acute leukemia in mice. J Clin Invest. 2005;115(8):2159-68.

124. Wildonger J, Mann RS. The t(8;21) translocation converts AML1 into a constitutive transcriptional repressor. Development. 2005;132(10):2263-72.

125. Higuchi M, O'Brien D, Kumaravelu P, Lenny N, Yeoh EH, Downing JR. Expression of a conditional AML1-ETO oncogene bypasses embryonic lethality and establishes a murine model of human t(8;21) acute myeloid leukemia. Cancer cell. 2002;1:63-74.

126. Grimwade D, Walker H, Oliver F, Wheatley K, Harrison C, Harrison G, et al. The importance of diagnostic cytogenetics on outcome in AML: analysis of 1,612 patients entered into the MRC AML 10 trial. The Medical Research Council Adult and Children's Leukaemia Working Parties. Blood. 1998;92(7):2322-33.

127. Grimwade D, Walker H, Harrison G, Oliver F, Chatters S, Harrison CJ, et al. The predictive value of hierarchical cytogenetic classification in older adults with acute myeloid leukemia (AML): analysis of 1065 patients entered into the United Kingdom Medical Research Council AML11 trial. Blood. 2001;98(5):1312-20.

128. Gulley ML, Shea TC, Fedoriw Y. Genetic tests to evaluate prognosis and predict therapeutic response in acute myeloid leukemia. J Mol Diagn. 2010;12(1):3-16.

129. Duployez N, Willekens C, Marceau-Renaut A, Boudry-Labis E, Preudhomme C. Prognosis and monitoring of core-binding factor acute myeloid leukemia: current and emerging factors. Expert Rev Hematol. 2015;8(1):43-56.

130. Yan M, Ahn EY, Hiebert SW, Zhang DE. RUNX1/AML1 DNA binding domain and ETO/MTG8 NHR2 dimerization domain are critical to AML1-ETO9a leukemogenesis. Blood. 2008:883-6.

131. Wichmann C, Becker Y, Chen-Wichmann L, Vogel V, Vojtkova A, Herglotz J, et al. Dimer-tetramer transition controls RUNX1/ETO leukemogenic activity. Blood. 2010;116(4):603-13.

132. Roudaia L, Cheney MD, Manuylova E, Chen W, Morrow M, Park S, et al. CBFbeta is critical for AML1-ETO and TEL-AML1 activity. Blood. 2009;113(13):3070-9.

133. Park S, Speck NA, Bushweller JH. The role of CBFbeta in AML1-ETO's activity. Blood. 2009;114(13):2849-50.

134. Kwok C, Zeisig BB, Qiu J, Dong S, So CW. Transforming activity of AML1-ETO is independent of CBFbeta and ETO interaction but requires formation of homo-oligomeric complexes. Proc Natl Acad Sci U S A. 2009;106(8):2853-8.

135. Zhang J, Kalkum M, Yamamura S, Chait BT, Roeder RG. E protein silencing by the leukemogenic AML1-ETO fusion protein. Science. 2004;305(5688):1286-9.

136. Fukuyama T, Sueoka E, Sugio Y, Otsuka T, Niho Y, Akagi K, et al. MTG8 proto-oncoprotein interacts with the regulatory subunit of type II cyclic AMP-dependent protein kinase in lymphocytes. Oncogene. 2001;20(43):6225-32.

137. Ahn EY, Yan M, Malakhova OA, Lo MC, Boyapati A, Ommen HB, et al. Disruption of the NHR4 domain structure in AML1-ETO abrogates SON binding and promotes leukemogenesis. Proc Natl Acad Sci U S A. 2008;105(44):17103-8.

138. Gelmetti V, Zhang J, Fanelli M, Minucci S, Pelicci PG, Lazar MA. Aberrant recruitment of the nuclear receptor corepressor-histone deacetylase complex by the acute myeloid leukemia fusion partner ETO. Mol Cell Biol. 1998;18(12):7185-91.

139. Lutterbach B, Westendorf JJ, Linggi B, Patten A, Moniwa M, Davie JR, et al. ETO, a target of t(8;21) in acute leukemia, interacts with the N-CoR and mSin3 corepressors. Mol Cell Biol. 1998;18:7176-84.

140. Wang J, Hoshino T, Redner RL, Kajigaya S, Liu JM. ETO, fusion partner in t(8;21) acute myeloid leukemia, represses transcription by interaction with the

human N-CoR/mSin3/HDAC complex. Proc Natl Acad Sci USA. 1998;95:10860-5.

141. Yan M, Burel SA, Peterson LF, Kanbe E, Iwasaki H, Boyapati A, et al. Deletion of an AML1-ETO C-terminal NcoR/SMRT-interacting region strongly induces leukemia development. Proc Natl Acad Sci U S A. 2004;101(49):17186-91.

142. Yan M, Kanbe E, Peterson LF, Boyapati A, Miao Y, Wang Y, et al. A previously unidentified alternatively spliced isoform of t(8;21) transcript promotes leukemogenesis. Nat Med. 2006;12(8):945-9.

143. Tang JL, Hou HA, Chen CY, Liu CY, Chou WC, Tseng MH, et al. AML1/RUNX1 mutations in 470 adult patients with de novo acute myeloid leukemia: prognostic implication and interaction with other gene alterations. Blood. 2009;114(26):5352-61.

144. Gaidzik VI, Bullinger L, Schlenk RF, Zimmermann AS, Rock J, Paschka P, et al. RUNX1 mutations in acute myeloid leukemia: results from a comprehensive genetic and clinical analysis from the AML study group. J Clin Oncol. 2011;29(10):1364-72.

145. Ben-Ami O, Friedman D, Leshkowitz D, Goldenberg D, Orlovsky K, Pencovich N, et al. Addiction of t(8;21) and inv(16) acute myeloid leukemia to native RUNX1. Cell Rep. 2013;4(6):1131-43.

146. Goyama S, Schibler J, Cunningham L, Zhang Y, Rao Y, Nishimoto N, et al. Transcription factor RUNX1 promotes survival of acute myeloid leukemia cells. J Clin Invest. 2013;123(9):3876-88.

147. Kwiatkowski N, Zhang T, Rahl PB, Abraham BJ, Reddy J, Ficarro SB, et al. Targeting transcription regulation in cancer with a covalent CDK7 inhibitor. Nature. 2014;511(7511):616-20.

148. Zhang L, Li Z, Yan J, Pradhan P, Corpora T, Cheney M, et al. Mutagenesis of the Runt domain defines two energetic hotspots for heterodimerization with the core binding factor ß subunit. J Biol Chem. 2003;278:33097-104.

149. Sun XJ, Wang Z, Wang L, Jiang Y, Kost N, Soong TD, et al. A stable transcription factor complex nucleated by oligomeric AML1-ETO controls leukaemogenesis. Nature. 2013;500(7460):93-7.

150. Bravo J, Li Z, Speck NA, Warren AJ. The leukaemia-associated AML1 (Runx1)-CBFb complex functions as a DNA-induced molecular clamp. Nat Struct Biol. 2001;8:371-7.

151. DeKelver RC, Yan M, Ahn EY, Shia WJ, Speck NA, Zhang DE. Attenuation of AML1-ETO cellular dysregulation correlates with increased leukemogenic potential. Blood. 2013;121(18):3714-7.

152. Young DW, Hassan MQ, Pratap J, Galindo M, Zaidi SK, Lee SH, et al. Mitotic occupancy and lineage-specific transcriptional control of rRNA genes by Runx2. Nature. 2007;445(7126):442-6.

153. Teplyuk NM, Zhang Y, Lou Y, Hawse JR, Hassan MQ, Teplyuk VI, et al. The osteogenic transcription factor runx2 controls genes involved in sterol/steroid

metabolism, including CYP11A1 in osteoblasts. Mol Endocrinol. 2009;23(6):849-61.

154.   Bohm HJ. The computer program LUDI: a new method for the de novo design of enzyme inhibitors. J Comput Aided Mol Des. 1992;6(1):61-78.

155.   Bohm HJ. Prediction of binding constants of protein ligands: a fast method for the prioritization of hits obtained from de novo design or 3D database search programs. J Comput Aided Mol Des. 1998;12(4):309-23.

156.   Gorczynski MJ, Grembecka J, Zhou Y, Kong Y, Roudaia L, Douvas MG, et al. Allosteric inhibition of the protein-protein interaction between the leukemia-associated proteins Runx1 and CBFbeta. Chem Biol. 2007;14(10):1186-97.

157.   Mayer M, Mayer B. Characterization of ligand binding by saturaton transfer difference NMR spectroscopy. Angewandte. 1999;38(12):1784-8.

158.   Mayer M, Meyer B. Group epitope mapping by saturation transfer difference NMR to identify segments of a ligand in direct contact with a protein receptor. J Am Chem Soc. 2001;123(25):6108-17.

159.   Cullion K, Draheim KM, Hermance N, Tammam J, Sharma VM, Ware C, et al. Targeting the Notch1 and mTOR pathways in a mouse T-ALL model. Blood. 2009;113(24):6172-81.

160.   Felsher DW, Bishop JM. Reversible tumorigenesis by MYC in hematopoietic lineages. Mol Cell. 1999;4(2):199-207.

161.   Ogata H, Goto S, Sato K, Fujibuchi W, Bono H, Kanehisa M. KEGG: Kyoto Encyclopedia of Genes and Genomes. Nucleic Acids Res. 1999;27(1):29-34.

162.   Huang da W, Sherman BT, Lempicki RA. Systematic and integrative analysis of large gene lists using DAVID bioinformatics resources. Nat Protoc. 2009;4(1):44-57.

163.   Lipinski CA. Drug-like properties and the causes of poor solubility and poor permeability. J Pharmacol Toxicol Methods. 2000;44(1):235-49.

164.   Bohm HJ. On the use of LUDI to search the Fine Chemicals Directory for ligands of proteins of known three-dimensional structure. J Comput Aided Mol Des. 1994;8(5):623-32.

165.   Matheny CJ, Speck ME, Cushing PR, Zhou Y, Corpora T, Regan M, et al. Disease mutations in RUNX1 and RUNX2 create nonfunctional, dominant-negative, or hypomorphic alleles. Embo J. 2007;26:1163-75.

166.   Perez-Alvarado GC, Munnerlyn A, Dyson HJ, Grosschedl R, Wright PE. Identification of the regions involved in DNA binding by the mouse PEBP2a protein. FEBS L. 2000;470:125-30.

167.   Li P, Shi L, Gao MN, Yang X, Xue W, Jin LH, et al. Antibacterial activities against rice bacterial leaf blight and tomato bacterial wilt of 2-mercapto-5-substituted-1,3,4-oxadiazole/thiadiazole derivatives. Bioorg Med Chem Lett. 2015;25(3):481-4.

168.   Bundgaard H, Johansen M. Prodrugs as drug delivery systems IV: N-Mannich bases as potential novel prodrugs for amides, ureides, amines, and other NH-acidic compounds. J Pharm Sci. 1980;69(1):44-6.

169.	Zuber J, Radtke I, Pardee TS, Zhao Z, Rappaport AR, Luo W, et al. Mouse models of human AML accurately predict chemotherapy response. Genes Dev. 2009;23(7):877-89.

170.	Teplyuk NM, Galindo M, Teplyuk VI, Pratap J, Young DW, Lapointe D, et al. Runx2 regulates G protein-coupled signaling pathways to control growth of osteoblast progenitors. J Biol Chem. 2008;283(41):27585-97.

171.	Wilson NK, Foster SD, Wang X, Knezevic K, Schutte J, Kaimakis P, et al. Combinatorial transcriptional control in blood stem/progenitor cells: genome-wide analysis of ten major transcriptional regulators. Cell Stem Cell. 2010;7(4):532-44.

172.	Hoogenkamp M, Lichtinger M, Krysinska H, Lancrin C, Clarke D, Williamson A, et al. Early chromatin unfolding by RUNX1 - a molecular explanation for differential requirements during specification versus maintenance of the hematopoietic gene expression program. Blood. 2009.

173.	Frye SV. The art of the chemical probe. Nat Chem Biol. 2010;6(3):159-61.

174.	Cunningham L, Finckbeiner S, Hyde RK, Southall N, Marugan J, Yedavalli VR, et al. Identification of benzodiazepine Ro5-3335 as an inhibitor of CBF leukemia through quantitative high throughput screen against RUNX1-CBFbeta interaction. Proc Natl Acad Sci U S A. 2012;109(36):14592-7.

175.	Sanda T, Lawton LN, Barrasa MI, Fan ZP, Kohlhammer H, Gutierrez A, et al. Core transcriptional regulatory circuit controlled by the TAL1 complex in human T cell acute lymphoblastic leukemia. Cancer cell. 2012;22(2):209-21.

176.	Mansour MR, Abraham BJ, Anders L, Berezovskaya A, Gutierrez A, Durbin AD, et al. Oncogene regulation. An oncogenic super-enhancer formed through somatic mutation of a noncoding intergenic element. Science. 2014;346(6215):1373-7.

177.	Saha A, Kumar R, Kumar R, Devakumar C. Green synthesis of 5-substituted-1,3,4-thiadiazole-2-thiols as new potent nitrification inhibitors. Journal of Heterocyclic Chemistry. 2010;47(4):838-45.

178.	Li P, Shi L, Gao M-N, Yang X, Xue W, Jin L-H, et al. Antibacterial activities against rice bacterial leaf blight and tomato bacterial wilt of 2-mercapto-5-substituted-1,3,4-oxadiazole/thiadiazole derivatives. Bioorganic & Medicinal Chemistry Letters. 2015;25(3):481-4.

179.	Wei M-X, Feng L, Li X-Q, Zhou X-Z, Shao Z-H. Synthesis of new chiral 2,5-disubstituted 1,3,4-thiadiazoles possessing γ-butenolide moiety and preliminary evaluation of in vitro anticancer activity. European Journal of Medicinal Chemistry. 2009;44(8):3340-4.

180.	Beriger E EW. Preparation of maecaptobis (1,3,4-oxadizoles and thiadiazoles) as agrochemical fungicides and nematocides. Eur Pat Appl. 1990:346,96.

181.	Lee S, Yi KY, Hwang SK, Lee BH, Yoo S-e, Lee K. (5-Arylfuran-2-ylcarbonyl)guanidines as Cardioprotectives through the Inhibition of Na+/H+ Exchanger Isoform-1. Journal of Medicinal Chemistry. 2005;48(8):2882-91.

182. Cui Z, Li Y, Ling Y, Huang J, Cui J, Wang R, et al. New class of potent antitumor acylhydrazone derivatives containing furan. European Journal of Medicinal Chemistry. 2010;45(12):5576-84.

183. Cui Z, Li X, Tian F, Yan X. Synthesis and Bioactivity of 5-Substituted-2-furoyl Diacylhydazide Derivatives with Aliphatic Chain. International Journal of Molecular Sciences. 2014;15(5):8941.

184. Schwieger M, Lohler J, Friel J, Scheller M, Horak I, Stocking C. AML1-ETO inhibits maturation of multiple lymphohematopoietic lineages and induces myeloblast transformation in synergy with ICSBP deficiency. J Exp Med. 2002;196:1227-40.

185. Rhoades KL, Hetherington CJ, Harakawa N, Yergeau DA, Zhou L, Liu LQ, et al. Analysis of the role of AML1-ETO in leukemogenesis, using an inducible transgenic mouse model. Blood. 2000;96:2108-15.

186. de Guzman CG, Warren AJ, Zhang Z, Gartland L, Erickson P, Drabkin H, et al. Hematopoietic stem cell expansion and distinct myeloid developmental abnormalities in a murine model of the AML1-ETO translocation. Mol Cell Biol. 2002;22:5506-17.

187. Buchholz F, Refaeli Y, Trumpp A, Bishop JM. Inducible chromosomal translocation of AML1 and ETO genes through Cre/loxP-mediated recombination in the mouse. EMBO Rep. 2000;1(2):133-9.

188. Yuan Y, Zhou L, Miyamoto T, Iwasaki H, Harakawa N, Hetherington CJ, et al. AML1-ETO expression is directly involved in the development of acute myeloid leukemia in the presence of additional mutations. Proc Natl Acad Sci USA. 2001;98:10398-403.

189. Beghini A, Peterlongo P, Ripamonti CB, Larizza L, Cairoli R, Morra E, et al. C-kit mutations in core binding factor leukemias. Blood. 2000;95(2):726-7.

190. Kottaridis PD, Gale RE, Frew ME, Harrison G, Langabeer SE, Belton AA, et al. The presence of a FLT3 internal tandem duplication in patients with acute myeloid leukemia (AML) adds important prognostic information to cytogenetic risk group and response to the first cycle of chemotherapy: analysis of 854 patients from the United Kingdom Medical Research Council AML 10 and 12 trials. Blood. 2001;98:1752-9.

191. Schnittger S, Kohl TM, Haferlach T, Kern W, Hiddemann W, Spiekermann K, et al. KIT-D816 mutations in AML1-ETO-positive AML are associated with impaired event-free and overall survival. Blood. 2006;107(5):1791-9.

192. Kuchenbauer F, Schnittger S, Look T, Gilliland G, Tenen D, Haferlach T, et al. Identification of additional cytogenetic and molecular genetic abnormalities in acute myeloid leukaemia with t(8;21)/AML1-ETO. Br J Haematol. 2006;134(6):616-9.

193. Boissel N, Leroy H, Brethon B, Philippe N, de Botton S, Auvrignon A, et al. Incidence and prognostic impact of c-Kit, FLT3, and Ras gene mutations in core binding factor acute myeloid leukemia (CBF-AML). Leukemia. 2006;20(6):965-70.

194. Golub TR, Barker GF, Bohlander SK, Hiebert S, Ward DC, Bray-Ward P, et al. Fusion of the *TEL* gene on 12p13 to the *AML1* gene on 21q22 in acute lymphoblastic leukemia. Proc Natl Acad Sci USA. 1995;92:4917-21.

195. Sanchez PV, Perry RL, Sarry JE, Perl AE, Murphy K, Swider CR, et al. A robust xenotransplantation model for acute myeloid leukemia. Leukemia. 2009;23(11):2109-17.

196. Kogan SC, Ward JM, Anver MR, Berman JJ, Brayton C, Cardiff RD, et al. Bethesda proposals for classification of nonlymphoid hematopoietic neoplasms in mice. Blood. 2002;100(1):238-45.

197. Mericskay M, Blanc J, Tritsch E, Moriez R, Aubert P, Neunlist M, et al. Inducible Mouse Model of Chronic Intestinal Pseudo-Obstruction by Smooth Muscle-Specific Inactivation of the SRF Gene. Gastroenterology. 2007;133(6):1960-70.

198. Bonora E, Bianco F, Cordeddu L, Bamshad M, Francescatto L, Dowless D, et al. Mutations in RAD21 Disrupt Regulation of APOB in Patients With Chronic Intestinal Pseudo-Obstruction. Gastroenterology. 2015;148(4):771-82.e11.

199. Galvao J, Davis B, Tilley M, Normando E, Duchen MR, Cordeiro MF. Unexpected low-dose toxicity of the universal solvent DMSO. The FASEB Journal. 2014;28(3):1317-30.

200. Ptasinska A, Assi SA, Mannari D, James SR, Williamson D, Dunne J, et al. Depletion of RUNX1/ETO in t(8;21) AML cells leads to genome-wide changes in chromatin structure and transcription factor binding. Leukemia. 2012;26(8):1829-41.

201. Hatlen M, Wang L, Nimer S. AML1-ETO driven acute leukemia: insights into pathogenesis and potential therapeutic approaches. Front Med. 2012;6(3):248-62.

202. Ptasinska A, Assi Salam A, Martinez-Soria N, Imperato Maria R, Piper J, Cauchy P, et al. Identification of a Dynamic Core Transcriptional Network in t(8;21) AML that Regulates Differentiation Block and Self-Renewal. Cell Reports. 2014;8(6):1974-88.

203. Alcalay M, Meani N, Gelmetti V, Fantozzi A, Fagioli M, Orleth A, et al. Acute myeloid leukemia fusion proteins deregulate genes involved in stem cell maintenance and DNA repair. The Journal of Clinical Investigation. 2003;112(11):1751-61.

204. Gardini A, Cesaroni M, Luzi L, Okumura AJ, Biggs JR, Minardi SP, et al. AML1/ETO Oncoprotein Is Directed to AML1 Binding Regions and Co-Localizes with AML1 and HEB on Its Targets. PLoS Genet. 2008;4(11):e1000275.

205. Fenske TS, Pengue G, Mathews V, Hanson PT, Hamm SE, Riaz N, et al. Stem cell expression of the AML1/ETO fusion protein induces a myeloproliferative disorder in mice. Proc Natl Acad Sci U S A. 2004;101(42):15184-9.

206. Yergeau DA, Hetherington CJ, Wang Q, Zhang P, Sharpe AH, Binder M, et al. Embryonic lethality and impairment of haematopoiesis in mice heterozygous for an AML1-ETO fusion gene. Nat Genet. 1997;15(3):303-6.

207. Okuda T, Cai Z, Yang S, Lenny N, Lyu C, van Deursen JMA, et al. Expression of a knocked-in *AML1-ETO* leukemia gene inhibits the establishment of normal definitive hematopoiesis and directly generates dysplastic hematopoietic progenitors. Blood. 1998;91:3134-43.

208. Li Q, Haigis KM, McDaniel A, Harding-Theobald E, Kogan SC, Akagi K, et al. Hematopoiesis and leukemogenesis in mice expressing oncogenic NrasG12D from the endogenous locus. Blood. 2011;117(6):2022-32.

209. Cabezas‐Wallscheid N, Eichwald V, de Graaf J, Löwer M, Lehr HA, Kreft A, et al. Instruction of haematopoietic lineage choices, evolution of transcriptional landscapes and cancer stem cell hierarchies derived from an AML1‐ETO mouse model. EMBO Molecular Medicine. 2013;5(12):1804-20.

210. Druker BJ. Imatinib as a Paradigm of Targeted Therapies. Advances in Cancer Research. Volume 91: Academic Press; 2004. p. 1-30.

211. Lydon NB, Druker BJ. Lessons learned from the development of imatinib. Leukemia Research. 2004;28, Supplement 1:29-38.

212. Perl A, Carroll M. Exploiting Signal Transduction Pathways in Acute Myelogenous Leukemia. Curr Treat Options in Oncol. 2007;8(4):265-76.

213. Wang X, Crowe PJ, Goldstein D, Yang JL. STAT3 inhibition, a novel approach to enhancing targeted therapy in human cancers (review). Int J Oncol. 2012;41(4):1181-91.

214. Moellering RE, Cornejo M, Davis TN, Bianco CD, Aster JC, Blacklow SC, et al. Direct inhibition of the NOTCH transcription factor complex. Nature. 2009;462(7270):182-8.